MICROFLUIDIC TECHNOLOGIES FOR RAPID, HIGH-THROUGHPUT SCREENING AND SELECTION OF MONOCLONAL ANTIBODIES FROM SINGLE CELLS

by

Anupam Singhal

B.A.Sc., The University of Toronto, 2004

A THESIS SUBMITTED IN PARTIAL FULFILLMENT OF

THE REQUIREMENTS FOR THE DEGREE OF

DOCTOR OF PHILOSOPHY

in

THE FACULTY OF GRADUATE STUDIES

(Chemical and Biological Engineering)

THE UNIVERSITY OF BRITISH COLUMBIA

(Vancouver)

November 2012

Abstract

This thesis describes the development of novel microfluidic technologies for rapid, high-throughput screening and selection of monoclonal antibodies (mAbs) from single cells. Microfluidic devices were used to compartmentalize single antibody-secreting cells (ASCs) in small-volume chambers (i.e. hundreds of picoliters to nanoliters) in order to concentrate secreted mAbs for measurement of antigen binding kinetics and affinities using a novel microfluidic fluorescence bead assay. Microfluidic single-cell antibody screening was performed on ASCs harvested from antigen-immunized mice and purified by fluorescence-activated cell sorting (FACS). Following microfluidic selection of ASCs producing antigen-specific mAbs, ASCs were sequentially recovered from the microfluidic device and subjected to single-cell RT-PCR to amplify the antibody-encoding heavy and light chain genes. Antibody genes for selected high-affinity mAbs are sequenced and cloned into expression vectors for recombinant production in mammalian cell lines. Nearly 200 high-affinity mouse mAbs to the model antigen hen egg lysozyme (HEL) were selected as a validation of this technology, representing a ten-fold increase in the number of high affinity anti-HEL mAbs previously selected using single-cell micro-technologies and the traditional hybridoma approach. Microfluidic single-cell mAb screening also yielded important insights into affinity maturation, immuno-dominance, and antibody stereotypy in the adaptive immune system. By circumventing time-consuming limiting dilution and clonal expansion in the hybridoma approach, microfluidic single-cell screening will enable selection of mAbs from other animal species (e.g. rabbits, humans) for both therapeutic and research applications.

Preface

I conducted the vast majority of the work described in this thesis, which was jointly designed by Dr. Carl Hansen, Dr. Charles Haynes, Dr. John Schrader and myself.

All animal work described in this thesis was conducted in collaboration with the laboratory of Dr. John Schrader at the Biomedical Research Centre located at the University of British Columbia (UBC). Animal immunizations, harvesting and purification of antibody-secreting cells, and ELISPOT assays were performed by Dr. Welson Wang, a postdoctoral fellow in Dr. Schrader's laboratory. Andy Johnson and Justin Wong performed all FACS sorting at the UBC Biomedical Research Centre and Life Sciences Institute. Dr. Michael Williams at the Biomedical Research Centre also assisted in the preparation of fluorescent protein conjugates and provided training in cell culture methods.

All LabView software (Appendix B) was developed in conjunction with an undergraduate engineering physics student, Daniel Da Costa, during an 8-month internship in the Hansen lab. When Dan started his co-op internship, he was provided with sample LabView code that I had previously developed and used to automate the microscope hardware. Dan re-wrote the majority of this software to produce a robust platform for screening many chambers in a single device using custom autofocus algorithms that we developed together. Dan also produced completely new LabView software (Appendix B.2) to perform semi-automated analysis of fluorescence images and binding kinetics. This replaced manual methods of image analysis that I previously used. Finally, Daniel assisted in fabrication of microfluidic devices used in this work. Dan also deserves credit for both the bead trap/filter and novel multiplexer designs

that were incorporated into the final microfluidic device architecture. Dan's contributions to this project are described in his co-op report, entitled "Microfluidic Technology for Screening and Selection of Monoclonal Antibodies from Single Cells".[1]

Most of Chapter 2 was previously published as a manuscript in the ACS journal Analytical Chemistry, entitled "Microfluidic measurement of antibody-antigen binding kinetics from low-abundance samples and single cells" by Singhal, A., Haynes, C.A. and Hansen, C.L. 82(20):8671-9 (2010). The work described in this publication was jointly designed by all three co-authors, and I performed all of the experiments and wrote the manuscript. Chapters 3 and 4 serve the basis for manuscripts currently in preparation.

All work conducted and described in this thesis was approved by the Research Board of Ethics at the University of British Columbia (Ethics Certificate Number A08-0493).

Table of Contents

List of Tables

List of Figures

Acknowledgements

I would like to thank my supervisors Dr. Carl Hansen and Dr. Charles Haynes. I owe both of these mean a great deal for for their mentorship, support, and encouragement both personally and professionally over the last 7 years. I would like to also thank the many members of the Hansen Lab that have helped me and made my experience so enjoyable and rewarding. Of particular note, I would like to thank Dan Da Costa, Tim Leaver, Veronika Sasse, Jeffrey Ng, Dr. Kevin Heyries, Jens Huft, Michael Van Insberghe, and Hans Zahn. I would also like to thank members of Schrader Lab and the Biomedical Research Centre for their training and countless valuable discussions: Dr. Michael Williams, Dr. Welson Wang, Dr. Yanni Wang and Dr. Christy Thompson.

This work would also not have been possible without the love and support of so many friends and family. Neha Bangar: you made so much of my life possible over the last several years. I will cherish every moment of this experience. My best friends Brad Atcheson and Adam White: your friendship is the greatest reward that I have received in Vancouver and I hope our paths "convergently evolve" in the future. To my new little brothers: Harshanvit Singh and Shreyas Rangan. And to everyone who supported me physically and mentally through the most physically challenging episode of my life: Jay Legouillux, Dr. Rob Lloyd-Smith, Dr. Michael Gilbart, and Dr. Rozeela Nand (!). To Dr. Ken Bryant (Ustad, Guruji, friend, mentor….): Thank you for helping me find my "sur"!

To my family: Mummy, Daddy, Didi, Tamara Didi, Tauji and Tia... I cannot describe in words how much I love you. This work is truly your's as much as it is mine.

Dedication

To all the fathers who made me who I am. To my grandfathers, Ram Kishore Aggarwal, Padam Prakash Aggarwal, and Kunwar Sen Goyal. I can only hope that I will one day measure up to some fraction of you all.

Chapter 1: Introduction

Antibodies are proteins produced by the vertebrate adaptive immune system to defend against infectious bacteria, viruses, and other foreign agents.[2] In addition to their natural role in immunity, antibodies that bind target antigens with high affinity and selectivity are routinely used for protein purification, cell sorting, histology, and other research and diagnostic applications.[3–8] Antibodies are also the most rapidly growing class of therapeutics and the second largest group of drugs after vaccines,[9] with 25 products approved for clinical use and over 425 others in development for the treatment of cancer, as well as cardiovascular, autoimmune, and infectious diseases.[10–12] Although several techniques for producing antibodies have been developed over the last three decades, the discovery of new antibodies remains an expensive and time-consuming process.[13–15]

This thesis describes the development of novel microfluidic technologies for rapid, high-throughput screening and selection of antibodies for both therapeutic and research applications. Described is a microfluidic pipeline (Figure 1.1) for screening and selection of monoclonal antibodies from single primary, antibody-secreting cells (ASCs). In this pipeline, animals are first immunized with a target antigen. Next, ASCs are harvested from the immunized animals and purified using fluorescence-activated cell sorting (FACS). Following purification, ASCs are arrayed as single cells into sub-nanoliter chambers in a microfluidic device and screened by a fluorescence bead assay for production of high affinity, antigen-specific mAbs. ASCs producing antigen-specific mAbs are sequentially recovered from the device and subjected to single-cell RT-PCR to amplify the antibody-encoding heavy and light chain genes.

Finally, antibody genes for high-affinity mAbs are sequenced and cloned into expression vectors for recombinant production in mammalian cell lines. This thesis describes the development and validation of this microfluidic single-cell antibody selection platform.

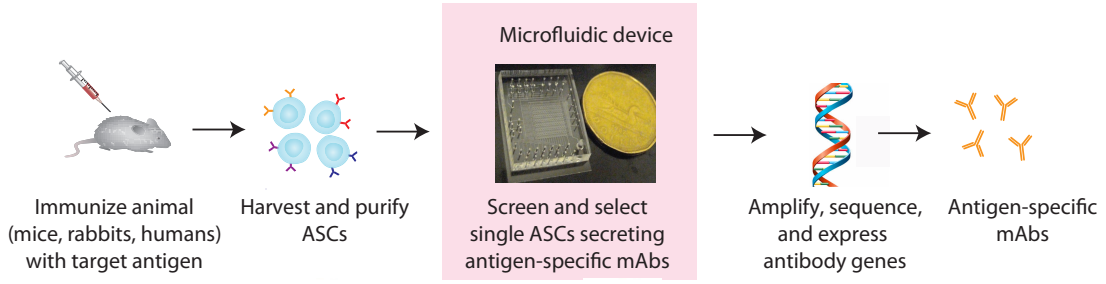

Figure 1.1 Microfluidic pipeline for single-cell antibody screening and selection.

1.1 Antibodies and the Vertebrate Adaptive Immune System

Antibodies have two primary functions: one is to bind target molecules, collectively referred to as antigens; the other is to recruit immune cells and other defense agents to degrade or clear the bound antigens from the host organism.[2] Distinct regions of the antibody molecule perform these two separate functions. Antibodies are symmetric "Y-shaped" proteins consisting of 4 polypeptide chains, two identical "heavy" chains and two identical "light chains" (Figure 1.2). The two arms of the Y-shaped antibody molecule contain identical antigen-binding sites and are called the antibody *variable* (F_v) *region*, so called because the gene sequence encoding this region varies between antibodies. Sequence diversity in the antibody variable region generates extensive conformational and chemical diversity. Antibodies bind target antigens through a combination of different molecular forces, including electrostatic and van der Waals, as well as hydrophobic and hydrogen

bonding interactions.[16] The base of the Y-shaped antibody molecule is referred to as the antibody *constant* (F_c) *region,* which can take one of four or five different forms, each of which recruits different immune effectors. For example, antibodies with a γ-type heavy chain within the F_c region, known as immunoglobulin G (IgG) antibodies, can bind phagocytic cells, such as macrophages and neutrophils, which engulf the bound antigen.[2] Conversely, IgE antibodies, which utilize an e type heavy chain within the F_c region, trigger inflammatory responses by binding to mast cells and basophils.[2] Unlike the antibody variable region, the gene sequence for the constant region is conserved across all antibodies of the same sub-type produced in the same species.

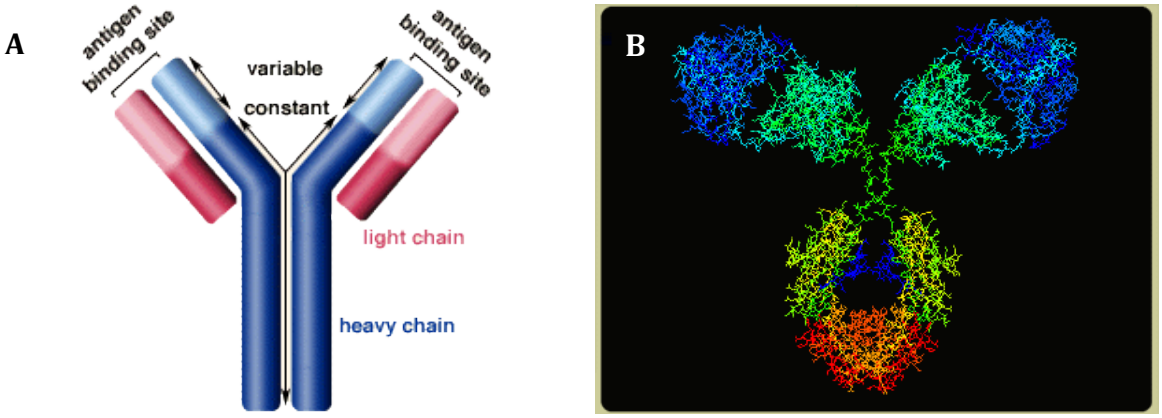

Figure 1.2 A schematic drawing (A) and crystal structure (B) of the antibody IgG molecule. Figures reproduced from the following websites: **http://www.biology.arizona.edu/immunology/tutorials/antibody/structure.html (A) and http://www.doctortipster.com/8245-immune-defense-against-viruses-not-based-on-antibody-production-study-says.html (B).**

Antibodies are naturally produced by bone marrow-derived cells (B cells) in jawed vertebrates, including mice, rabbits, and humans. B cells undergo gene recombination in order to produce two antibody-encoding genes, encoding the antibody heavy and light chain protein chains, respectively.[2] A human heavy chain gene is generated by combining three different gene segments: 1 out of ~60 different variable (V) regions, 1 out of ~25 diversity (D) regions, and 1 out of 6 junction (J) regions (Table 1.1).[2] This combinatorial process, called VDJ recombination, can in theory produce over 7000 unique heavy chain genes. Similarly, each human B cell produces only one of roughly 500 light chain genes by recombining 1 out of 40 Vκ (kappa) genes with 1 of 5 Jκ -genes, or by recombining 1 of 30 Vλ (lambda) genes with 1 of 4 Jλ genes (Table 1.1).[2] Combinatorial pairing of heavy and light chains can therefore produce well over a million different antibodies, each characterized by a distinct antigen-binding site. The antibody repertoire is further diversified by nucleotide trimming and enzymatic addition of non-templated bases at the junctions of recombined gene segments. Importantly, recombination of a single heavy and light chain gene in each B cell excludes all other possible recombination events (allelic exclusion); thus, all antibodies produced by a single B cell share an identical sequence, structure, and function. Accounting for both combinatorial and junctional diversity, human B cells are thought to be capable of producing roughly one hundred trillion (~10^{14}) unique antibody molecules (Table 1.1). However, since a human produces between 10^{10} - 10^{11} B cells, any particular individual produces only a small percentage (~0.01%) of the total antibody diversity.[17]

Table 1.1 Diversity of human antibodies generated by combinatorial (imprecise) gene recombination and heavy/light chain pairing. Antibody genes are further diversified by somatic hypermutation. Data for table taken from Janeway, Arnaout et al., and Tiller et al.[2,18,19]

Human Antibodies		
Antibody Chain	**Heavy**	**Light (κ or λ)**
Variable (V) Segments	56-65	40(κ) 30(λ)
Diversity (D) Segments	23-27	-
Joining (J) Segments	6	5(κ) 4(λ)
V(D)J combinations	~7500-10,000	~300
# of Heavy + Light Pairs	$\sim 2\text{-}3 \times 10^6$	
Junctional Diversity	$\sim 3 \times 10^7$	
Total Antibody Diversity	$\sim 10^{14}$	

The immense diversity of antigen-binding sites makes it likely that a subset of B cells will express an antibody that binds any antigen. Naïve B cells, those cells that have yet to encounter antigen, express their antibody as cell-surface receptors (the B cell receptor, or BCR). The binding of antigen to these receptors triggers the B cell to rapidly proliferate: dividing two to four times daily for 3 to 5 days, resulting in a clone of approximately 1000 antibody-producing daughter cells.[2] B cells undergoing clonal expansion also produce high levels of the enzyme activation-induced deaminase (AID), which acts on antibody genes to induce somatic hypermutation. These mutations are often concentrated in three hypervariable regions, known as complementary-determining regions (CDRs), in both the antibody heavy and light chains (Figure 1.3). Collectively, the heavy and light chain

CDR regions define most of the antigen-binding surface of the antibody molecule; thus, mutations to these regions often result in amino acid substitutions that alter antibody-antigen binding specificity and affinity (Figure 1.4). While many of these substitutions will abolish antibody-antigen binding, others result in increased binding specificity and affinity, conferring the B cell with a selective advantage over the original parent B cell. Through this iterative "affinity maturation" process, antibodies that bind their target antigen with very high affinity and specificity can evolve over several weeks or months (Figure 1.5).[20]

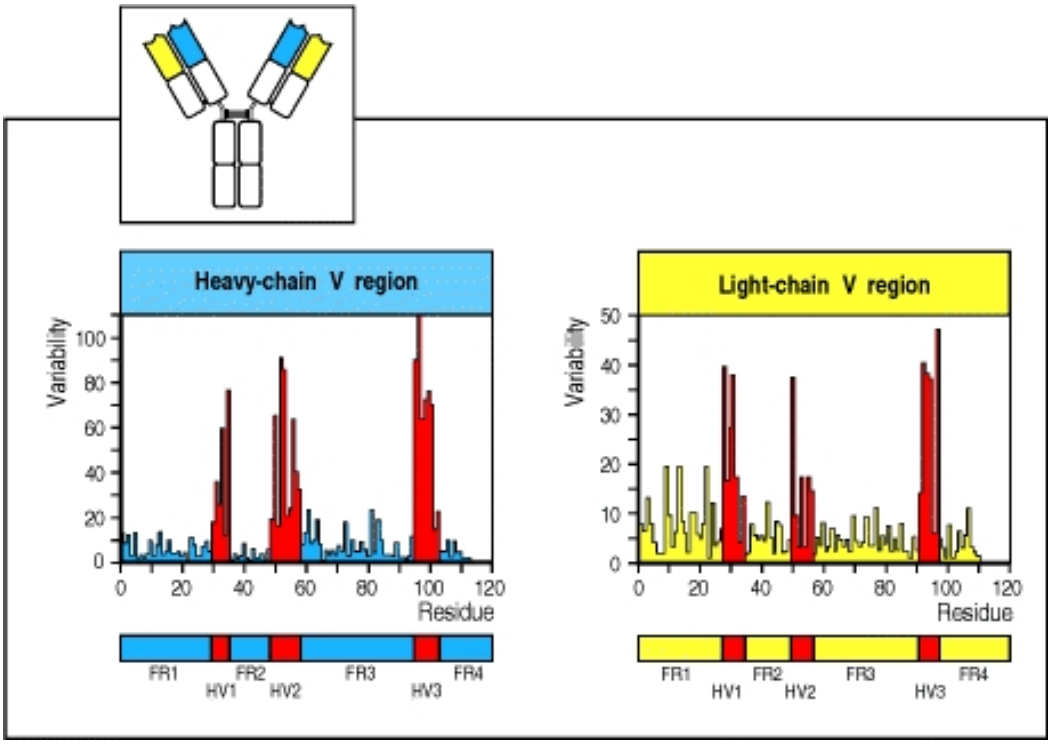

Figure 1.3 Antibody heavy and light chains can be divided into 3 hypervariable regions (complementary-determining regions, CDRs) and 4 framework regions. Comparison of antibody heavy and light chains reveals that sequence differences are largely concentrated to the CDR regions. The heavy and light CDR3 regions, which are the sites of V(D)J recombination, exhibit the greatest sequence diversity. Figure reproduced from Janeway's Immunobiology with permission from Garland Science / Taylor and Francis LLC, 2011.[2]

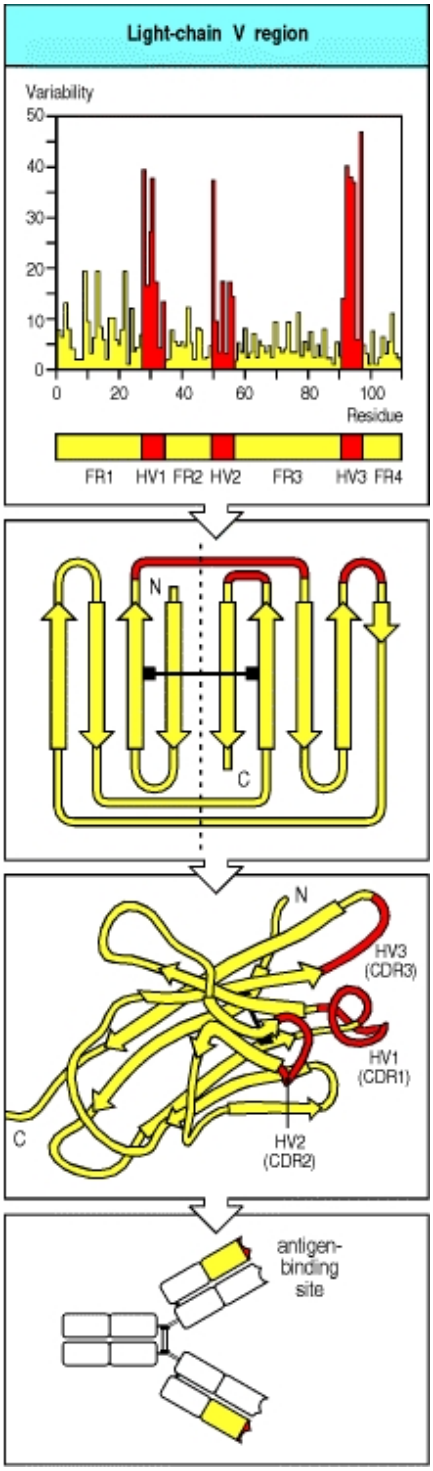

Figure 1.4 The hypervariable (CDR) regions of both antibody heavy and light chains lie in the antigen-binding domain of the folded antibody molecule. Figure reproduced from Janeway's Immunobiology with permission from Garland Science / Taylor and Francis LLC, 2011.[2]

During clonal selection and affinity maturation, B-cells give rise to two classes of cellular progeny: plasma cells and "memory" B cells. Plasma cells are terminally-differentiated B cells that no longer respond to antigen stimulation, and whose primary function is to serve as antibody-producing "factories", with antibodies accounting for 10-20% of all protein synthesis in these cells.[2] While some of these antibodies may still be displayed on the plasma cell membrane, most of these antibodies are secreted into the blood and other tissues at extraordinary rates, reaching several thousand molecules per second.[21] Plasma cells are enriched in the spleen, lymph nodes, and bone marrow, and have been reported to migrate to the blood 1 week after antigen re-stimulation ("boost").[22,23] Memory B cells are quiescent cells that circulate throughout the body long after the primary antigenic challenge, and are named for their role in accelerating the immune response to re-infection with the same antigen. Unlike plasma cells, memory B cells do not secrete antibodies; rather, they display antigen-specific antibodies on their cell surface. Binding of antigen to memory B cells triggers a vigorous response, consisting of rapid cellular proliferation and differentiation into plasma cells.[24]

This thesis focuses on methods for screening and selection of antigen-specific antibodies from plasma cells, which are uniquely tractable for single-cell analysis because of their high rates of production and secretion of antibody mRNA and protein, respectively.

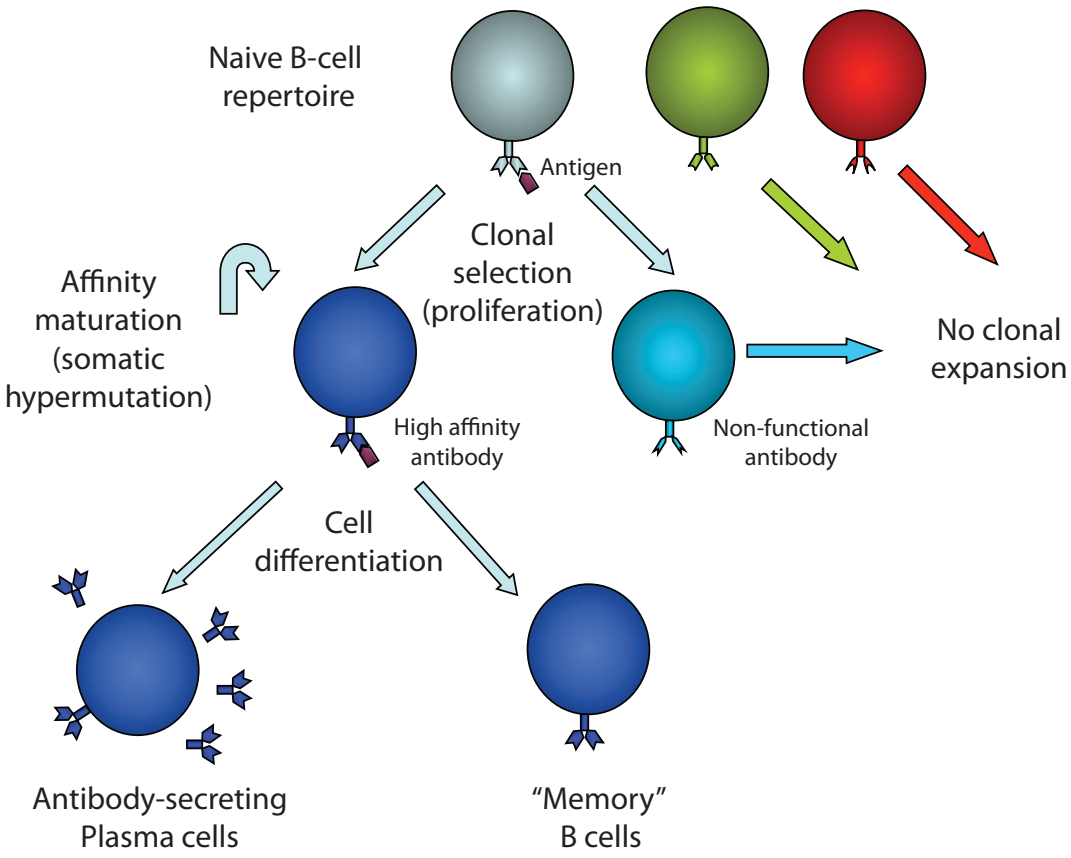

Figure 1.5 Generation of antigen-specific antibodies by the adaptive immune system. Antigen binds surface-displayed antibody on a subset of naïve B cells, which are subsequently stimulated to proliferate (clonal selection). Somatic mutations in proliferating cells alter the expressed antibodies, and the clonal selection process is iterated to generate antibodies that bind antigen with high affinity and specificity (affinity maturation). This process creates two cell-types: plasma cells that secrete soluble antibodies into the blood and other tissues and memory B cells that accelerate the immune response to host re-infection with the same antigen.

1.2 Methods for Antibody Screening and Selection

At the end of the 19th century, Paul Ehrlich, Emil von Behring and Shibasaburo Kitasato conducting pioneering studies that demonstrated the presence of therapeutic antibodies in the blood sera of antigen-immunized animals.[25,26] This work laid the foundations for vaccination and passive serotherapy strategies against diphtheria, tetanus, and other pathogens. However, antibody serum derived from other animal species induces cross-reactive antibodies in humans and often results in undesirable off-target effects, in part because the antibodies are derived from many cells (i.e. polyclonal) and are therefore multi-reactive.[27] Widespread adoption of antibodies in both research and therapeutic applications was facilitated by Kohler and Milstein's seminal invention in 1975 of the "hybridoma" method for producing antibodies of a defined specificity.[28] In this method, spleen cells (i.e. splenocytes) from immunized rodents (e.g. mice, rats, hamsters) are harvested and fused with a cancer (i.e. myeloma) cell-line to generate hybrid cells (hybridoma) that both secrete antibodies and can be expanded in cell culture using selective media (Figure 1.6). These cells are grown for over a week in order to obtain sufficiently high antibody concentrations such that the culture supernatant can be screened by, for example, an enzyme-linked immunoassay (ELISA), to identify cell subpopulations secreting antigen-specific antibodies. This screening process is typically iterated several times using limiting cell dilutions to select clones that are producing antigen-specific antibodies of a single specificity, termed monoclonal antibodies (mAbs).[29]

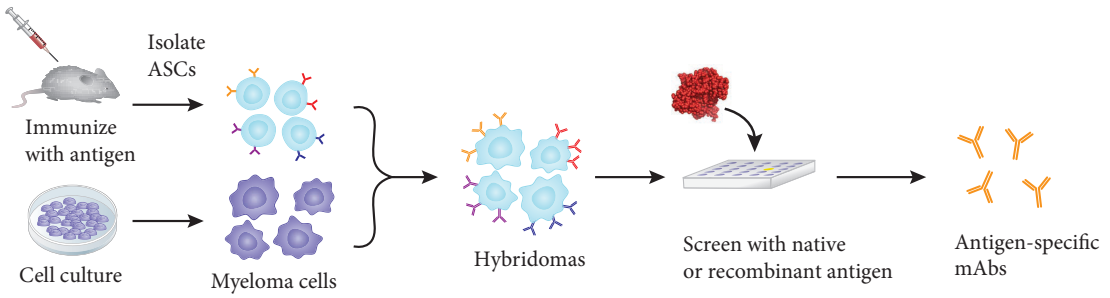

Figure 1.6 Hybridoma method for producing antibodies of a defined specificity. Antibody-secreting cells (ASCs) from animals (e.g. mice) immunized with antigen are fused to cancer (myeloma) cells in order to generate immortalized ASCs (hybridoma). The hybridoma cells are screened by limiting dilution to identify stable clones that secrete antigen-specific mAbs. Figure adapted with permission from Joyce et al (Nature Publishing Group, 2010).[30]

The success of the conventional hybridoma technique for producing rodent mAbs has spurred great interest in adapting this technique for the production of antibodies from larger animals. For example, Knight and coworkers developed a rabbit plasmacytoma cell line capable of forming rabbit hybridoma, thus enabling the selection of antibodies to antigens not immunogenic in rodents.[31] In order to circumvent the immunogenicity of mouse or rabbit mAbs when used as human therapeutics, mAbs generated using the hybridoma approach can be "humanized" by substituting human sequences into regions of the mouse mAbs that are not in direct contact with the antigen.[32–34] Although several therapeutic mAbs (e.g. Herceptin) have been produced in this way, "humanization" of mAbs is a laborious, iterative process since the process of humanization often produces mAbs that either no longer bind the target antigen or remain sufficiently immunogenic in humans to preclude their use as therapeutics.[35] Efforts have therefore been made to develop human mAbs by fusion of human ASCs with human cancer cell-lines, though technical limitations have limited widespread adoption of this approach.[36]

Alternatively, hybridoma cell lines have been generated by fusing mouse myeloma cell-lines with ASCs from transgenic "humanized" mice in which the endogenous mouse Ab genes have been inactivated and replaced with functional human Ab genes.[37–40] Most clinically approved "fully" human therapeutic mAbs (6 out of 7) have been developed using humanized mice.[41]

Common to all hybridoma methods is the problem that many of the fused cells either stop secreting mAbs or fail to expand in culture due to genetic instability. Whereas the spleen of an immunized mouse may contain tens to hundreds of thousands of antigen-specific ASCs, a typical fusion will generate fewer than 50 hybridoma clones secreting antigen-specific mAbs, many of which are genetically unstable or secrete low-affinity mAbs.[28,42,43] The pool of hybridoma clones therefore grossly underrepresents the true antibody diversity in the immunized animal. Generation of high-quality commercial mAbs (e.g. high affinity and/or antigen specificity) may require screening hundreds or thousands of clones from multiple animal immunizations and hybridoma fusions, representing a considerable investment in time and cost.[35] Alternative methods for immortalizing ASCs in cell culture, such as viral transformation, have similarly low transformation efficiencies and, hence, also underrepresent the native antibody repertoire.[44,45]

Antibody screening techniques based on generation of synthetic antibody libraries can circumvent both animal immunization and hybridoma generation.[46] In these methods, diverse libraries of antibody genes are generated *in vitro* by error-prone polymerase chain reaction (PCR), DNA shuffling or other recombinant methods, and these antibody genes are expressed on the surface of phage, yeast, or

other recombinant vectors (Figure 1.7).[46] The library of surface-displayed antibodies is screened by panning over an antigen-covered surface or by fluorescence-activated cell sorting (FACS) in order to select for antigen-specific antibodies. The process is iterated using the selected antibodies in order to select for high binding affinity and/or specificity. These newer approaches can be expensive and time-consuming due to difficulties in generating and maintaining a diverse antibody library, as well as the challenge to establishing an effective post-screening validation step to discard unstable, insoluble, or non-specific binders. As a result, most research-grade antibodies continue to be produced using the hybridoma method. The application of these methods to discovery of therapeutic mAbs is likewise challenging. In order to reduce possible immunogenicity for therapeutic applications, synthetic libraries are often generated entirely from human antibody gene sequences. However, the use of human genes as starting materials for library generation is not sufficient to guarantee the creation of a "truly human" antibody since *in vitro* screening cannot re-capitulate the negative selection processes that reject self-reactive antibodies in humans.[47] Indeed, almost a third of rheumatoid arthritis patients treated with Humira, a clinically approved human therapeutic mAb developed using phage display technologies, were found to develop anti-Humira antibodies and were, in turn, less likely to have clinical benefit or remission.[48]

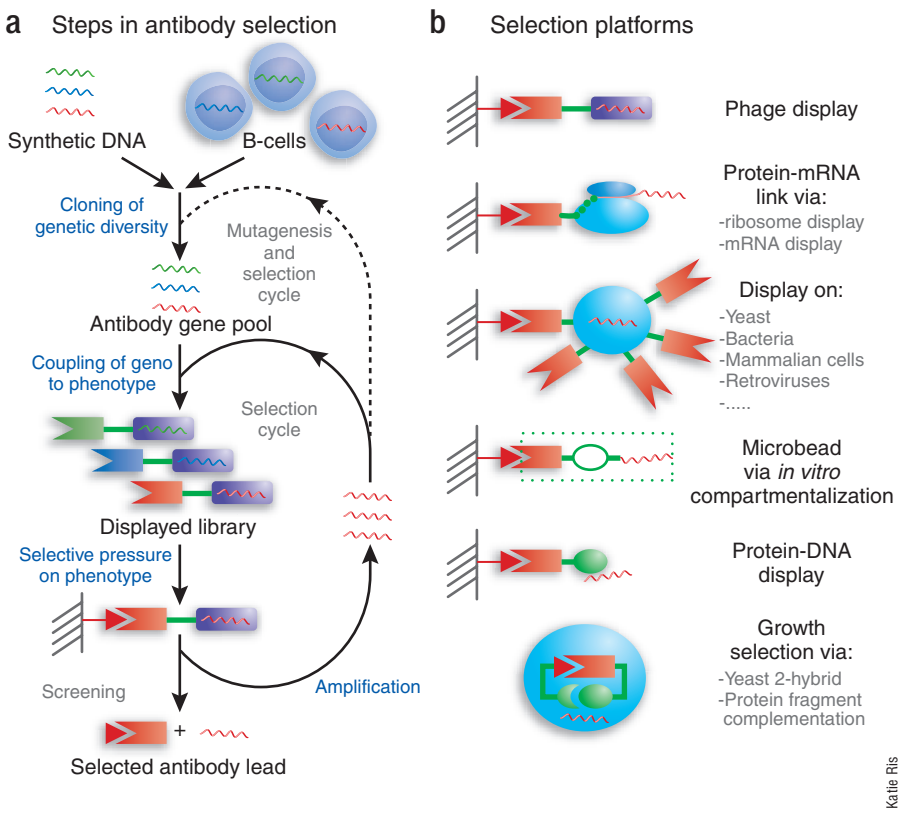

Figure 1.7 Screening and selection of synthetic antibody libraries. (A) Antibody genes are synthesized or amplified from B cells and diversified by *in vitro* mutagenesis (e.g. error-prone PCR or DNA shuffling). The antibody genes are expressed on the surface of a vector (B) and panned with antigen in order to select antigen-specific mAbs. The process is iterated several times in order to increase affinity and/or specificity of the selected antibodies. Figure reproduced from Hoogenboom with permission from Nature Publishing Group, 2005.[46]

1.2.1 Single-Cell Methods for Antibody Selection

In order to reduce the time and expense of both hybridoma and synthetic library screening, a number of approaches have recently been developed to isolate antigen-specific mAbs directly from single antibody-secreting cells (ASCs).[23,49–57] In these methods, tissue samples (e.g. blood, cerebrospinal fluid, spleen, bone marrow) are harvested from immunized animals or naturally infected humans. ASCs are enriched from these tissue samples by incubating cells with fluorescently-labeled antibodies to known plasma cell-surface markers (e.g. $CD138^+$ in mice or $CD19^+$ in

humans) followed by fluorescence-activated cell sorting (FACS).[19,58] Antibody heavy and light chain genes are amplified by single-cell reverse transcription polymerase chain reaction (RT-PCR), cloned into expression vectors and expressed recombinantly in bacterial, yeast, or mammalian cells. The expressed antibodies are subsequently screened for binding affinity and specificity to the target antigen. This general workflow has yielded antibodies from highly enriched antigen-specific ASC populations produced by humans exposed to tetanus toxoid, anthrax, dengue virus, rotavirus, and influenza virus.[23,59–62] Remarkably, up to 80% of human ASCs from blood taken 7 days after a booster shot with influenza vaccine were found to produce influenza-specific mAbs.[23] It remains to be seen whether this approach can be generally applied for the selection of antibodies to more poorly immunogenic antigens that may fail to generate highly enriched ASC populations, such as mutated proteins expressed in human cancers and endogenous proteins overexpressed in autoimmune disorders. Under these circumstances, laborious and time-consuming cloning and expression of thousands of antibodies may be required for downstream screening.

An assay for screening antibodies secreted by single ASCs could facilitate rapid and inexpensive single-cell antibody selection without the need to amplify, clone and express mAbs from all (i.e. antigen-specific *and* antigen-nonspecific) ASCs. Among the most successful examples of this strategy is the Selected Lymphocyte Antibody Method (SLAM), in which a hemolytic plaque assay is used to identify single cells secreting antigen-specific mAbs (Figure 1.8).[50] In SLAM, antigen is chemically conjugated to the surface of sheep red blood cells (SRBCs). The SRBCs

are then mixed with ASCs and blood complement, such that the SRBCs vastly outnumber the ASCs. The mixture is then placed in between two wax-sealed glass slides and incubated at 37°C for less than an hour. During this time, antibodies secreted by ASCs bind to the antigen-covered SRBCs. Blood complement then binds to these antibodies, which triggers the lysis of the SRBCs (i.e. hemolysis). Antigen-specific ASCs are located in regions on the glass slide devoid of SRBCs ("plaques") (Figure 1.8). Each ASC is then manually recovered using a micropipette and can be subjected to single-cell reverse transcription polymerase chain reaction (RT-PCR) to amplify the antibody heavy and light chain genes. The amplified genes are sequenced, cloned and expressed in mammalian cell-lines for production. Despite success of the SLAM method, the hemolytic plaque assay is not suitable for selecting mAbs based on antigen-binding affinity and selectivity and is further not amenable to high-throughput automation. The development of new technologies for sensitive, high-throughput screening of mAbs from single cells could facilitate rapid generation of mAbs for both research and therapeutic applications.

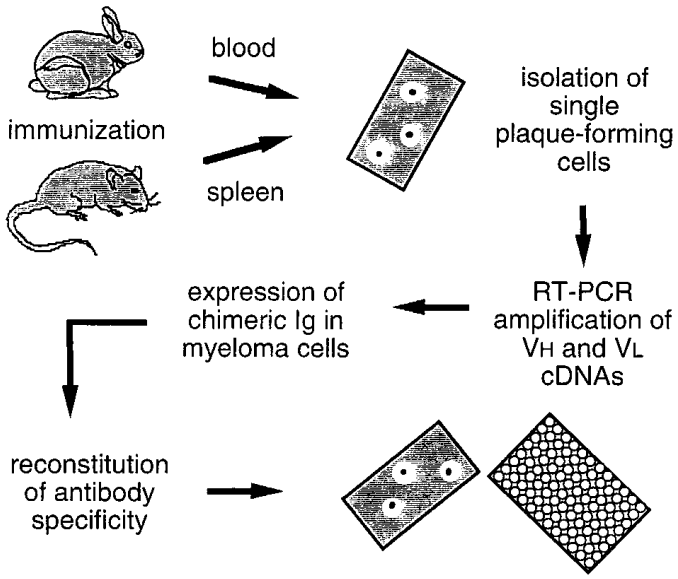

Figure 1.8 Selected Lymphocyte Antibody Method (SLAM) for identifying antigen-specific mAbs from single antibody-secreting cells (ASCs). ASCs are mixed with antigen-coated sheep red blood cells (SRBCs) and blood complement on a glass slide and incubated at 37°C for an hour. Binding of secreted antibodies to antigen triggers lysis of red blood cells in the area around each ASC, thus forming visible "plaques" on a sealed glass slide. ASCs are manually recovered and subjected to single-cell RT-PCR followed by cloning and expression of antibody genes. Figure reproduced with permission from Babcook et al. (PNAS, 1996).[50]

1.3 Microfluidics – An Enabling Technology for Screening and Selection of Antibodies from Single Cells

Microfluidics can be broadly defined as technologies that manipulate small volumes of fluids (femtoliters to nanoliters, or 10^{-15} – 10^{-12} L) in channels with dimensions of tens to hundreds of microns.[63] Microfluidics offer fundamental advantages in chemical analysis, namely precise control of reagents, reduced analysis times, and lower cost compared with traditional analytical methods. In the last two decades, microfluidic technologies have progressed from an initial proof-of-concept demonstration[64] to commercial applications in chromatography,[65] molecular detection,[66] and high-throughput DNA sequencing[67]. Microfluidic

technology has also enabled high-throughput biochemistry,[68,69] drug discovery,[70] chemical synthesis,[71] structural biology,[72–74] molecular diagnostics,[75–77] and single-cell analysis.[78–83]

Rapid prototyping of complex microfluidic devices has been enabled by two inventions: firstly, the invention of a replica molding technique, called soft lithography, for fabricating microfluidic channels from lithographically-patterned master molds (Figure 1.9A);[84,85] and, secondly, a method to fabricate valves by multilayer soft lithography (MSL) whereby channels are fabricated and aligned in multiple layers of a single device[86] (Figure 1.9B). Both of these fabrication methods utilize a silicone rubber known as polydimethylsiloxane (PDMS), which is manufactured as a two-part viscous fluid that, when mixed, solidifies by room-temperature vulcanization (RTV). PDMS exhibits a range of useful material properties for microfluidic devices, the most important of which are gas permeability for maintaining viability of biological specimens and for enabling dead-end loading of liquids into channels, transparency to allow imaging of devices using standard optical and fluorescence microscopes, and a relatively low Young's modulus (< 1 MPa). This latter property enables the simple fabrication of pneumatic valves whereby application of pressure to a fluid-filled channel on one layer deflects a thin elastomeric membrane to seal off a channel on an adjacent layer of the microfluidic device (Figure 1.9C). MSL facilitates the integration of thousands of micro-valves in a single PDMS device, which can be used to build higher-level components including fluidic mixers, peristaltic pumps, and fluidic multiplexing structures (Figure 1.10).

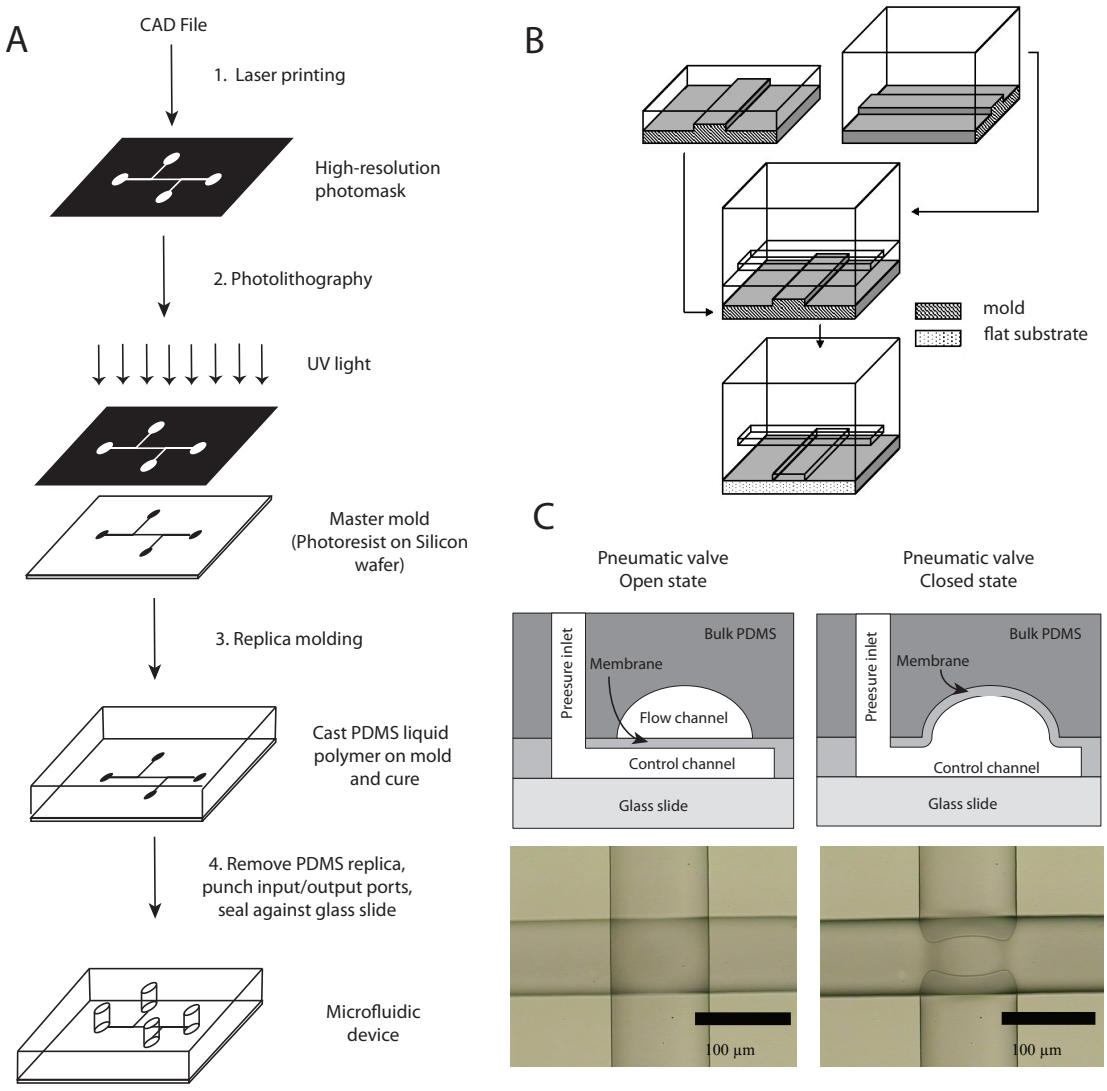

Figure 1.9 Fabrication of single (A) and multilayer (B & c) polydimethylsiloxane (PDMS) microfluidic devices. (A) Soft lithography. Replica molding of lithographically-patterned master molds using PDMS liquid polymer. After the PDMS polymer is cured into a solid substrate, it is removed from the master mold, input/output ports are manually punched through the device and the microfluidic channels are sealed against a glass slide. (B) Multilayer soft lithography (MSL). Replica molding is performed using multiple master molds, and the resulting PDMS layers are aligned and bonded into a monolithic structure. (C) Pressure applied to a fluid-filled channel on the control layer deflects the elastomeric membrane separating it from the channel on the flow layer, thus closing the reversible valve structure. Figures (A) adapted with permission from McDonald et al. (Electrophoresis, 2000),[85] (B) reproduced from Unger et al. (Science, 2000),[86] and (C) courtesy of C. Hansen.

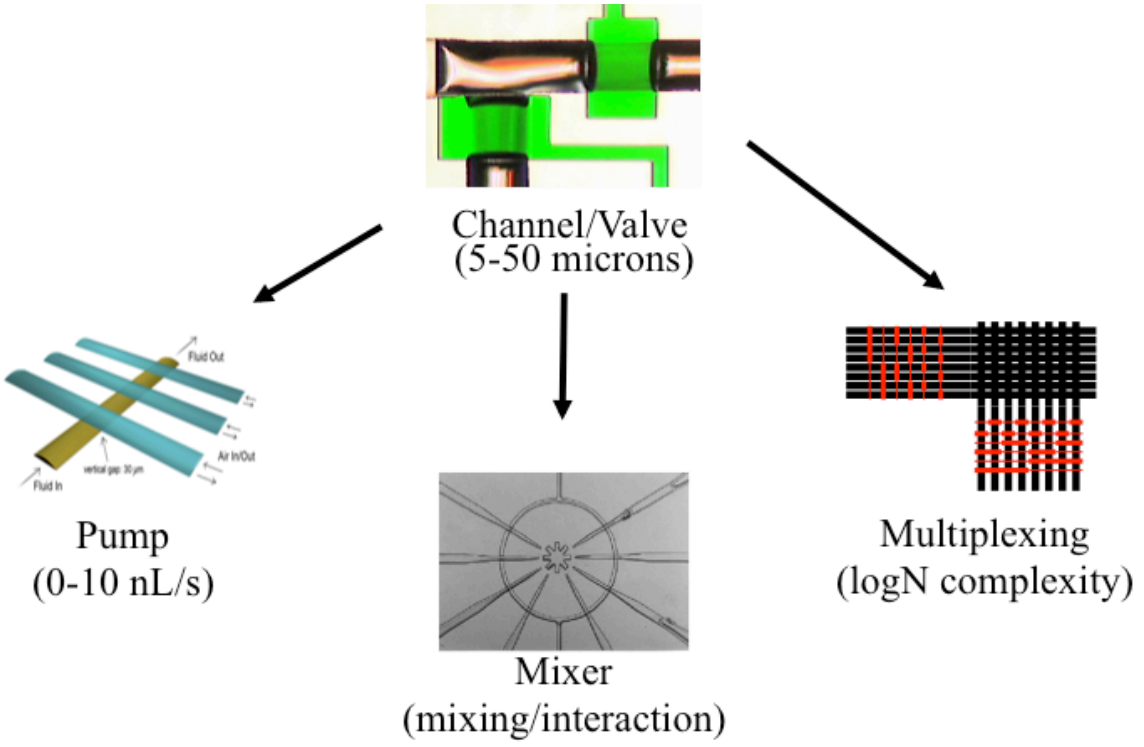

Figure 1.10 Integration of multiple microfluidic valves into higher-order fluidic structures (pumps, fluidic mixers, and fluidic multiplexing structures) in single microfluidic devices fabricated by multilayer soft lithography.[73,86,87] Pumps are used to meter precise volumes of fluidic reagents, ranging from 100 pL to 1 nL. Viscous forces dominate inertial forces for fluid flow in microfluidic channels (i.e. laminar flow), and thus fluidic mixers are required to accelerate the mixing of chemical reagents. Multiplexing structures facilitate the selection of one or more fluidic reagents with a reduced number of valves (2logN) compared to the number of reagent inputs (N). Figure courtesy of C. Hansen with permission.

Miniaturization offers a particular advantage for the detection of mAbs secreted by single antibody-secreting cells (ASCs). Despite secreting thousands of antibody molecules per second[21], single ASCs in conventional 96- or 384-well plates (>10 μL volumes) would require approximately 10 weeks to secrete antibody concentrations detectable by standard enzyme-linked immunoassays (ELISA) (Figure 1.11). Confining single ASCs to small (e.g. sub-nanoliter) volumes can enable efficient detection of secreted antibodies from single ASCs within hours of harvesting and laboratory culture (Figure 1.11). Indeed, Nossal and Lederberg

confined single ASCs in microdroplets and demonstrated that single ASCs secrete antibodies of a single specificity, in a seminal study from 1958 that first provided experimental evidence for the "one cell-one antibody" theory.[88,89]

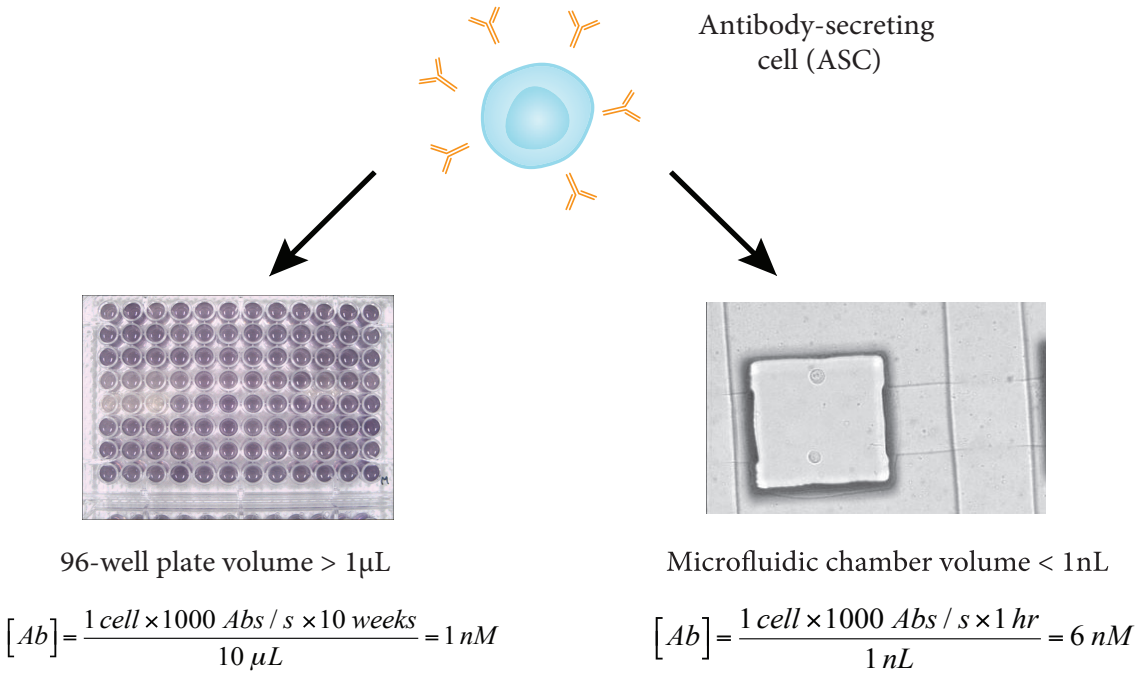

Figure 1.11 Concentration enhancement in small-volume chambers (<1 nL) enables detection of antibodies secreted by single antibody-secreting cells (ASCs). ASCs harvested from immunized animals typically survive for ~1-2 days in culture. Thus, mAbs from single ASCs cannot be detected in cell-culture plates using standard laboratory tests (>1 nM detection limit).

A number of groups have recently used small-volume compartmentalization to screen mAbs from single ASCs using either micro-fabricated wells[14,51,90] or emulsion (i.e. water-in-oil) droplets[91,92]. Love and coworkers used a microengraving method to fabricate small micro-wells in a PDMS substrate (Figure 1.12A).[14] ASCs were manually pipetted on to the surface of the substrate and single ASCs were allowed to settle into the wells by gravity. The PDMS substrate was then sealed against a functionalized glass slide that captured secreted antibody from each well

to produce a printed "microarray" that was then incubated with fluorescently labeled antigen and secondary antibodies. Fluorescence imaging of the microarray was performed to determine which wells contained single ASCs secreting antigen-specific mAbs. Repeating this method with multiple slides and incubating each printed microarray with a different concentration of fluorescent antigen, the apparent affinity of each secreted mAb was estimated.[90] In a similar manner, Kishi and coworkers demonstrated that mAbs from single ASCs in micro-fabricated wells can be detected using a fluorescence surface assay (immunospot array assay on a chip, ISAAC) and that selected ASCs can be retrieved from the array by micromanipulation in order to amplify heavy and light chain genes for subsequent cloning and expression of mAbs (Figure 1.12B).[51] Finally, Merten and coworkers developed microfluidic devices to encapsulate single hybridoma cells in aqueous droplets (Figure 1.12C) and demonstrated the detection, sorting and enrichment of droplets containing ASCs secreting mAbs that inhibit enzymatic activity (e.g. angiotensin converting enzyme 1, ACE-1) based on a fluorescence assay.[92] Despite screening tens to hundreds of thousands of ASCs, these micro-technologies typically identify very few ASCs secreting antigen-specific mAbs (~20), of which the vast majority of mAbs bind target antigen with low affinities (K_d < 100nM);[51,90] thus, these methods produce comparable yield and quality of mAbs to conventional hybridoma methods (see Chapter 1, Section 1.2 above). Of these micro-technologies, only the ISAAC method has previously been used to recover ASCs for amplification, cloning, and expression of antibody genes. Thus, the work described in this thesis focused on the development of a novel micro-technology for rapid, high-throughput

selection of high affinity antigen-specific mAbs from single ASCs. Specifically, a fully integrated microfluidic device was designed and fabricated by multilayer soft lithography for single-cell handling, screening of high affinity antigen-specific mAbs, and selective recovery of ASCs for downstream amplification, cloning, and expression of antigen-specific mAbs.

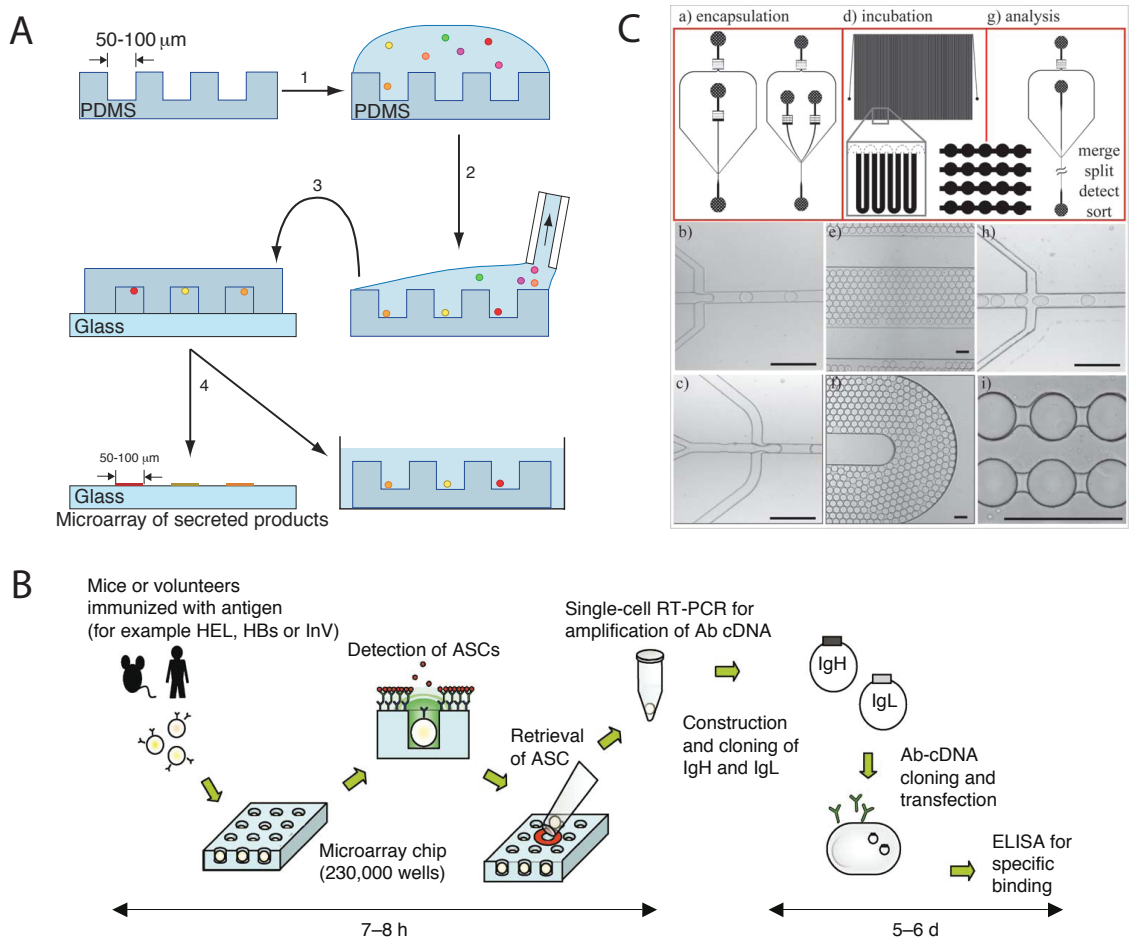

Figure 1.12 Methods for screening antibodies secreted by single cells using micro-fabricated wells (A and B) and droplet encapsulation (C). (A) Microengraving method. Single cells in PDMS micro-wells secrete antibodies that are captured on a "printed microarray" that is imaged after incubation with fluorescently-labeled antigen. (B) ISAAC method (see text for details). (C) Schematic (above) and microscope images (below) of microfluidic devices to encapsulate single cells in water-in-oil emulsion droplets, incubate and detect secreted antibodies. Scale bars are 100 μm. Figures reproduced with permission from Love et al. (Nature Publishing Group, 2006) (A)[14], Jin et al. (Nature Publishing Group, 2009) (B)[51], and Köster et al. (Lab on a Chip, 2008) (C)[91].

1.4 Aims of this Thesis

This thesis describes the design and fabrication of a novel fully-integrated microfluidic system that enables sensitive screening and selection of mAbs from single antibody-secreting cells (ASCs) through direct and accurate measurement of their binding affinities and selectivity to a target antigen, as well as automated recovery of single cells for RT-PCR amplification of antibody genes in order to sequence, clone, and express antigen-specific mAbs produced by these cells. This work involved:

1. The development of an ultrasensitive microfluidic fluorescence bead assay for measuring antibody-antigen binding kinetics and selectivity from small amounts of antibody sample (Chapter 2);
2. The development of methods to sort and recover single cells from microfluidic devices and RT-PCR amplify heavy and light chain genes encoding antigen-specific mAbs (Chapter 3);
3. The integration of antibody screening from hundreds of single cells with recovery and amplification of antibody genes from cells producing novel, antigen-specific mAbs (Chapter 4).

By screening monoclonal antibodies from single cells, the proposed technology will enable rapid and high-throughput selection of monoclonal antibodies for therapeutic and biomedical research applications.

Chapter 2: Microfluidic Measurement of Antibody-Antigen Binding Kinetics from Low Abundance Samples

An ultrasensitive microfluidic fluorescence bead assay for measuring antibody-antigen binding kinetics from low abundance samples is described.

2.1 Antibody-Antigen Binding Properties: Binding Affinity, Selectivity and Kinetics

The binding of antibodies to target antigens is typically characterized by two properties: affinity and selectivity. Selectivity refers to the ability of an antibody to bind variants of a target antigen; that is, a cross-reactive antibody will bind many different structural isoforms (glycoforms, post-translational modifications, or species homologues) of an antigen, whereas a selective antibody will bind a specific structural isoform of an antigen. On the other hand, antibody affinity refers to the "strength" with which it binds to a target antigen, and is governed by a combination of net favorable electrostatic and van der Waals forces, as well as hydrophobic and hydrogen bonding interactions. Based on differences in the number, types and geometries of molecular contacts, antibody-antigen interactions can exhibit a broad range of binding affinities, with equilibrium dissociation constants ranging from micromolar to sub-nanomolar (10^{-5} – 10^{-10} M).[93]

2.1.1 Mathematical Model for Antibody-Antigen Binding

Antibody-antigen interactions are non-covalent and usually reversible.[94] In such cases, the kinetics of the binding reaction can be described by the following first-order differential equation:

$$\frac{d}{dt}[AbAg] = k_f[Ab][Ag] - k_r[AbAg] \qquad (2.1),$$

in which [*Ab*], [*Ag*], and [*AbAg*], represent molar concentrations of antibody, antigen and antibody-antigen bound complex, respectively. This equation, often referred to as the law of mass action, can be physically interpreted in the following manner: 1) antibody and antigen molecules collide in solution due to random diffusion and, thus, the probability of collision and binding is directly proportional to the antibody and antigen solution concentrations; 2) the dissociation of antibody-antigen complex is a random event and is therefore only proportional to the concentration of antibody-antigen complex. The proportionality constants, k_f and k_r, are called the forward and reverse kinetic rate constants, respectively. This equation can be solved analytically when one of the two interacting molecules is present in excess or is immobilized on a substrate, such that $[Ab] = [Ab]_{t=0} + [AbAg] \approx [Ab]_{t=0}$. Under these circumstances, the analytical solution to equation 2.1 is described by the equations in Table 2.1 and depicted in Figure 2.1.

Table 2.1 Analytical solutions to first-order differential equations describing antibody-antigen binding under the condition that $[Ab] \approx [Ab]_{t=0} >> [Ag]_0$.

Association phase: $[AbAg] = [Ab]_0 \frac{[Ag]_0}{[Ag]_0 + K_d}\left(1 - e^{-t/\tau}\right)$ (2.2a) $\tau = \frac{1}{k_f[Ag]_0 + k_r}$ (2.2b)
Chemical Equilibrium: $[AbAg] = \frac{[Ag]_0}{[Ag]_0 + K_d}$ (2.3a) $K_d = \frac{k_f}{k_r}$ (2.3b)
Dissociation phase: $[AbAg] = [Ab]_0 \frac{[Ag]_0}{[Ag]_0 + K_d}\left(e^{-t/\tau}\right)$ (2.4a) $\tau = \frac{1}{k_r}$ (2.4b)

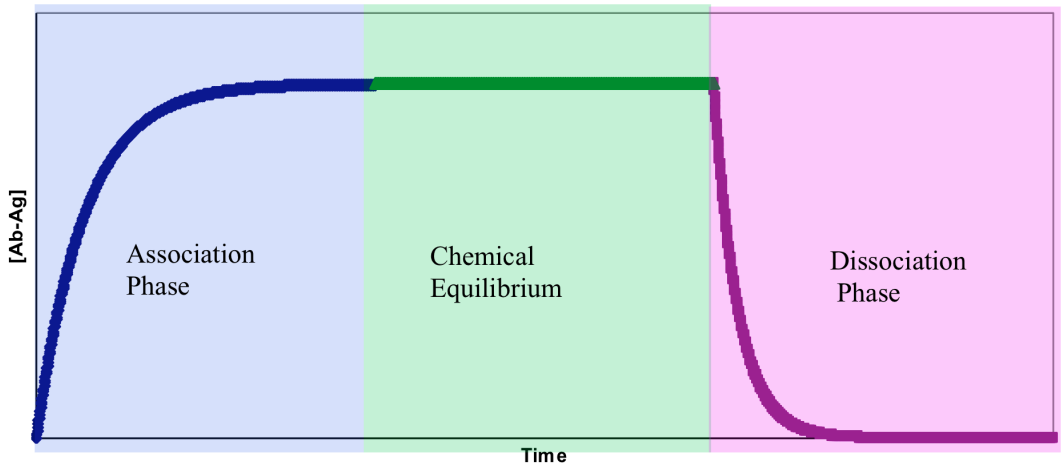

Figure 2.1 Graphical depiction of first-order antibody-antigen binding kinetics. Concentration of antibody-antigen complex is on the y-axis, whereas time is on the x-axis. Antibody-antigen complex follows bimolecular exponential association kinetics during the association phase, and first-order exponential kinetics during the dissociation phase. Equations describing the rates of growth and decay in concentration of antibody-antigen complex are presented in Table 2.1.

According to this simple but proven model, antibody-antigen binding is predicted to occur at an exponential rate, with a time constant dependent on the total antigen concentration as well as both the forward and reverse rate constants (equation 2.2). The concentration of antibody-antigen complex reaches a plateau at a maximum value, corresponding to the condition of chemical equilibrium, where the rate of antibody-antigen association equals the rate of dissociation of the antibody-antigen complex. The amount of antibody-antigen complex formed at chemical equilibrium can be conveniently quantified with respect to the equilibrium dissociation constant ($K_{d,}$ in units of molarity), where a lower value of K_d represents a higher binding affinity (equation 2.3). For a system containing antibody-antigen complex initially at equilibrium, this model also predicts that the amount of antibody-antigen complex decreases exponentially, governed solely by the reverse rate constant, when the free

(unbound) state of one of the interacting molecules is completely removed from solution (equation 2.4).

By considering the antibody-antigen interaction as two independent physical processes of diffusive transport and intrinsic reaction, the forward and reverse kinetic rate constants can be expressed as:

$$k_f = \frac{k_+ k_{on}}{k_+ + k_{on}} \qquad (2.5a)$$

$$k_r = \frac{k_+ k_{off}}{k_+ + k_{on}} \qquad (2.5b),$$

where k_{on} and k_{off} are the intrinsic on-rate and off-rate constants, and k_+ is the characteristic diffusive rate constant.[95] The diffusive rate constant k_+ is highly dependent upon the geometric and solution conditions under which antibody-antigen interactions occur. If antibody-antigen binding occurs on a spherical surface, as when antibodies are expressed on a cell surface, the diffusive rate constant can be expressed as:

$$k_+ = (4\pi D a) N_A \qquad (2.6),$$

where D represents the effective diffusion coefficient, a represents the radius of the spherical binding surface, and N_A represents Avogadro's number. If one assumes that the antigen is a small protein ($D < 10^{-10}$ m^2/s) and the antibody is expressed on a cell with diameter of 1 to 10 μm, the diffusion rate constant is then predicted to be on the order of 10^{12} M^{-1}s^{-1}. Stringent orientation requirements limit kinetic on-rate constants for most antibody-antigen complexes to less than 10^5-10^7 M^{-1}s^{-1}.[96,97] Thus, antibody-antigen binding on the cell surface is reaction-limited ($k_+ >> k_{on}$), making the forward and reverse rate constants equal to the intrinsic on-rate and off-rate

constants, respectively (equations 2.5). The half-lives of antibody-antigen interactions typically range from several minutes to several hours, corresponding to k_{off} values greater than 10^{-3} - 10^{-4} s^{-1}. Taken together, the majority of naturally produced antibodies therefore bind their antigen with an equilibrium dissociation constant ranging from 100 pM to 10 μM.[59,98] Antibodies with K_d values close to 100pM are estimated to be near the affinity limits that can be selected by the immune system, as antibodies that bind antigen with longer half-lives than cellular endocytosis rates should theoretically provide no selective advantage during the adaptive immune response.[93] It is possible, however, that antibodies with K_d values less than 100 pM are produced by the immune system simply by chance.

2.2 Methods and Parameters for Antibody Screening and Selection

Antigen binding affinity and selectivity are the two parameters that typically determine the suitability of an antibody for particular research and therapeutic applications. For instance, therapeutic antibodies for long-term protection to human influenza virus would ideally cross-react with a variety of hemagglutinin (HA) surface proteins present on different viral strains.[49] Conversely, antibodies used for treatment of cancerous tumors must often specifically bind a particular genetically mutated or glycosylated state of a protein.[99] The most useful antibodies for both research and therapeutic applications are typically those that bind their target antigen with moderate to high binding affinities (i.e. equilibrium dissociation constants less than or equal to 10 nM).[12]

Antibody binding affinity and selectivity are typically assessed using an enzyme-linked immunosorbent assay (ELISA) or related assay, in which varying amounts of antibody are titrated on a surface with bound antigen and the amount of bound antibody-antigen complex is measured using a secondary antibody with a fluorescent reporter. ELISA measurements do not provide any information about antibody-antigen binding kinetics. However, there are numerous applications in which knowledge of antibody-antigen binding kinetics may be useful for the selection of research-grade or therapeutic mAbs. For instance, antibodies with high on-rate constants ($>10^6$ $M^{-1}s^{-1}$) may be particularly useful for diagnostics and bio-sensing, as well as for viral neutralization.[100,101] Conversely, therapeutic antibodies that bind their target antigens with off-rate constants less than 10^{-4} s^{-1} (i.e. half-lives of hours to days) could, in principle, be administered in lower dosages, reducing the cost and side-effects of these therapies.[11,102]

A number of detection techniques exist to measure antibody-antigen binding kinetics, including surface plasmon resonance (SPR) spectroscopy, fluorescence polarization, ellipsometry, quartz crystal microbalance (QCM) sensing, and interferometry.[103–108] SPR spectroscopy, the most widely used of these techniques, facilitates real-time, label-free detection of antigen binding to surface-immobilized antibodies by detecting refractive index changes at the binding surface. SPR arrays have previously been used to screen antibodies produced by phage display and rabbit hybridoma.[109,110] However, since refractive index changes are proportional to the mass bound to the sensor surface, SPR spectroscopic measurements are poorly suited for the detection of low molecular weight molecules (<200 Da), as well as low

abundance samples (<200 pg) such as antibodies secreted by single cells.[111] Back-scattering interferometry (BSI) is an alternative, label-free technique capable of measuring binding of low molecular weight molecules and has lower detection limits than SPR spectroscopy.[106] However, as a solution-phase method, BSI does not enable direct measurement of dissociation kinetics, cannot be easily extended to make multiplexed kinetic measurements of multiple antibody-antigen interactions, and is limited in its ability to measure binding kinetics in complex mixtures. Moreover, in both BSI and SPR spectroscopy, measurement sensitivity is affected by temperature fluctuations and bulk refractive index shifts during buffer exchange. More importantly, neither these nor other currently available methods allow for measurement of antibody-antigen binding kinetics from very low abundance samples. To address this need, a microfluidic fluorescence bead assay was developed to enable screening of antibody-antigen association and dissociation kinetics in order to characterize and select antibodies secreted by single cells.

2.3 Materials and Methods

2.3.1 Microfluidic Device Fabrication and Control

All microfluidic devices were fabricated using multilayer soft lithography.[86,87] Devices were composed of two layers of poly(dimethylsiloxane) (PDMS) elastomer (GE RTV 615) bonded to No 1.5 glass coverslips (Ted Pella, Inc.). The microfluidic device was fabricated with a push-down geometry, in which the flow channels were bonded by oxygen plasma directly to the cover-glass, while the control channels were situated above the flow channels, separated by a thin (~10 μm), deflectable

PDMS membrane. Thus, reagent samples were brought in direct contact with the cover-glass, allowing for imaging of the device with a 100X high numerical aperture (N.A. 1.30) oil-immersion objective (working distance ~ 200 μm). The devices were designed in AutoCAD software (Autodesk) and printed on high-resolution (20,000 dpi) transparency masks (CAD/Art Services). Master molds were fabricated in photoresist on silicon wafers (Silicon Quest) by standard optical lithography. The control master molds were fabricated out of 20-25 μm high SU-8 2025 photoresist (Microchem). The flow master molds were fabricated with 12 μm rounded SPR220-7.0 photoresist channels (Rohm and Haas) and 6μm SU-8 5 photoresist (Microchem) channels with rectangular cross-section. Microfluidic valves were actuated at 30 psi pressure that was controlled using off-chip solenoid valves (Fluidigm Corp) controlled using LabView 7.1 software and a NI-6533 DAQ card (National Instruments). Compressed air (3-4 psi) was used to push reagent solutions into and through the device.

2.3.2 Reagent Preparation

Protein A-coated 5.5 μm diameter polystyrene beads (Bangs labs) were incubated with a 1 mg/mL solution of Rabbit anti-mouse polyclonal antibodies (pAbs) purchased from Jackson Immunoresearch and used without further purification. All antibody and antigen solutions were prepared in PBS/BSA/Tween solution consisting of 1X PBS, pH 7.4 (Gibco) with 10 mg/mL BSA (Sigma) and 0.5% Polyoxyethylene (20) sorbitan monolaurate (similar to Tween-20, EMD Biosciences). Lysozyme from chicken egg white (HEL) was purchased from Sigma,

and the D1.3 and HyHEL-5 mouse monoclonal antibodies (mAbs) to lysozyme were generously provided by Dr. Richard Willson (University of Houston). The anti-GFP mouse mAb (LGB-1) was purchased from Abcam. Fluorescent protein conjugates were prepared using Dylight488 and Dylight633 NHS esters (Pierce) and were purified using Slide-A-Lyzer™ dialysis cassettes (Pierce). The concentration of fluorescent conjugates was measured by spectrophotometry (Nanodrop). In order to minimize protein denaturation, fluorescent HEL conjugates were labeled at a dye-to-protein ratio (D/P) of less than 1, whereas the D1.3-Dylight488 conjugate was prepared at a D/P of ~5.

2.3.3 Fluorescence Microscopy

The microfluidic devices were imaged on a Nikon TE200 Eclipse inverted epifluorescence microscope equipped with green (470/40 nm excitation, 535/30 nm emission) and red (600/60 nm excitation, 655 nm long-pass emission) fluorescence filter cubes (Chroma Technology). Fluorescence images were taken using a 16-bit, cooled CCD camera (Apogee Alta U2000) and a 100X oil immersion objective (N.A. 1.30, Nikon Plan Fluor). The fluorescence sensitivity was adjusted by binning pixels on the CCD detection camera and by modulating the fluorescence exposure times (20 ms - 1 s) with a computer-controlled mechanical shutter (Ludl Electronic Products). During antibody-antigen binding experiments, the image focal position was held constant on the center of the beads by minimizing the bead diffraction pattern observed under bright-field illumination.

2.3.4 Cell Culture

Mouse D1.3 hybridoma cells were grown in 6 mL petri dishes (Nunc) using RPMI 1640 medium (Gibco) with 10% fetal calf serum (FCS) in a cell culture incubator (37°C, 5% CO_2). Cells were passaged approximately once a week by serial dilutions (5-fold) in fresh medium. Prior to loading into the device, cells were washed by centrifugation at 1500 rpm and re-suspended in 1X PBS, pH 7.4 (Gibco) in order to remove free antibodies in the cell medium. Cell concentration was quantified using a haemocytometer and brightfield microscope.

2.3.5 Assay Operation

The microfluidic device consisted of six flow input channels, each used for loading a distinct reagent and controlled with an independent control valve, which join into a common flow output channel (Figure 2.2 A and B). The output channel was partitioned into discrete ~200 pL chambers by actuating a set of microfluidic "sieve" valves which, when actuated, acted as filters to immobilize large particles (> 1μm) while still allowing fluid exchange.[83] The microfluidic device consisted of low fluidic dead volume upstream of the bead capture area (<4 nL), such that this volume was displaced in approximately 1 second based on the typical flow rates used in this study (~10 μL/hr).

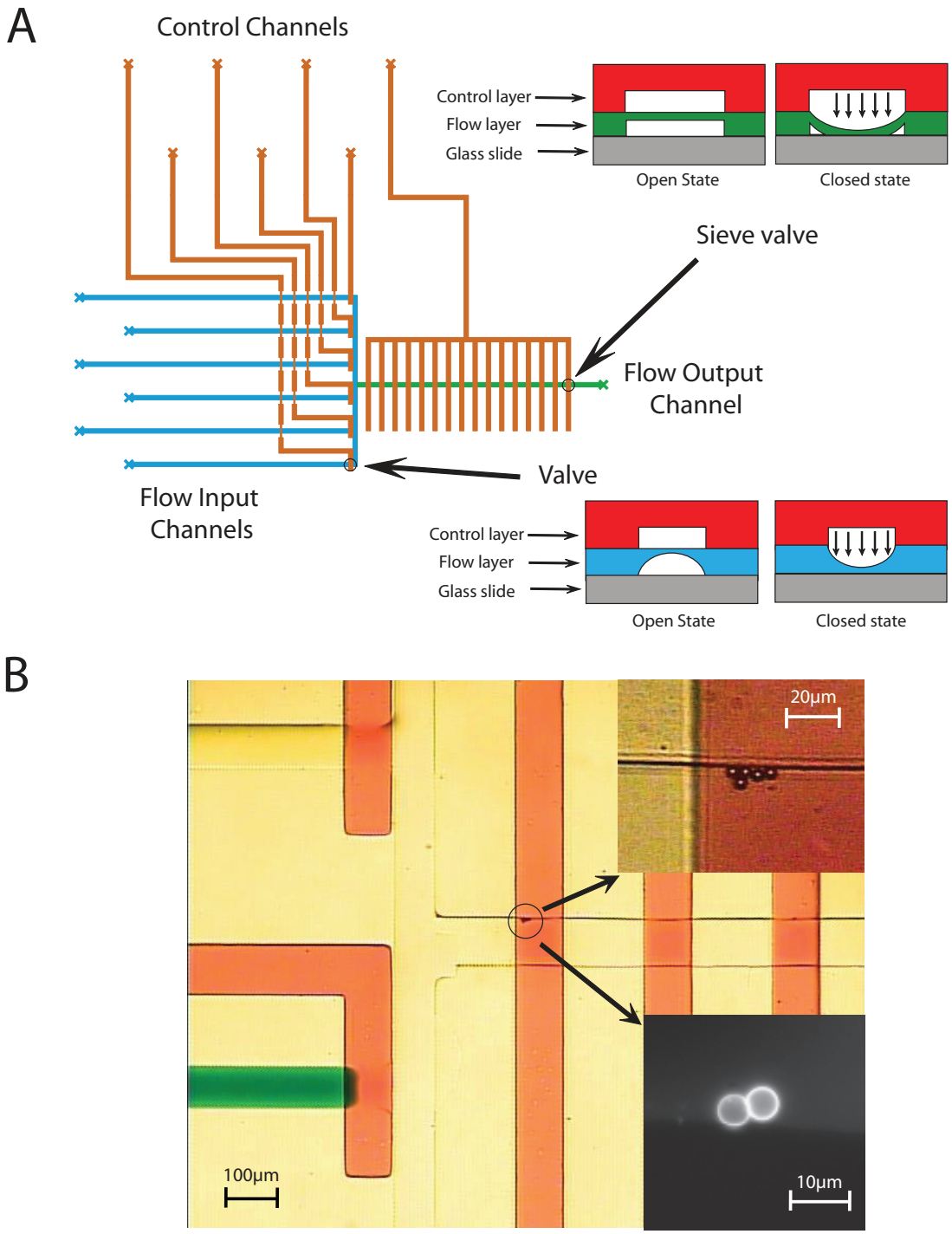

Figure 2.2 Microfluidic fluorescence bead measurements of antibody-antigen binding kinetics. (A) Device schematic showing control channels (orange) for selecting six reagent inlets (blue) and actuating sieve valves on the reagent outlet channel (green). (B) Microscope image of device with food coloring to visualize distinct reagent inlets (yellow and green) and control channels (red). (Insets) Brightfield (top) and fluorescence (bottom) images of beads trapped using sieve valves at 20X and 100X magnification, respectively. [continued on next page]

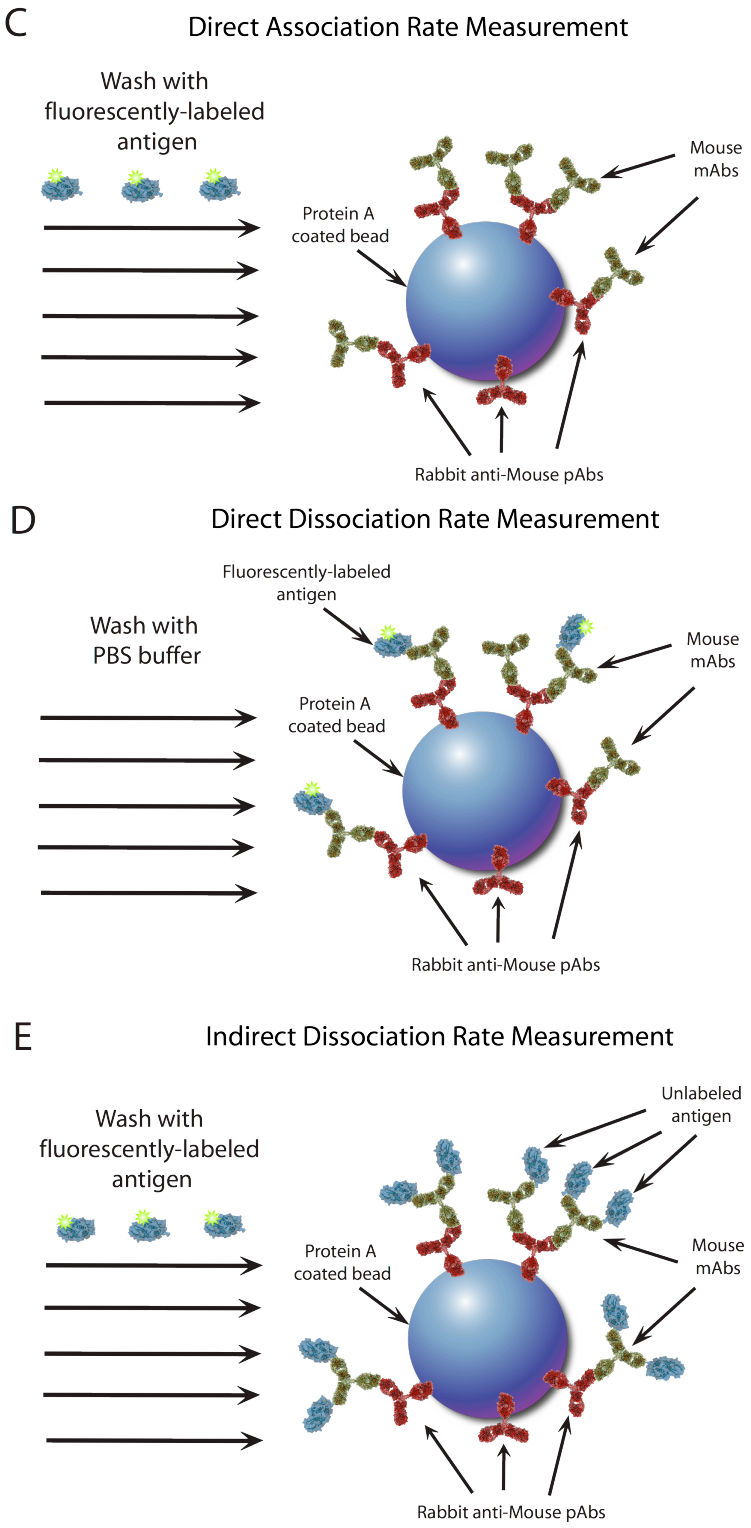

Figure 2.2 [continued from previous page] (C-E) Schematics of bead assay for direct measurement of association and dissociation kinetics of immobilized mAbs and fluorescently labeled antigen (C and D, respectively), and indirect measurement of dissociation kinetics of immobilized mAbs and unlabeled antigen molecules (E). Adapted with permission from Singhal et al.[112] (American Chemical Society, 2010).

At the start of the experiment, the flow output channel was flushed with a PBS/BSA/Tween solution from the top and bottom flow inlets in order to pre-coat the hydrophobic channel walls to reduce nonspecific binding. Next, a solution containing Protein A beads coated with Rabbit anti-mouse pAb (d = 5.5 μm, ~10^6-10^7 beads/mL) was loaded through the device to the fluidic outlet. The microfluidic sieve valves were then actuated to immobilize the beads against the traps, and the fluidic outlet channel was again washed for 1 min with PBS/BSA/Tween solution to remove any free rabbit pAb in solution. The beads were then incubated for ~1-10 min with a 1-100 μg/mL solution containing the mouse mAb of interest. Again, free mouse antibody was washed out of the fluidic output channel using PBS/BSA/Tween solution for 1 min. To measure the rate of antibody-antigen association, the beads were flushed with a solution of fluorescently labeled antigen and fluorescently imaged at defined time intervals (Figure 1C). When chemical equilibrium between the antibody and antigen was reached, as detected by a plateau in bead fluorescence, the beads were flushed with PBS buffer and imaged to measure the rate of antibody-antigen dissociation. The process was repeated with multiple solutions of varying concentrations of fluorescently labeled antigen (10 pM – 500 nM), each loaded onto the microfluidic device from a separate fluidic inlet. At the concentrations used in this study, we did not detect any increase in fluorescence intensity relative to the bead autofluorescence when fluorescent antigen was flushed over control beads without antigen-specific mouse mAbs.

A second version of microfluidic bead assay was implemented to indirectly measure dissociation kinetics between antibodies and unlabeled antigen molecules

by displacement with fluorescently labeled antigen (Figure 1D). In this assay, the antibody of interest was captured on Rabbit anti-mouse pAb-coated Protein A beads, and the beads were subsequently washed with unlabeled antigen at high concentration (>1 μM) to saturate all antibody binding sites. Beads were then washed with a solution of fluorescently labeled antigen (10 nM) while imaging at defined time intervals. Dissociation of the unlabeled antigen was then inferred by accumulated fluorescence on the beads.

In order to measure the antigen binding kinetics from antibodies secreted by single cells, a solution of RPMI-1640 medium containing freshly washed hybridoma cells (~10^5 cells/mL) was loaded into the device. The control valve was momentarily opened to allow for a single hybridoma cell to be trapped by the first sieve valve in the fluidic outlet channel. Subsequently, a solution of RPMI-1640 medium containing Protein A beads coated with Rabbit anti-mouse pAb (d = 5.5 μm, ~10^6-10^7 beads/mL) was loaded into the device, such that 1-2 beads were brought into close proximity with the hybridoma cell. The hybridoma cell was then allowed to incubate next to the beads for 1 hour, and subsequently washed for 1 min with PBS/BSA/Tween buffer to wash out any free antibody in solution and halt antibody secretion from the cell. Kinetic measurements of antibody-antigen binding were then performed while flushing the beads with cycles of increasing fluorescent antigen solution (~5-50 nM) and PBS/BSA/Tween buffer.

2.3.6 Data Analysis

Fluorescent images were analyzed using MaximDL 4 imaging software. Fluorescent intensities were measured by selecting line profiles through the beads and recording the maximum intensity at the bead surface (Appendix A). Analysis of multiple beads in a single field-of-view during antibody-antigen binding experiments confirmed that measured binding kinetics were insensitive to systematic variations caused by non-uniform binding of antigen to the bead surface, differences in bead-to-bead binding capacity, variation in position in the flow channel and non-uniform illumination over the field of view (Figure 2.3). Error in all measurements was estimated to be less than 10% of the fluorescence intensity. The measured fluorescence bead intensities were assumed to be proportional to the concentration of antibody-antigen complex ([*AbAg*]) and were fit to the following standard first-order mass-action equations (Section 2.1.1) using nonlinear least squares minimization:

$$F(t) = (F_{max} - F_0)\frac{[Ag]_0}{[Ag]_0+K_d}\left(1 - e^{-(k_{on}[Ag]_0+k_{off})t}\right) + F_0 \qquad (2.7a)$$

$$F(t) = (F_{max} - F_0)\frac{[Ag]_0}{[Ag]_0+K_d}\left(e^{-k_{off}t}\right) + F_0 \qquad (2.7b)$$

$$F(t) = (F_{max} - F_0)\frac{[Ag]_0}{[Ag]_0+K_d} + F_0 \qquad (2.7c),$$

in which $F(t)$ represents the measured bead fluorescence at time t, F_0 and F_{max} represent the background and maximum bead fluorescence, respectively, $[Ag]_0$ represents the solution concentration of antigen (in M), K_d is the equilibrium dissociation constant (in M), and k_{on} and k_{off} represent the intrinsic association and

dissociation rate constants, in units of $M^{-1}s^{-1}$ and s^{-1}, respectively. In addition to the binding rate constants (K_d, k_{on} and k_{off}), F_0 and F_{max} were constants fitted by the model. In agreement with this model, all measured antibody-antigen interactions obeyed simple bimolecular association and first-order dissociation kinetics. All reported errors represent the calculated standard deviation from multiple replicate measurements.

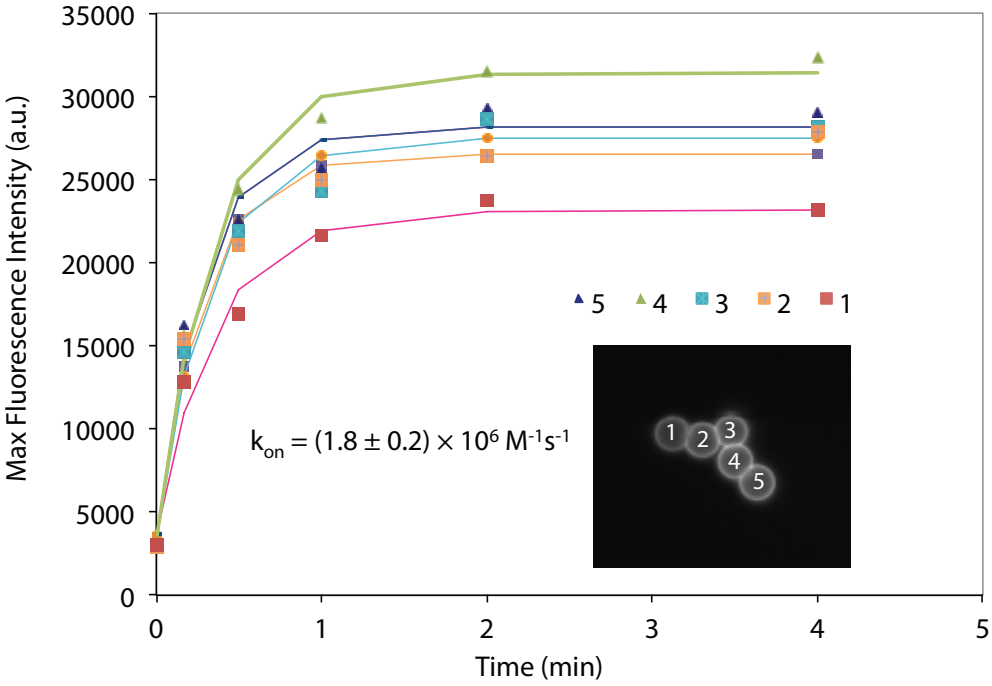

Figure 2.3 Antibody-antigen association kinetics measured from multiple beads in a single field-of-view (FOV). In this experiment, fluorescently labeled hen egg lysozyme is binding bead-immobilized anti-HEL D1.3 mouse mAb. Reported error represents the calculated standard deviation from multiple replicate measurements. Dissociation kinetics measured on multiple beads in a single FOV were also consistent to within 20% (data not shown).

2.4 Results

Measurements of antibody-antigen binding kinetics using the microfluidic fluorescence bead assay were validated using the model antigen hen egg lysozyme

(HEL). HEL is a 14.7 kDa protein of known structure that can hydrolyze polysaccharides, such as those present in bacterial cell walls.[113] HEL is frequently used as a model antigen in immunological research because it is inexpensive, very soluble in water (~20 mg/mL), and highly immunogenic in mice. The latter fact has enabled the production of dozens of hybridoma cell-lines secreting monoclonal antibodies that bind HEL with a wide range of affinities (10 μM > K_d > 10 pM).[114] Of these, two particular mAbs, D1.3 and HyHEL-5, have significantly different binding kinetics and were, thus, selected for testing and validation of the microfluidic fluorescence bead assay (Figure 2.4A and 2.4B and Table 2.2).

Association and dissociation rate constants measured in device for the D1.3/HEL interaction were 1.87 ± 0.48 × 10^6 $M^{-1}s^{-1}$ and 2.10 ± 0.25 × 10^{-3} s^{-1}, respectively, and were consistent with values of 1.0 - 2.0 × 10^6 $M^{-1}s^{-1}$ and 1.15 - 3.04 × 10^{-3} s^{-1} previously measured using surface plasmon resonance (SPR) spectroscopy, stopped-flow fluorescence quenching, and competitive ELISA.[115,116] A ten-fold smaller association rate constant previously reported for the D1.3/HEL interaction (1.67 × 10^5 $M^{-1}s^{-1}$) may be attributed to differences between the full D1.3 mAb used in the microfluidic bead-based measurements and the recombinant single-chain antibody fragment used by Bedouelle and coworkers.[117]

A variation of the microfluidic bead assay using fluorescently-labeled HEL as a competitive antigen was used to indirectly measure the dissociation rate constant between D1.3 mAb and unlabeled HEL (Figure 2.2E and 2.4D). In this assay, D1.3 mAbs immobilized on beads were first saturated with unlabeled HEL and subsequently washed with fluorescently-labeled HEL. Measurements of the

accumulated bead fluorescence faithfully reflected the D1.3/HEL dissociation kinetics provided the labeled HEL was at a sufficiently high concentration to ensure that dissociation was rate-limiting (i.e. $k_{on}[Ag] > k_{off}$, or, equivalently, $[Ag] > K_d$). Using this method, the dissociation rate constant of D1.3 and unlabeled HEL was measured to be $1.45 \pm 0.30 \times 10^{-3}$ s^{-1}, in close agreement with direct dissociation measurements between D1.3 and fluorescently-labeled HEL (Table 2.2).

Table 2.2 Antibody-antigen binding kinetics measured using the microfluidic fluorescence bead assay.
Reported error represents the calculated standard deviation of multiple replicate measurements. Data taken from Singhal et al.[112]

Antibody/Antigen pair	k_{on} ($M^{-1}s^{-1}$)	k_{off} (s^{-1})	$K_d = k_{off} / k_{on}$
D1.3 mAb/HEL-Dylight488	$(1.87 \pm 0.48)\times10^{6}$	$(2.10 \pm 0.25)\times10^{-3}$	1.20 ± 0.42nM
D1.3 mAb/HEL-Dylight633	$(1.27 \pm 0.22)\times10^{6}$	$(2.15 \pm 0.23)\times10^{-3}$	1.75 ± 0.46nM
HyHEL-5 mAb/HEL-Dylight488	$(5.75 \pm 0.71)\times10^{6}$	$(1.69 \pm 0.30)\times10^{-4}$	30.0 ± 7.4pM
LGB-1 mAb/EGFP	$(5.00 \pm 0.72)\times10^{4}$	$(5.15 \pm 0.89)\times10^{-3}$	106 ± 28nM

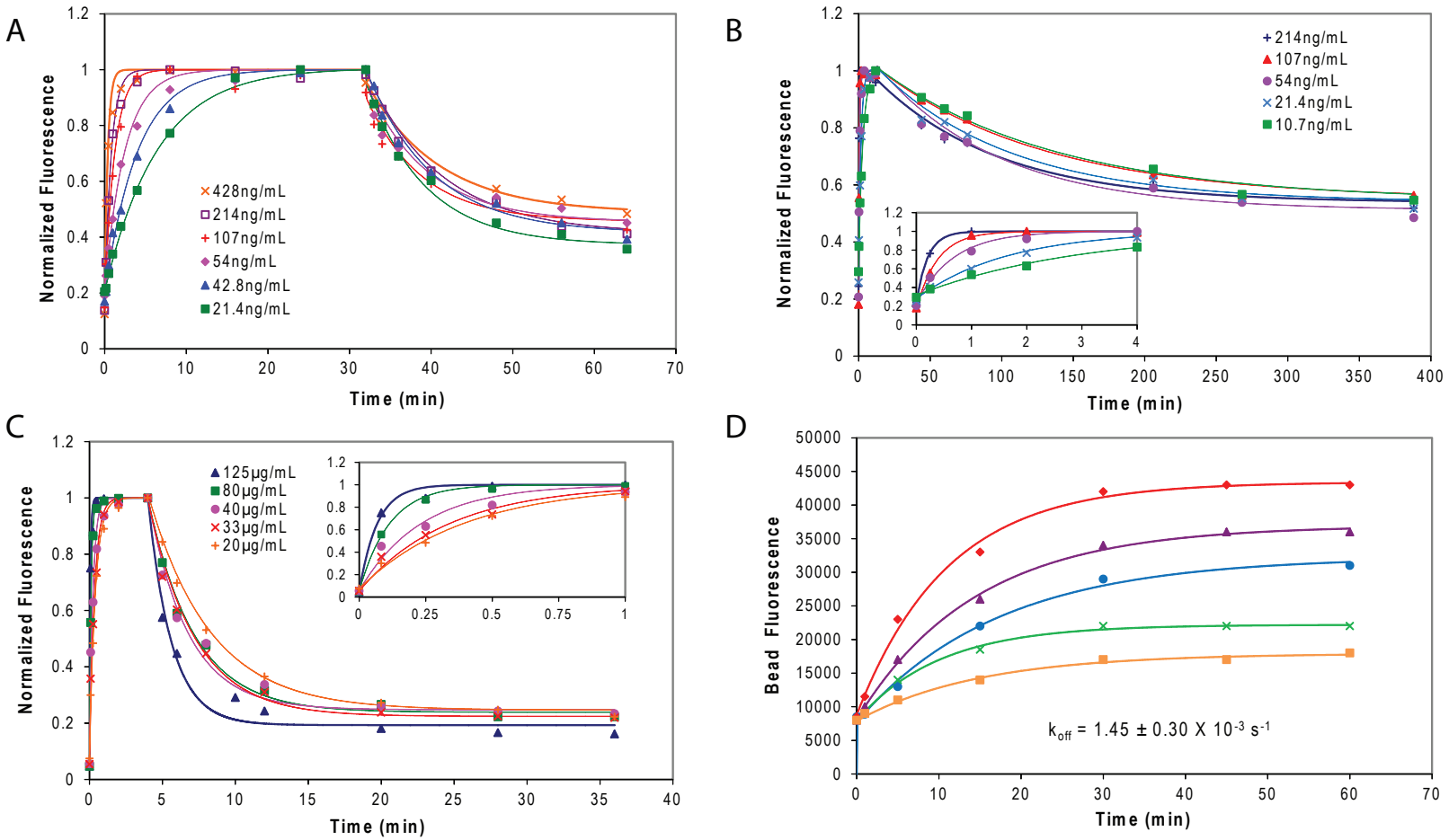

Figure 2.4 Microfluidic fluorescence bead measurements of antibody-antigen binding kinetics. Direct fluorescent measurements of association and dissociation kinetics of (A) D1.3 mAb and HEL-Dylight488 conjugate, (B) HyHEL-5 mAb and HEL-Dylight488 conjugate, (C) LGB-1 mAb and enhanced green fluorescent protein (EGFP). (D) Indirect measurement of dissociation kinetics of D1.3 mAb and HEL using HEL-Dylight488 conjugate. Solid lines represent experimental fits using mass-action equations (equations 2.7a-c). Reported error represents the calculated standard deviation of multiple replicate measurements. Adapted with permission from Singhal et al. (American Chemical Society, 2010).[112]

In comparison to the D1.3 mAb, HyHEL-5 binds HEL with a nearly four-fold larger association rate constant ($5.75 \pm 0.71 \times 10^6$ $M^{-1}s^{-1}$) and ten-fold smaller dissociation rate constant ($1.69 \pm 0.30 \times 10^{-4}$ s^{-1}) (Figure 2.4B). Thus, HyHEL-5 is found to bind HEL with a ~40-fold smaller equilibrium dissociation constant than D1.3 (30 pM vs. 1.2 nM) (Table 2.2). Previous measurements of the HyHEL-5/HEL interaction using particle-counting fluorescence immunoassay (PCFIA) and stopped-flow fluorescence polarization produced a similar equilibrium dissociation constant (25 pM) and dissociation rate constant (2.2×10^{-4} s^{-1}), but a three- to five-fold larger association rate constant ($1.5–3.3\times10^7$ $M^{-1}s^{-1}$).[105] Immobilization of the mAb in the microfluidic bead assay may result in slower association kinetics when compared with solution-phase fluorescence polarization measurements. HyHEL-5 mAb and HEL are known to bind with near diffusion-limited kinetics, a regime in which the association rate constant scales linearly with the effective diffusion coefficient (equation 2.6, where $D \cong D_{mAb} + D_{HEL}$).[95,105] Since the translational diffusion coefficient of HEL is much larger than that of the HyHEL-5 mAb ($D_{HEL} \geq 3\times D_{mAb}$), immobilization of the mAb would reduce the apparent association rate constant by less than 25%.[118,119] Similarly, mAb immobilization would reduce the effective rotational diffusion by less than 10%, based on the rotational diffusion coefficients of HEL and the three- to five-fold larger HyHEL-5 mAb molecule ($D_R \propto 1/R^3$ where R = radius of the molecule).[118,120] Although mAb immobilization does not have an appreciable effect on effective diffusion of the HyHEL-5/HEL pair, it is possible that binding of HEL to bead-immobilized HyHEL-5 mAb results in steric hindrance of adjacent mAb molecules, resulting in slower association kinetics

measured using the bead assay when compared to solution-phase fluorescence polarization measurements.

To demonstrate that the microfluidic bead assay can be used to measure binding kinetics of a previously uncharacterized antibody, binding kinetics were measured for a commercially available mouse monoclonal antibody (LGB-1, Abcam) to enhanced green fluorescent protein (eGFP) (Figure 2.4C). In this instance, native eGFP fluorescence was measured, eliminating the need for an exogenous fluorescent label. The measured association and dissociation rate constants for the LGB-1/eGFP interaction were $5.00 \pm 0.72 \times 10^{4}$ $M^{-1}s^{-1}$ and $5.15 \pm 0.89 \times 10^{-3}$ s^{-1}, respectively (Table 2.2).

Collectively, the measured binding kinetics of the anti-lysozyme and anti-eGFP mAbs span nearly four orders of magnitude in equilibrium dissociation constants (30 pM to 0.1 μM), with association rate constants varying from 5×10^{4}-10^{6} $M^{-1}s^{-1}$ and dissociation rate constants ranging from 10^{-3}-10^{-4} s^{-1} (Table 2.2). In principle, the microfluidic bead assay can be used to characterize stronger antibody-antigen interactions than the HyHEL-5/HEL interaction; however, measurements of binding interactions with dissociation rate constants lower than $10^{-4}s^{-1}$ must be taken over several days or weeks. On the other hand, the bead-based assay can be readily used to measure binding interactions weaker than the LGB-1/eGFP interaction. By optimizing the fluidics for rapid solution exchange (<1 s), the practical upper limit in measurable rate constants is approximately 10^{-1} s^{-1}. Thus, the microfluidic bead-based assay should enable characterization of antibody-

antigen interactions that span greater than five orders of magnitude in kinetic rate constants and at least seven orders of magnitude in equilibrium binding affinities.

2.4.1 Microfluidic Fluorescence Bead Measurements Reflect Intrinsic Antibody-Antigen Binding Kinetics.

A series of experiments were performed in order to verify that bead-based fluorescence measurements reflected intrinsic antibody-antigen binding kinetics, and were unaffected by artifacts arising from fluorescent labeling of the antigen, antibody immobilization, or mass transport effects.

Fluorescent labeling of HEL did not alter the intrinsic D1.3/HEL binding kinetics, as indicated by the agreement between microfluidic bead measurements using fluorescently labeled HEL and previously reported measurements using SPR spectroscopy with unlabeled HEL.[121] In addition, no differences were observed in bead-based kinetic measurements of the D1.3 mAb binding to HEL labeled with two different fluorophores, Dylight488 and Dylight633 (Table 2.2). Photobleaching of fluorophores did not affect the measured binding kinetics, as was confirmed by measuring the photobleaching rates of the fluorescent dyes used in this study (Dylight488, Dylight633, and eGFP) and selecting fluorescence exposure times (e.g. 100ms) that resulted in less than 5% reduction in bead fluorescence (Figure 2.5A). Indeed, measured binding kinetics were consistent over a large range of fluorescence exposure times (20 – 500 ms), whereas exposure times of greater than 1 s resulted in substantial photobleaching and an artificial increase in measured

association and dissociation binding kinetics when compared to intrinsic kinetics (Figure 2.5B).

Association and dissociation rate measurements for the D1.3/HEL interaction were also unaffected by the antibody bead immobilization chemistry employed, as demonstrated by measurements using both silica and polystyrene beads coated with either rabbit or goat anti-mouse polyclonal antibody (Figure 2.6). We further verified that multivalent binding between the rabbit anti-mouse pAbs and fluorescently-labeled D1.3 mAb resulted in no detectable dissociation over the course of 3 days, which would otherwise artificially accelerate the measured antibody-antigen binding kinetics (Figure 2.7). Indeed, the nearly irreversible bond between rabbit pAb and the mouse mAbs was critical for this bead assay, as attempts to measure D1.3/HEL binding kinetics using Protein A beads without Rabbit anti-mouse pAbs were unsuccessful due to rapid dissociation (and low affinity) of protein A / mouse mAb complexes (data not shown).

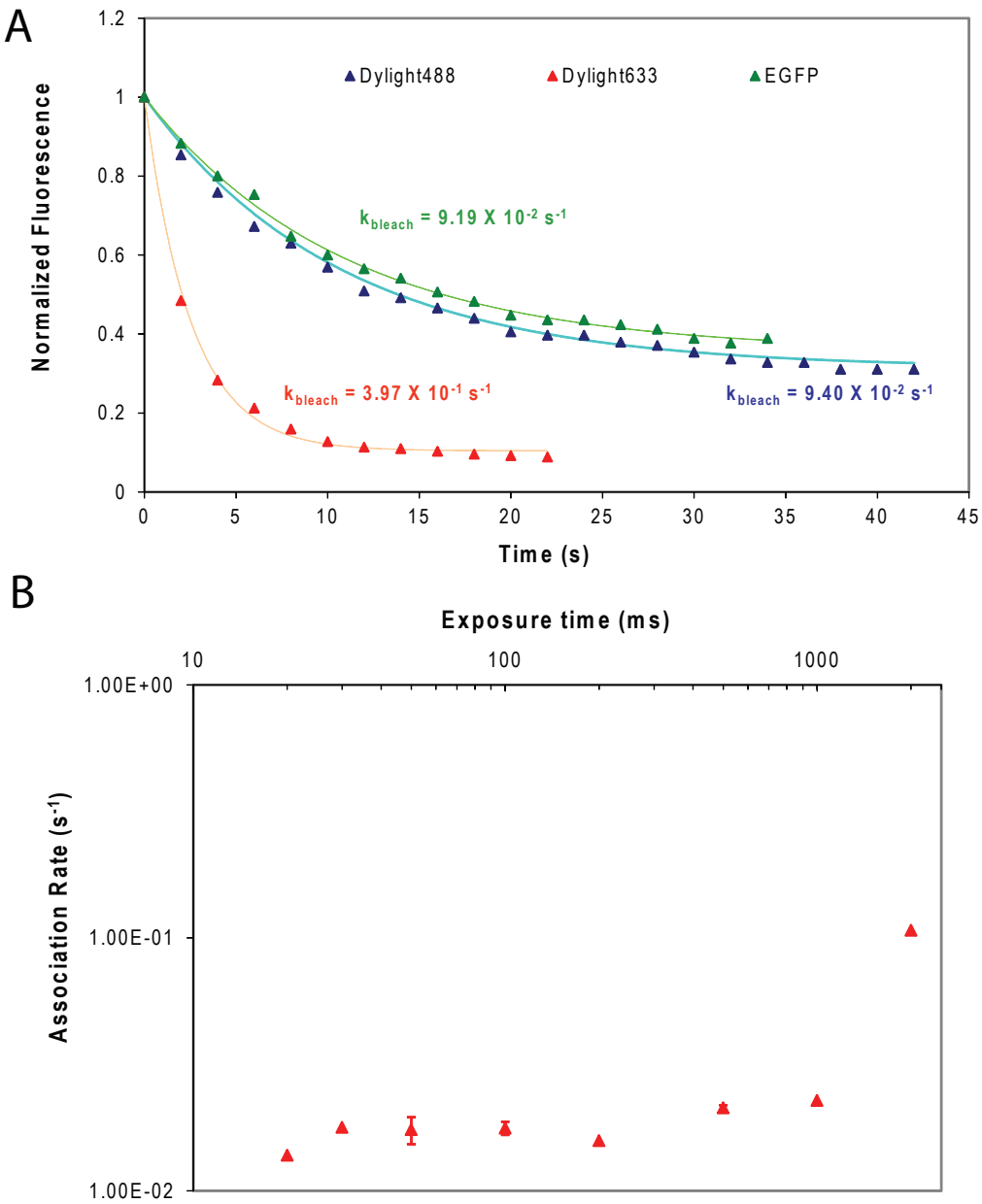

Figure 2.5 Effect of fluorophore stability on measured antibody-antigen binding kinetics. (A) Photobleaching rates of fluorescent dye molecules under 100W Hg lamp illumination using 100X oil-immersion objective (NA 1.30). (B) Effect of fluorescent exposure times on measured association kinetics of D1.3 mAb and HEL-Dylight488. Reported error represents the calculated standard deviation of multiple replicate measurements. Values measured only once are reported without error bars. Adapted with permission from Singhal et al. (American Chemical Society, 2010).[112]

Several experiments were conducted to verify that mass transport, including diffusion limitation, did not affect microfluidic bead measurements of antibody-antigen binding kinetics. In the diffusion-limited regime, antibodies adjacent on the bead surface compete for fluorescent antigen, thus reducing the apparent association rate constant. Similarly, antigen that dissociates and then rebinds to adjacent antibodies would reduce the apparent dissociation rate.[25,21] However, nearly identical association and dissociation kinetics were measured for the D1.3-HEL interaction by varying the amount of bead-immobilized D1.3 mAb over two orders of magnitude (Figure 2.10B). Moreover, dissociation kinetics of the D1.3 antibody and fluorescently labeled HEL were similar both in the presence and absence of a high concentration (~2mg/mL) of competitive unlabeled HEL antigen (Figure 2.8). Thus, no diffusion limitation was observed in the form of competition between antibodies adjacent to one another on the beads. Association and dissociation rate constants of the D1.3-HEL interaction remained constant over a range of flow rates from 3-14 μL/hr, suggesting no other effects of mass transport on the measured kinetics (Figure 2.9).

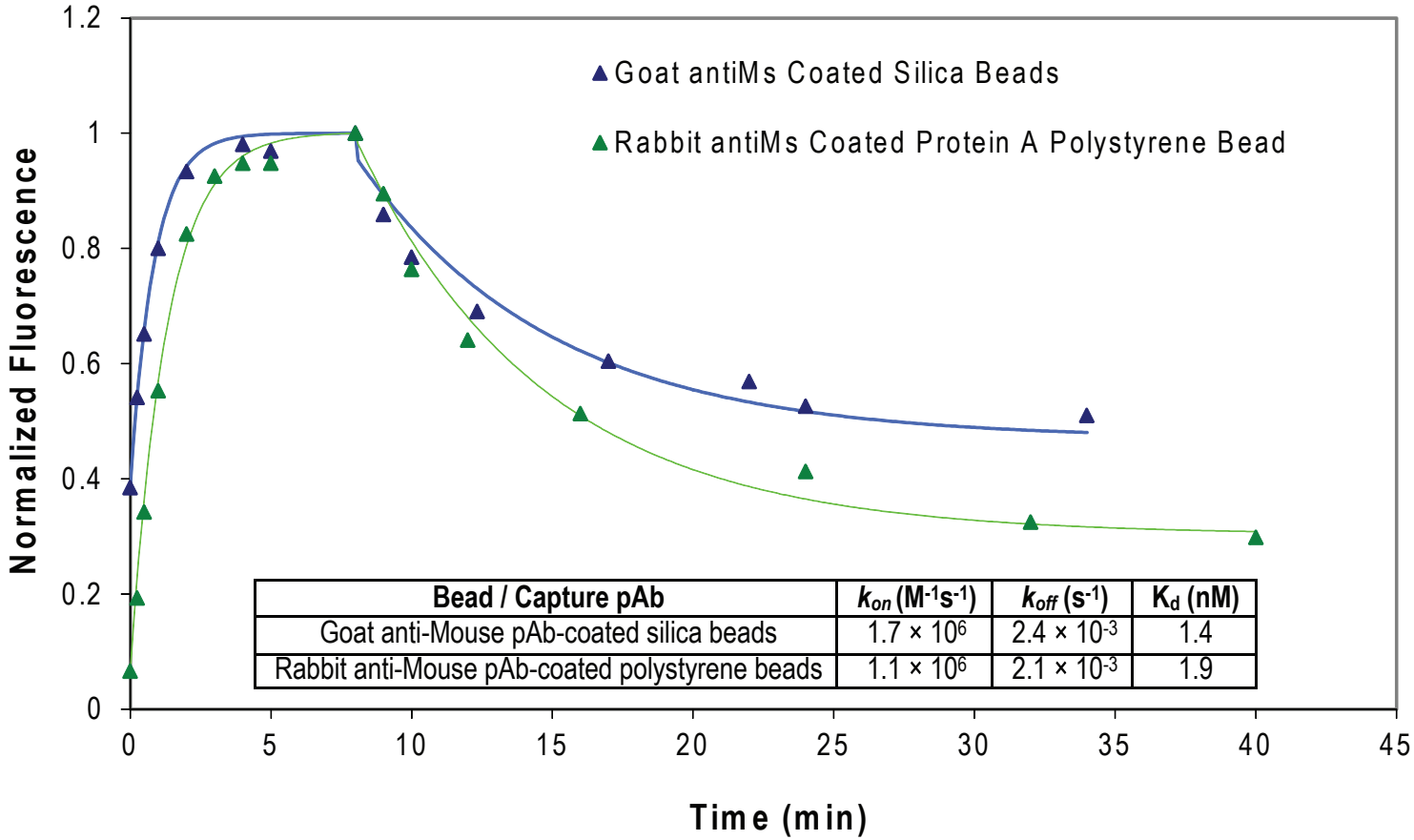

Bead / Capture pAb	k_{on} ($M^{-1}s^{-1}$)	k_{off} (s^{-1})	K_d (nM)
Goat anti-Mouse pAb-coated silica beads	1.7×10^6	2.4×10^{-3}	1.4
Rabbit anti-Mouse pAb-coated polystyrene beads	1.1×10^6	2.1×10^{-3}	1.9

Figure 2.6 Effect of different bead composition and capture antibodies on measured antibody-antigen binding kinetics. Measured binding kinetics and affinities from both conditions were consistent within experimental error (see Table 2.1). Adapted with permission from Singhal et al.[112] (American Chemical Society, 2010).[112]

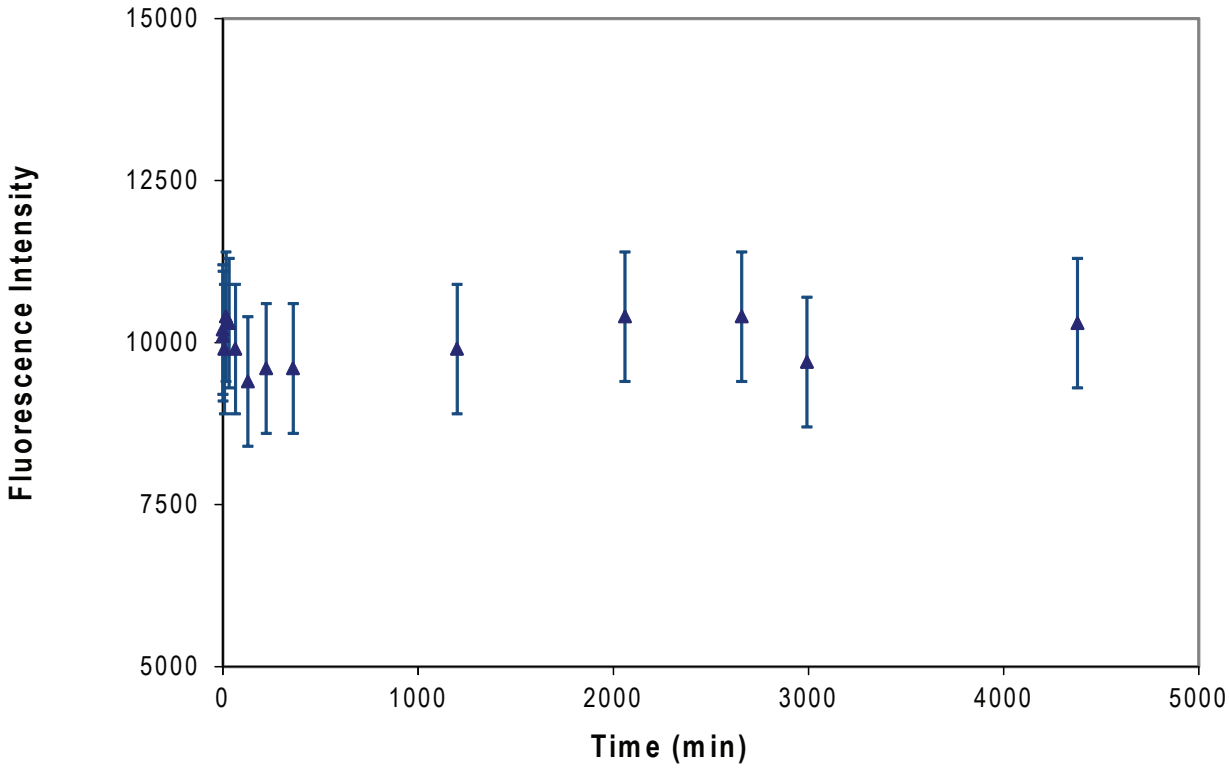

Figure 2.7 **Measured dissociation kinetics of mouse mAb from antibody capture beads. No dissociation of D1.3 mAb-Dylight488 conjugate from Rabbit anti-Ms pAb coated beads was observed over 3 days. Reported error represents the calculated standard deviation of multiple replicate measurements. Adapted with permission from Singhal et al.[112] (American Chemical Society, 2010).[112]**

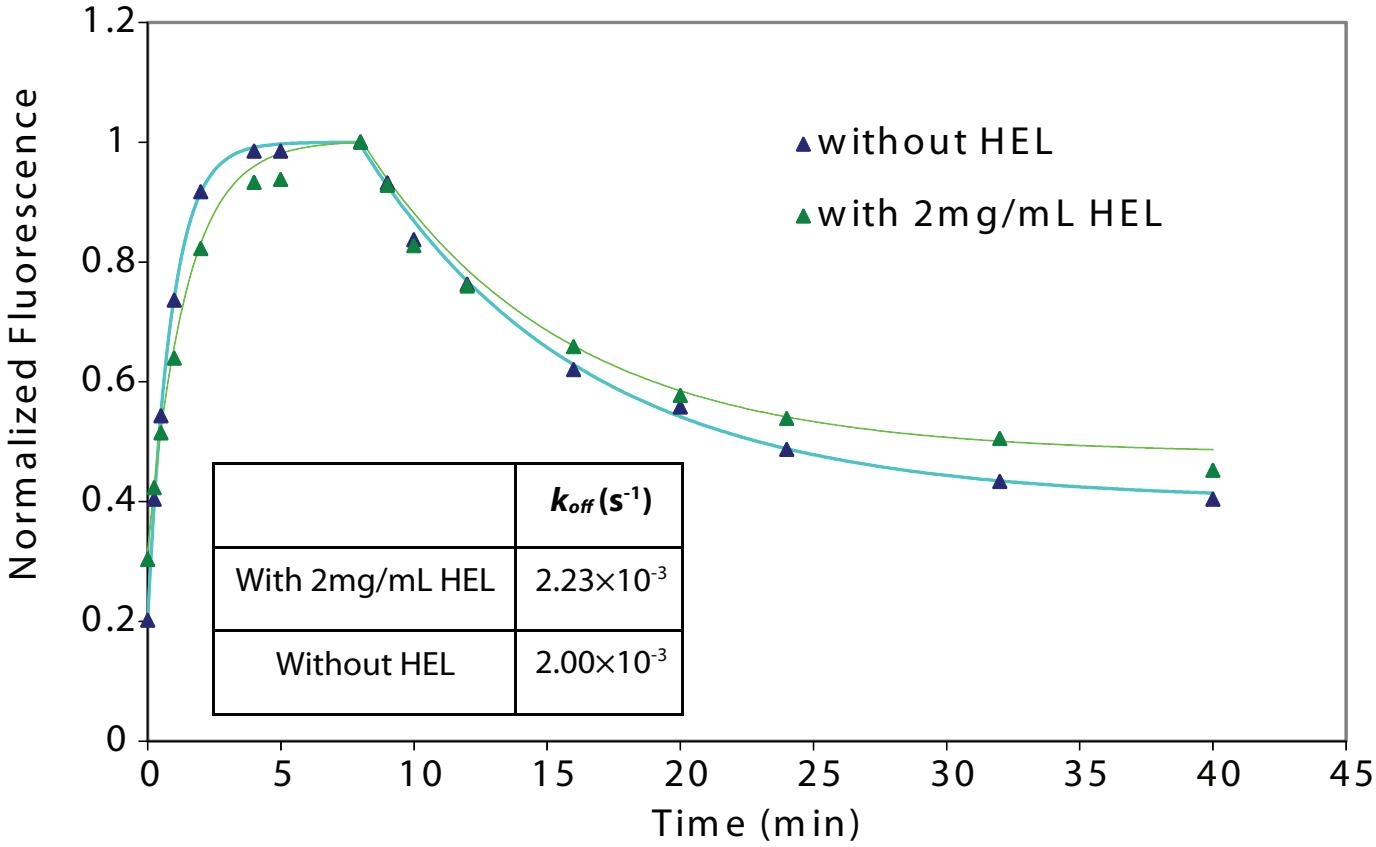

Figure 2.8 Effect of antigen re-binding on measured antibody-antigen dissociation kinetics. Dissociation kinetics of D1.3 mAb and HEL-Dylight488 conjugate were similar both in the presence and absence of a large concentration of competitive antigen (2 mg/mL HEL). Measured binding kinetics from both conditions were consistent within experimental error (see Table 2.1). Adapted with permission from Singhal et al.[112] (American Chemical Society, 2010).[112]

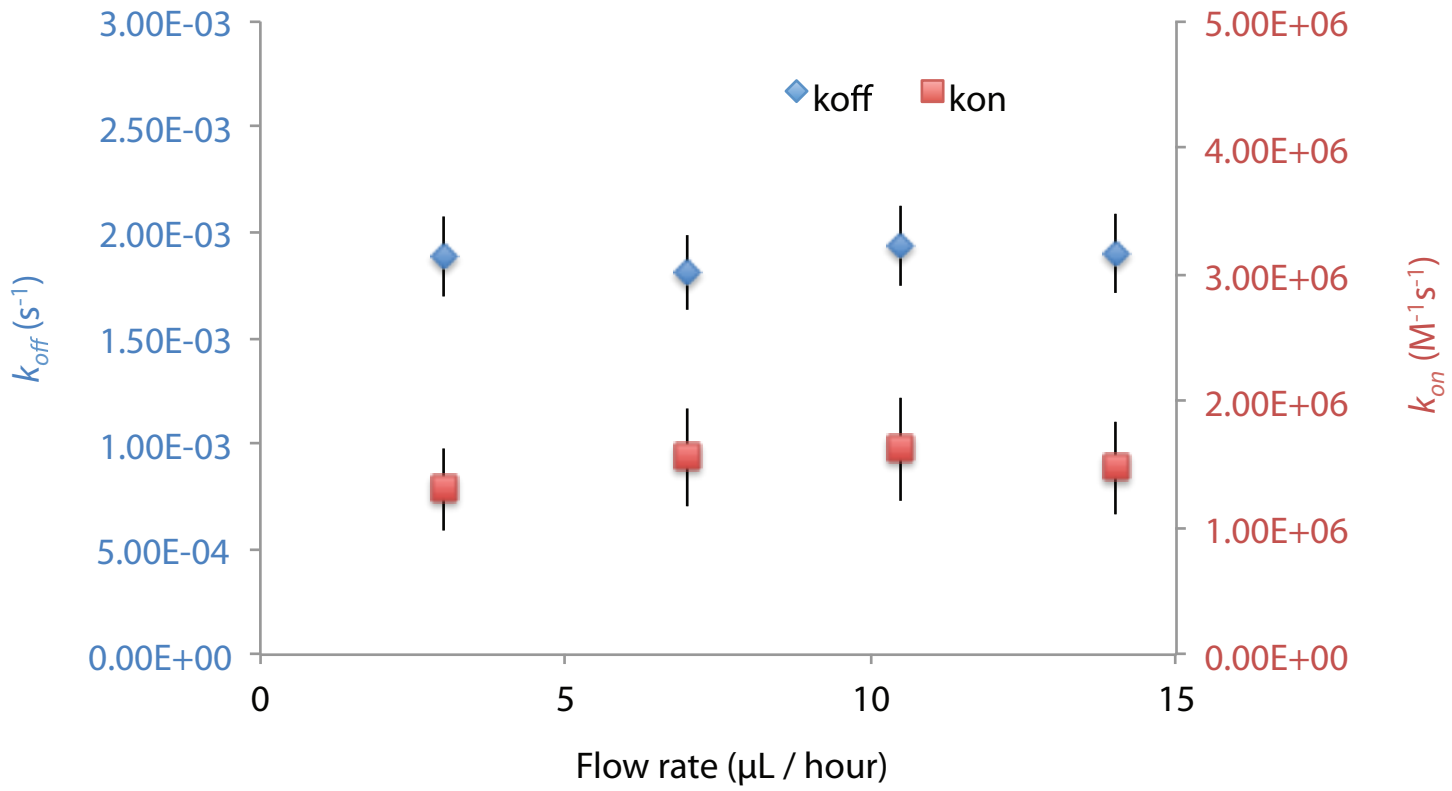

Figure 2.9 Effect of mass transport on measured antibody-antigen binding kinetics. Association and dissociation kinetics of D1.3 mAb and HEL-Dylight488 conjugate were similar over a range of flow rates (~3-14 µL/hr). Fixed error bars represent the calculated ratio of the standard deviation to mean value of measured D1.3/HEL kinetic rate constants reported in Table 2.1 (25% and 10% for k_{on} and k_{off}, respectively). Adapted with permission from Singhal et al.[112] (American Chemical Society, 2010).[112]

2.4.2 Microfluidic Fluorescence Bead Measurements Exhibit Low Detection Limits and Minimal Sample Consumption.

In order to quantify the limit of detection (LOD) and minimal sample consumption required for the microfluidic bead assay, measurements of antibody-antigen binding kinetics were made using varying amounts of bead-immobilized mAb. Using the measured kinetic on-rate constant for fluorescently-labeled D1.3 mAb binding to Rabbit anti-mouse pAb coated Protein A beads (k_{on} = 1.10 ± 0.11 × 10^6 $M^{-1}s^{-1}$), the amount of bead-immobilized D1.3 mAb was varied over two orders of magnitude by modulating the loading time of mAb on the bead (Figure 2.10). The limit of detection (LOD) was determined to be 2% of the bead antibody-binding capacity by setting a threshold three standard deviations larger than the mean equilibrium bead fluorescence from replicate measurements of control beads without D1.3 mAb (i.e. 0% immobilization).

From both the manufacturer's specifications and steric considerations, a single 5.5μm diameter bead can bind at most 4×10^6 antibody molecules (~6.6 amol); thus, the measured LOD of 2% of the bead surface corresponds to approximately ~8×10^4 antibodies or ~132 zeptomoles (Figure 2.10C). In contrast, SPR spectroscopy requires at least 200 pg (~10^9 molecules) of immobilized antibody in order to generate a detectable refractive index change.[111] D1.3/HEL binding kinetics were measured using as little as 2 million D1.3 mAb molecules (~3 attomoles) loaded into the microfluidic device.

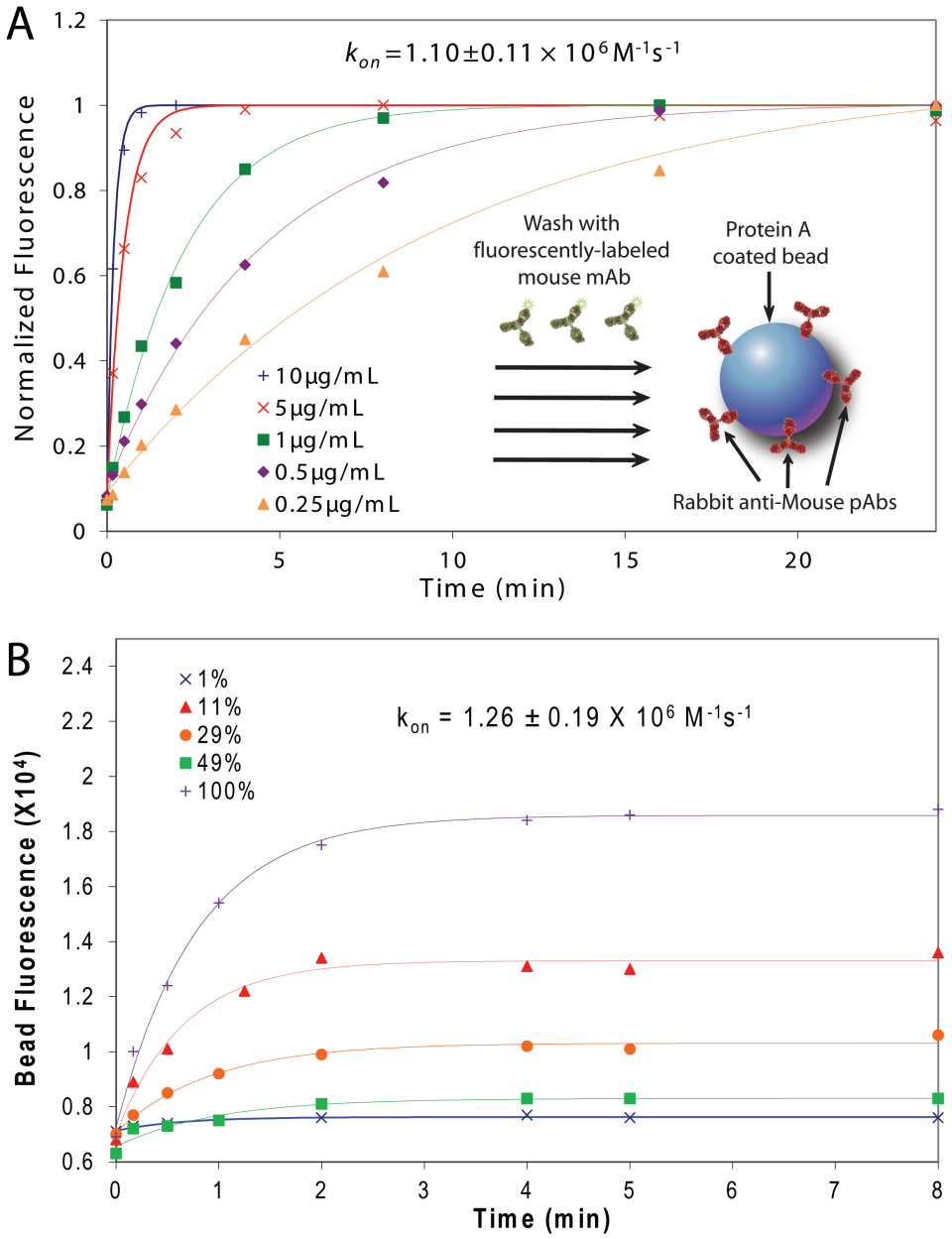

Figure 2.10 Sensitivity and detection limit of antibody-antigen binding kinetics measurements. (A) Measured association kinetics of D1.3 mAb-Dylight488 conjugate on rabbit anti-mouse pAb coated beads. (Inset) Schematic of bead assay for measuring binding kinetics of fluorescently labeled mouse mAb and rabbit anti-mouse pAb coated beads. Solid lines represent experimental fits using mass-action equations (equations 2.7a-c). (B) Association kinetics of HEL-Dylight488 conjugate on beads with varying amounts of immobilized D1.3 mAb (shown in % bead coverage). Bead fluorescence data is plotted after subtraction of bead autofluorescence at time zero. No change in bead fluorescence was observed when beads were not covered with D1.3 mAb (0% bead coverage). Reported error represents the calculated standard deviation of multiple replicate measurements. [continued on next page]

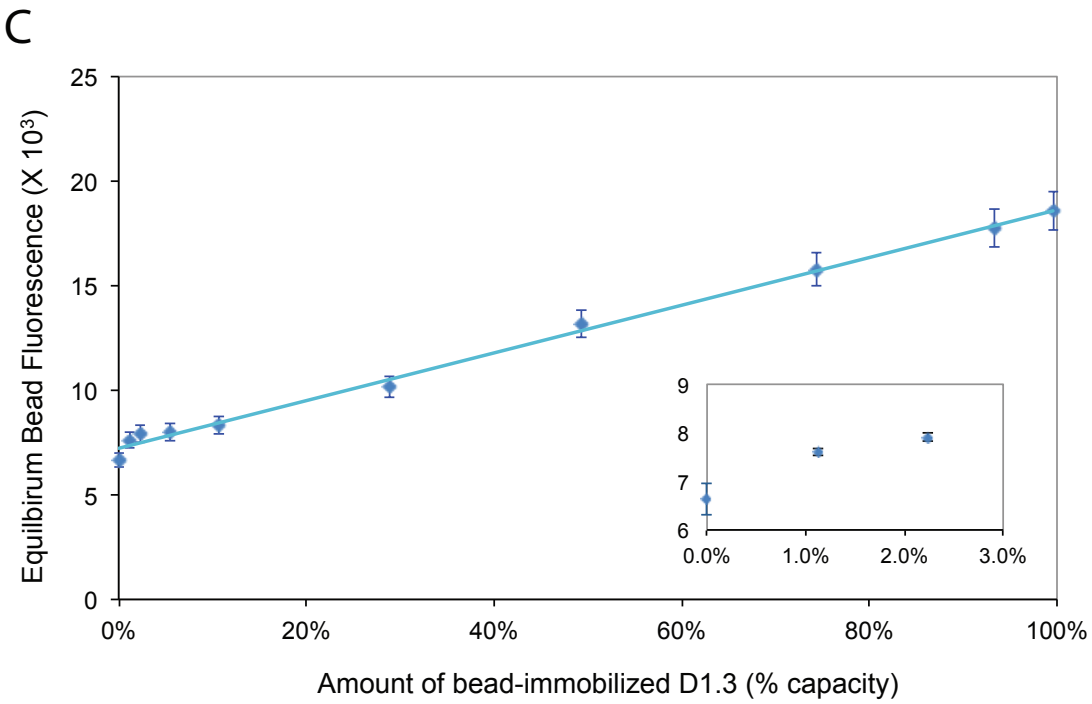

Figure 2.10 [continued from previous page] (C) Equilibrium bead fluorescence of HEL-Dylight488 conjugate varies linearly with the amount of immobilized D1.3 mAb. (Inset) Expanded view of graph to highlight detection limit of bead assay. Solid lines represent experimental fits using mass-action equations (A and B, equations 2.7a-c) and a line-of-best-fit (C). Adapted with permission from Singhal et al.[112] (American Chemical Society, 2010).[112]

In theory, the minimum sample consumption of the microfluidic bead assay could be reduced even further by reducing losses associated with channel dead volumes, optimizing the capture efficiency of antibodies on beads, as well as using microfluidic pumps to achieve flow rates less than 1 μL/hr.[86] In its present form, the microfluidic bead assay reported here enables antigen-antibody binding kinetics measurements with a four-order of magnitude reduction in both LOD and sample consumption when compared with SPR spectroscopy and a previously reported microfluidic fluorescence assay for measuring protein-protein binding kinetics.[111,122]

2.4.3 Measurement of Binding Kinetics of Antigen and Antibody Secreted from Single Cells.

The low detection limit of the fluorescence bead assay enabled measurements of antigen binding kinetics from antibodies secreted by single cells. To this end, rabbit anti-mouse pAb coated Protein A beads and single D1.3 hybridoma cells were loaded adjacent to one another in the microfluidic device and were co-incubated for 1 hour at room temperature (Figure 2.11). Subsequently, antibody-antigen binding kinetics were measured by recording the fluorescence of a single bead washed with buffer and successively higher concentrations of fluorescent antigen, in a manner analogous to the single-cycle kinetics technique used with SPR spectroscopy.[121,123] Association and dissociation rate constants for the D1.3/HEL interaction were successfully measured using antibodies secreted by a single D1.3 hybridoma cell, and the single-cell measurements were consistent with measurements on purified antibodies (Figure 2.11 and Table 2.2). By loading the beads into the microfluidic device after the cell, free antibodies from the cell medium were washed out of the device, thereby ensuring that only mAbs secreted by a single cell bound to the adjacent beads. No antibody-antigen binding was detected in control experiments in which beads were loaded into the fluidic output channel previously loaded with cell-free medium containing anti-HEL mAbs, confirming minimal mixing of reagents during sequential loading into the device.

Antibody-secreting cells are known to secrete thousands of antibodies per second at 37°C, and would therefore secrete enough antibodies in approximately one hour to saturate the surface of a single 5.5 μm diameter bead with maximum

binding capacity of ~4×10^6 antibody molecules.[21,124] However, hybridoma cells likely secrete antibodies at a reduced rate when incubated in the microfluidic device at room temperature (i.e. non-physiological conditions). Although direct measurements of actual antibody secretion rates were confounded by time-varying concentrations of secreted antibodies and an unknown bead capture efficiency, the cell/bead incubation time was varied in order to estimate the minimum antibody secretion rate. Based on the minimum incubation time (~5 min) and detection limit of the assay (~8×10^4 antibodies), single hybridoma cells secreted at least 200 antibodies/second when incubated at room temperature in the microfluidic device.

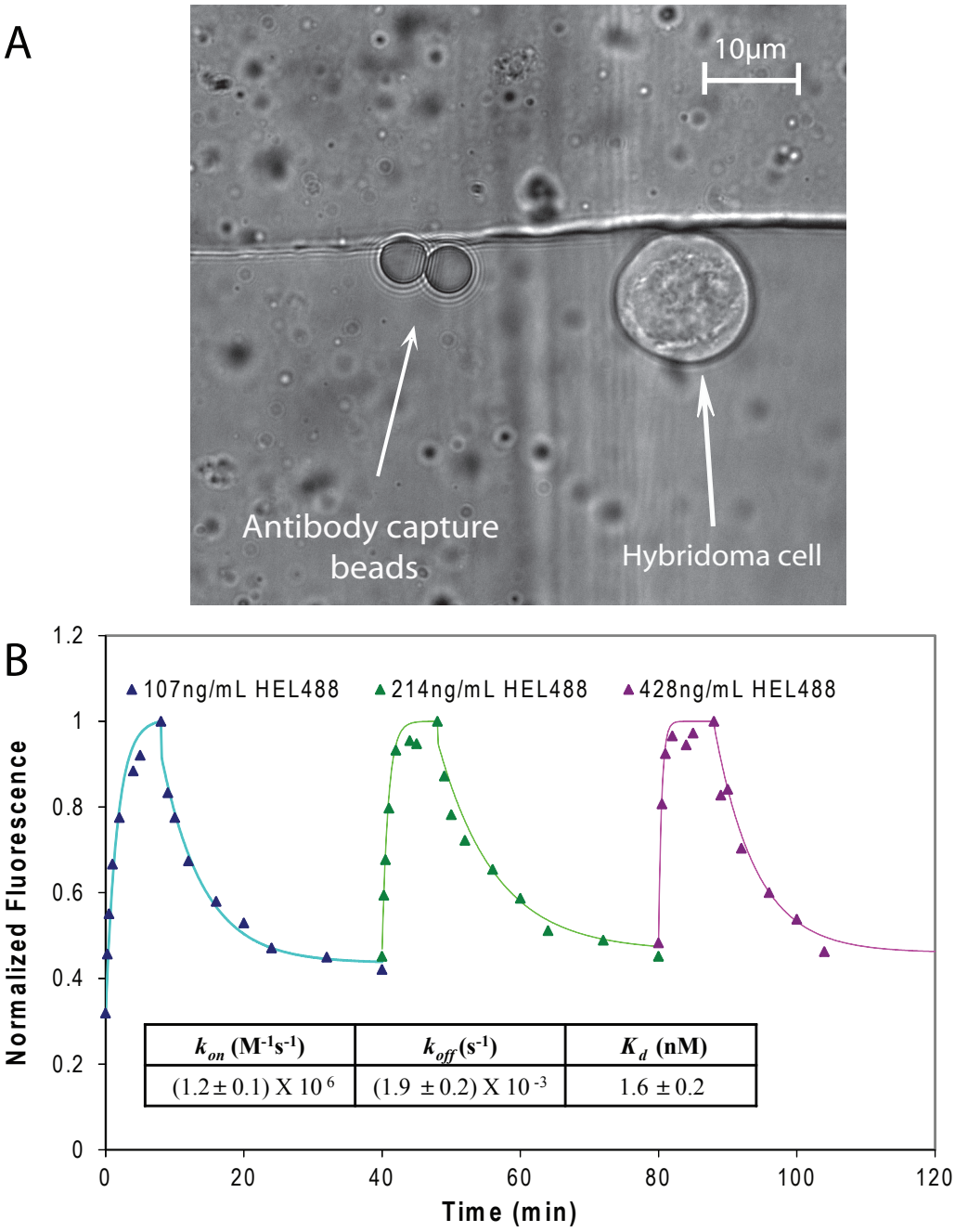

Figure 2.11 Antibody-antigen binding kinetics measured using antibodies secreted from a single cell. (A) Microscope image of D1.3 hybridoma cell loaded into microfluidic device adjacent to rabbit anti-mouse pAb coated beads trapped using a sieve valve. (B) "Single-cycle" binding kinetics from a single bead containing D1.3 mAbs secreted from a single cell and subject to increasing concentrations of HEL-Dylight488 conjugate. Solid lines represent three experimental fits using mass-action equations corresponding to each concentration of fluorescently labeled HEL. Reported error represents the calculated standard deviation of multiple replicate measurements. Adapted with permission from Singhal et al.[112] (American Chemical Society, 2010).[112]

2.4.4 Extensions of the Microfluidic Fluorescence Bead Assay

2.4.4.1 Direct Measurements of Antibody-Antigen Equilibrium Binding Affinities

The microfluidic fluorescence bead assay was used to directly measure the equilibrium binding affinities of antibody-antigen interactions. In particular, the equilibrium bead fluorescence was measured at different concentrations of fluorescently labeled HEL using beads loaded with a fixed amount of immobilized D1.3 mAb (Figure 2.12). By fitting the equilibrium bead fluorescence measurements with a Langmuir isotherm (equation 2.7c), the D1.3 mAb/HEL interaction was found to have an equilibrium dissociation constant equal to 1.67 nM, consistent with kinetic measurements from the fluorescence bead assay (Table 2.2).

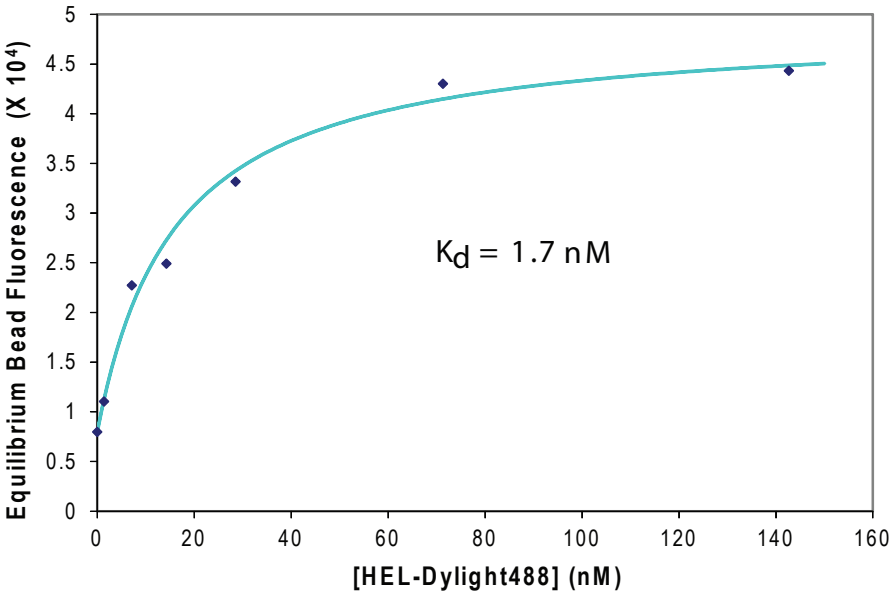

Figure 2.12 Direct measurement of equilibrium dissociation constants by measuring equilibrium bead fluorescence using immobilized D1.3 mAb and varying concentrations of HEL-Dylight488. Solid line represents experimental fits using a Langmuir isotherm equation. Value of K_d estimated by the concentration at which the equilibrium bead fluorescence was equal to the half-maximal value. Adapted with permission from Singhal et al.[112] (American Chemical Society, 2010).[112]

Alternatively, the equilibrium binding affinity of an antigen-antibody complex can be measured relative to a known affinity for the same antibody bound to a second capture reagent (such as anti-immunoglobulin, denoted antiAb). Assuming the two binding reactions are independent, both reactions take the form of the classic single-sorbate Langmuir isotherm:

$$[AbAg] = [Ag]_0 \frac{[Ab]_0}{[Ab]_0 + K_{d,AbAg}} \quad (2.8a),$$

$$[AbAntiAb] = [AntiAb]_0 \frac{[Ab]_0}{[Ab]_0 + K_{d,AbAntiAb}} \quad (2.8b),$$

Taking the ratio of these two equations:

$$\frac{[AbAntiAb]}{[AbAg]} = \frac{[AbAntiAb]_0}{[AbAg]_0} \frac{[Ab]_0 + K_{d,AbAg}}{[Ab]_0 + K_{d,AbAntiAb}} \quad (2.9a),$$

When the free antibody concentration is less than the equilibrium dissociation constants of both reactions ($[Ab]_0 << K_d$), this equation reduces to:

$$\frac{[AbAntiAb]}{[AbAg]} = \frac{[AbAntiAb]_0}{[AbAg]_0} \frac{K_{d,AbAg}}{K_{d,AbAntiAb}} \quad (2.9b),$$

Using this equation, the equilibrium dissociation constant for an antibody-antigen interaction can be deduced by measuring the relative bead fluorescence after co-incubating antibodies of interest with two different bead populations, one coated with the antigen and the other coated with a secondary antibody. Importantly, the solution concentration of antibody does not need to be known to perform these measurements, making this approach suitable for characterizing antibodies secreted by single cells at unknown rates.

A significant challenge to the relative equilibrium affinity measurements is the assumption that the antibody-antigen and antibody-antiAb reactions are independent (i.e. non-competitive). This assumption is valid in the limit where secreted antibody molecules are in vast excess to the available antigen and antiAb molecules. Thus, the number of antigen and antiAb molecules conjugated to the beads should be less than 10% of the number of secreted antibodies, or 10^3-10^5 molecules per bead given that ASCs secreting thousands of antibodies per second will produce approximately 10^5-10^6 molecules after a 1-hour incubation. As described above, 5 μm diameter beads are capable of covalently displaying ~10^5-10^6 protein molecules based on steric considerations. Thus, in order to reduce their protein-binding capacity, either the size of the beads or the surface density of binding sites must be reduced. Reducing the surface ligand density of the beads by 1 to 2 orders of magnitude will also reduce the dynamic range of fluorescence detection of the bead assay. This reduction in dynamic range could hamper the relative concentration measurements necessary for the assay, which has a sensitivity of approximately 2 orders of magnitude (Figure 2.10C). In contrast, reducing the size of the beads to <1 μm would reduce the bead binding capacity, but would make the beads significantly more difficult to trap reliably using a sieve valve (Figure 2.2A and 2.2B). In this case, passive hydrodynamic flow traps may be more suitable for capturing beads and allowing them to be washed with different solutions.[125]

2.4.4.2 Measurement of Antibody-Antigen Binding Kinetics and Selectivity Using Optical and Spatial Multiplexing.

The binding kinetics and selectivity of multiple antibodies binding multiple distinct antigens were measured simultaneously using both optical and spatial multiplexing of the bead-based assay (Figure 2.13). In principle, any combination of $m \times n$ antibody-antigen interactions can be screened simultaneously by immobilizing m distinct antibodies each on a distinct bead and exposing this bead population to a solution of n antigens, each with a spectrally-resolvable fluorescent label. By sequentially trapping each distinct bead using sieve valves, a population of beads was immobilized in a single field-of-view and the spatial address of each bead was used to identify each antibody. The beads were imaged with different fluorescence filter sets corresponding to a spectrally distinct fluorophore for each antigen.

In this manner, the kinetics and selectivity of 3 different monoclonal antibodies (D1.3, HyHEL-5 and LGB-1) binding to two different fluorescent antigens (HEL-Dylight633 and eGFP) were simultaneously measured (Figure 2.13). By employing this strategy, beads coated with anti-lysozyme mAbs or anti-eGFP mAbs were spectrally distinguished, whereas the two anti-lysozyme mAbs (D1.3 and HyHEL-5) were discriminated based on their unique binding kinetics for HEL. The fluorescence intensities of HyHEL-5 mAb-coated beads were significantly higher than the D1.3 mAb-coated beads, consistent with the fact that HyHEL-5 binds HEL with significantly higher affinity (~30-fold) than D1.3 (Table 2.2).

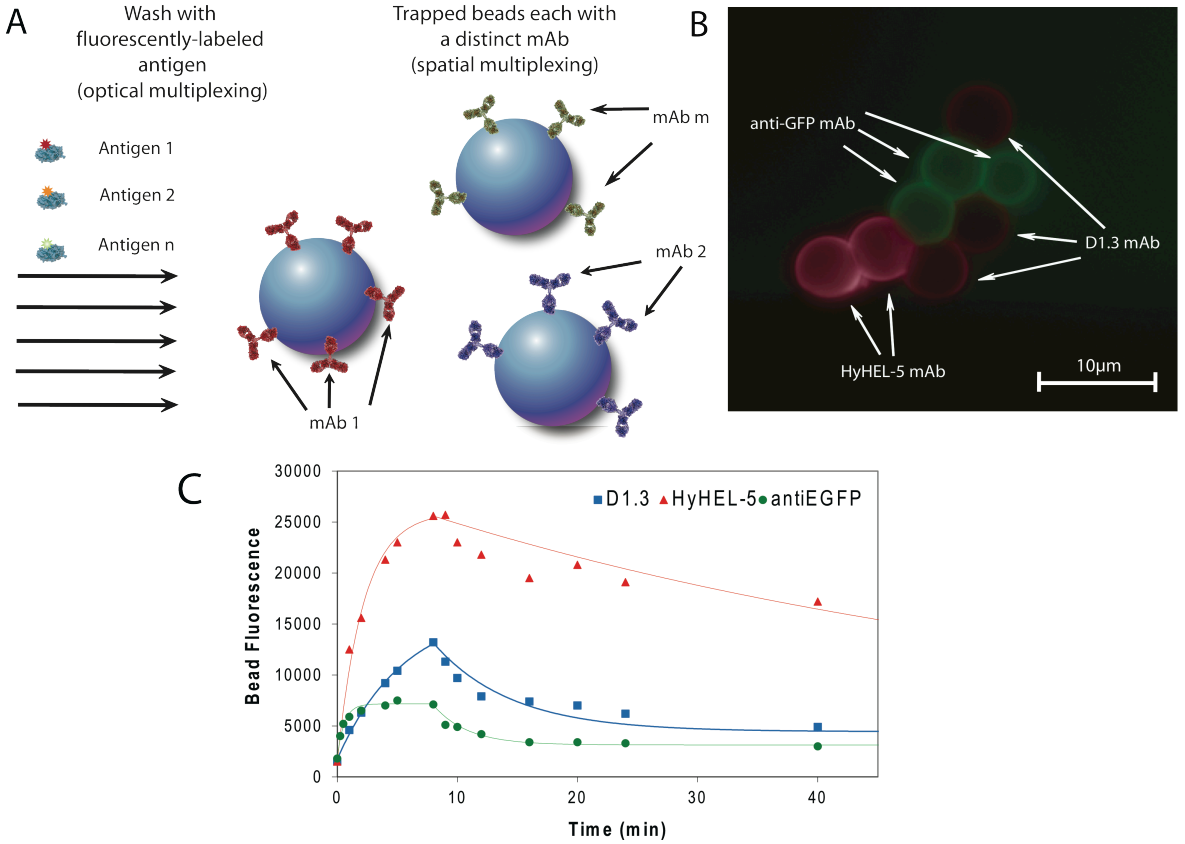

Figure 2.13 Simultaneous screening of binding kinetics and selectivity of multiple antibody-antigen interactions using optical and spatial multiplexing. (A) Schematic of assay to screen binding of *m* antibodies to *n* distinct antigens each labeled with a spectrally unique fluorophore. (B) False-colored, overlay of images taken with distinct fluorescence filter cubes to identify anti-lysozyme mAbs (red) and anti-EGFP mAbs (green). (C) Measured association and dissociation kinetics of 3 distinct mAbs (HyHEL-5, D1.3, and LGB-1) interacting with 2 different antigens (HEL-Dylight633 conjugate and EGFP). Solid lines represent experimental fits using mass-action equations. Adapted with permission from Singhal et al.[112] (American Chemical Society, 2010).[112]

In practice, several hundred antibody-antigen interactions could be measured simultaneously by imaging up to 100 beads in a single field of view with five to six spectrally distinct fluorophores. Multiplexed bead measurements could be used for simultaneously analyzing the binding kinetics and binding specificities of a panel of mAbs to multiple antigens in serum and other complex mixtures.

2.5 Conclusion

This chapter described a simple and sensitive microfluidic fluorescence bead assay for measuring antibody-antigen binding kinetics. This assay is useful for measuring antibody-antigen interactions with a wide of range of binding affinities and kinetics, as well as enabling the characterization of antibody binding selectivity. The microfluidic bead assay should also be useful for measuring other biomolecular interactions, such as protein-carbohydrate binding, protein-DNA (i.e. transcription factor binding), and protein-RNA interactions. Importantly, the microfluidic fluorescence bead assay is suitable for measuring binding kinetics using low abundance samples, such as antibodies secreted from single cells. Chapter 4 of this thesis describes the extension of this assay for screening hundreds of antibody-secreting cells from immunized animals in order to select high-affinity antibodies for both research and therapeutic applications.

Chapter 3: Microfluidic Single-cell Sorting, Recovery, and Robust Amplification of Antibody Heavy and Light Chain Genes from Single Cells

Described are methods for microfluidic sorting and recovery of selected antibody-secreting cells (ASCs) for single-cell RT-PCR amplification of antibody heavy and light chain genes. A particular focus was placed on developing methods compatible with microfluidic measurements of antibodies secreted by single ASCs (described in Chapter 2) in order to facilitate a complete pipeline for functional screening and selection of antibodies from single ASCs (see Chapter 4). As each antibody-producing cell may contain only a few thousand antibody-encoding messenger RNA (mRNA) molecules,[126] amplification of antibody heavy and light chain genes from single cells is required to obtain sufficient template to sequence antibody genes of interest and permit cloning into expression vectors for recombinant antibody production using *E. Coli*, yeast, insect, plant or mammalian cells.[19,127–130]

In the last two decades, numerous groups have reported the successful amplification of antibody heavy and light chain genes from single B cells, including naïve B cells, memory B cells, and plasma cells.[19,23,49–56,59,131,132] All of these amplification strategies employ reverse transcription polymerase chain (RT-PCR) of antibody genes using custom-designed primers for the antibody constant and variable regions of both heavy and light chain genes. Despite the large number of studies reporting single-cell RT-PCR of antibody genes, a systematic comparison of these different RT-PCR primer designs and reaction conditions has yet to be

conducted and the success-rate of RT-PCR amplification from single cells is typically low (< 50%). For example, using a combination of custom-designed and previously-published primers, Tiller et al. reported successful amplification of heavy and light chain genes from 20-40% and 30-60% of mouse[58] and human B cells[19], respectively. Differences in the antibody gene sequence and mRNA abundance between B cells are likely the two major factors accounting for amplification failures.

The work described in this chapter focused on developing methods to rigorously test the sensitivity of RT-PCR reactions using dilutions of purified mRNA from ASCs in order to optimize amplification of antibody genes from single ASCs. In particular, purified mRNA from mouse hybridoma cells was subjected to RT-PCR using a range of primer designs, primer concentrations, and annealing temperatures. Robust amplification of antibody genes was performed on fractions of single-cell mRNA equivalents, and the optimized RT-PCR reaction conditions also successfully amplified antibody genes from single-cell mRNA equivalents of primary antibody-secreted cells (ASCs) harvested from antigen-immunized mice. By microfluidic single-cell sorting and recovery, success rates for single-cell RT-PCR exceeded 90% from mouse hybridoma cells.

The following sections describe the structure of antibody genes and the design of primers for RT-PCR amplification of these genes.

3.1 Structure of Antibody Heavy and Light Chain Genes

All antibodies are encoded by two distinct genes, called the immunoglobulin heavy and light chain genes, respectively (Figure 3.1). Each of these genes can, in turn, be sub-divided into multiple gene segments, which are located on distant parts of the same chromosome in B cells.[2] In the process of forming an antibody, B cells undergo somatic recombination of gene segments in order to produce the variable regions of heavy (V_H) and light chain (V_L) genes. The V_H region is formed by recombination of three gene segments termed the variable (V), diversity (D), and junction (J) regions, respectively. In contrast, the V_L region is formed by recombination of two gene segments: V and J. Both the V_H and V_L gene regions are joined to the fragments coding for the constant (C) and leader (L) regions of an antibody by mRNA splicing. The constant region defines the antibody effector function, whereas the leader region (L) encodes a peptide that directs the antibody protein to the cellular secretion machinery and is cleaved post-transcriptionally.[2]

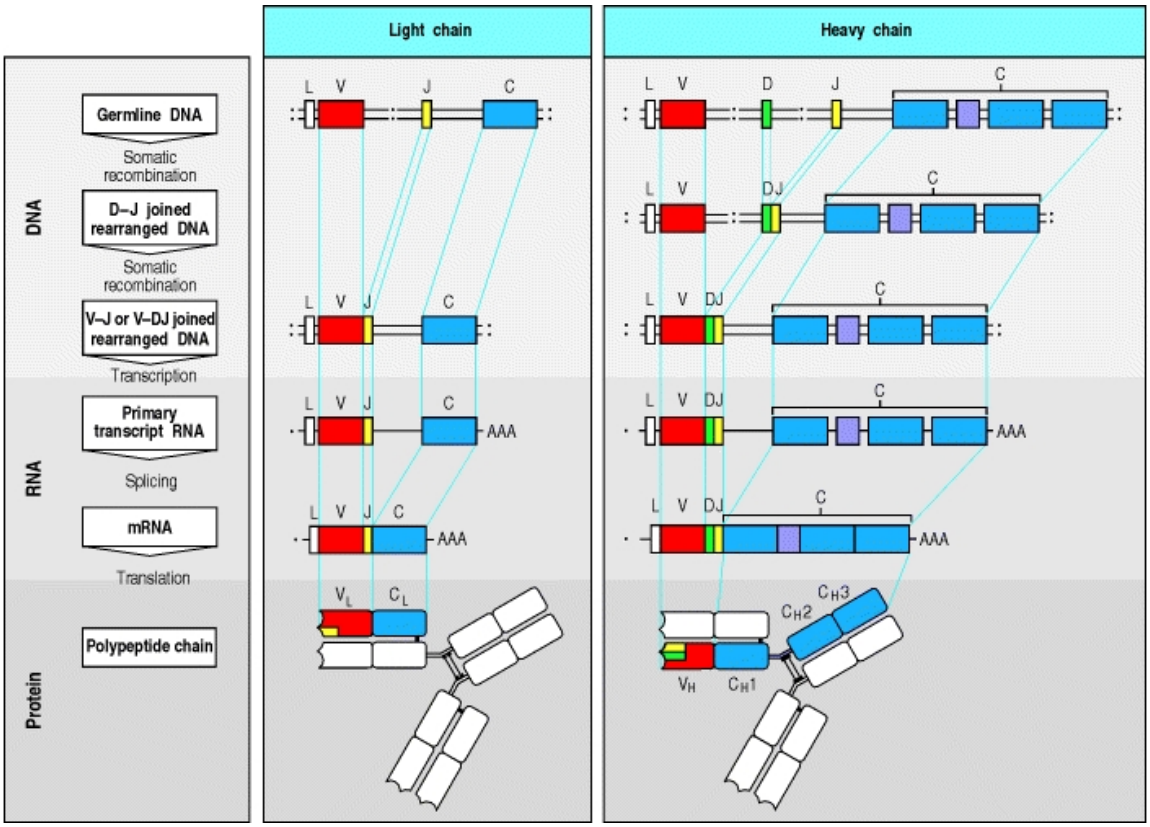

Figure 3.1 Antibody heavy and light chain genes are constructed from variable region segments (V,D,J) that are joined by somatic recombination. Leader (L) and constant (C) regions are joined by mRNA splicing. Figure reproduced from Janeway's Immunobiology with permission from Garland Science / Taylor and Francis LLC, 2011.[2]

A large number of VDJ gene segments can be combined in order to confer antibodies with a broad diversity of antigen binding domains (Table 3.1). These gene segments are clustered into three distinct genetic loci, named the kappa (κ), lambda (λ), and heavy (H) chain loci. In humans, the κ, λ, and H gene clusters are present on chromosomes 2, 22, and 14, respectively. Gene segments present in a single gene cluster can share as little as 50% sequence homology.[58] Antibody light chains in both humans and mice can be encoded by genes in either κ or λ loci. Whereas humans produce roughly equal amounts of antibodies with the κ and λ light chains, the vast majority (95%) of mouse antibody light chains are κ

isotype.[133,134] Interestingly, the mouse genome encodes a much greater diversity of both heavy and kappa chains than the human genome (Table 3.1).

Table 3.1 Number of V region gene segments that encode human and mouse antibody heavy and light chains. A range of values provided for some gene segments to reflect differences in the published literature. Data selected from Janeway,[2] Arnaout et al.,[18] and Tiller et al.[19,58]

Species	*Human*			*Mouse*		
Gene segment	**κ**	**λ**	**H**	**κ**	**λ**	**H**
Variable (V)	40	30	56-65	95	3	100-110
Diversity (D)	0	0	23-27	0	0	10
Junction (J)	5	4	6	4	3	4

3.2 Primer Design for Reverse-Transcription Polymerase Chain Reaction (RT-PCR) of Antibody Heavy and Light Chain Genes

Standard DNA amplification methods based on the polymerase chain reaction (PCR) require the design of primers with sequences complementary to both ends of the target gene.[135] Most strategies for amplifying antibody genes utilize reverse-transcription polymerase chain reaction (RT-PCR) in order to take advantage of the fact that heavy and light chain mRNA transcripts contain conserved constant region gene sequences downstream of both V_H and V_L genes (Figure 3.2).

Thus, a handful of short oligonucleotides can be designed to the constant region gene segments and used as 3' primers. In contrast, design of 5' primers to the antibody heavy and light chain mRNA transcripts is complicated by the broad sequence diversity of both V_H and V_L genes (Table 3.1). Thus, degenerate primers are designed complementary to the leader region or the first framework region (FWR1) at the 5' end of heavy and light chain mRNA (Figure 3.2). Degenerate primers are mixes of similar but not identical primers that are often used to amplify target genes with highly similar sequences, such as homologous genes in different organisms. The level of degeneracy of a primer can be calculated by multiplying the number of bases present at each position where the sequence varies (Figure 3.3). RT-PCR amplification of antibody heavy and light chain genes has previously been performed using relatively few primers with high degeneracy (>500-fold) as well as many primers with low degeneracy (<10-fold).[58,134]

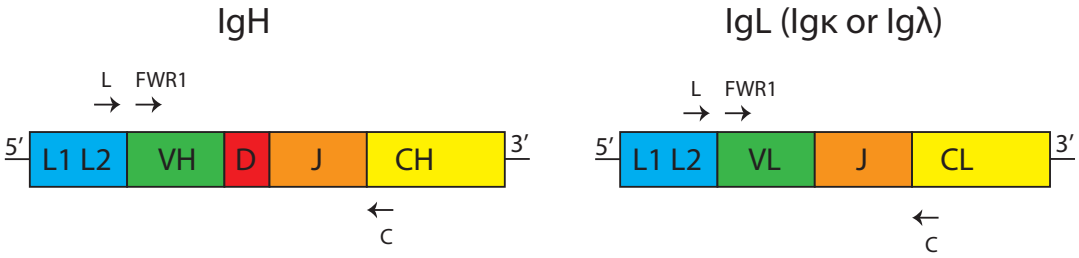

Figure 3.2 Design of primers for PCR amplification of antibody heavy (IgH) and light (IgL) chain genes. 3' primers are designed to the antibody constant (C) region. Degenerate primers to the 5' region can be designed either to the leader (L) or 1st framework (FWR1) region of V_H and V_L genes.

Figure 3.3 Degenerate primers are mixtures of oligonucleotides with similar sequences designed to amplify genes with highly related sequences. The level of degeneracy depends on the number of base positions and the variation at each position. In this example, the 5' primer has 4-fold degeneracy (2 positions X 2 bases at each variable position) whereas the 3' primer has 6-fold degeneracy (3 bases at 1st variable position X 2 bases at 2nd variable position).

One potential drawback of using degenerate primers for RT-PCR of antibody genes is the amplification of non-specific products as a result of the reduced specificity of degenerate primers. One approach for compensating for the reduced specificity of degenerate primers is to perform nested PCR, in which multiple rounds of PCR are performed using a unique set of primers internal to the target gene at each successive round (Figure 1.4). In order to optimize RT-PCR amplification of mouse antibody heavy and light chain genes from low abundance template (e.g. single cells), a variety of conditions were tested, including different primer concentrations, annealing temperatures, primers with varying levels of degeneracy, as well as nested PCR primers.

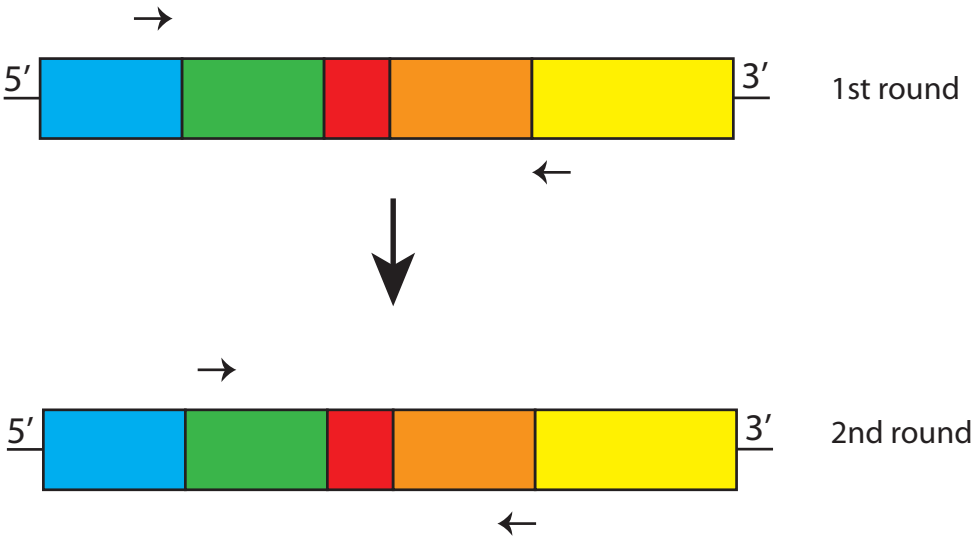

Figure 3.4 Nested PCR. Multiple rounds of PCR are performed, in which a unique set of primers internal to the template DNA are used in each successive PCR round. In semi-nested PCR, one primer is re-used and one internal primer is designed for each successive round of PCR. Nested PCR is used to increase amplification specificity for the target gene.

3.3 Materials and Methods

3.3.1 Cell Culture

Mouse hybridoma cells (D1.3, HyHEL-5, CD1d) were grown in 6 mL petri dishes (Nunc) using RPMI 1640 medium (Gibco) with 10% fetal calf serum (FCS) in a cell culture incubator (37°C, 5% CO_2). Cells were passaged approximately once a week by serial dilutions (5-fold) in fresh medium. Prior to RT-PCR experiments, cells were washed by centrifugation at 1500 rpm and re-suspended in 1X PBS, pH 7.4 (Gibco) in order to remove cell medium. Cell concentration was quantified using a haemocytometer and brightfield microscope.

3.3.2 Cell Lysis and mRNA Purification

10^5–10^6 antibody-secreting cells (e.g. mouse hybridoma cells) were concentrated into a pellet by centrifugation at 1500 rpm and the supernatant was decanted. Cells were re-suspended in alkaline or non-ionic lysis buffer. Alkaline lysis buffer consisted of 100 mM Tris-HCl, pH 7.5, 500 mM LiCl, 10 mM EDTA, pH 8, 1% Lithium dodecyl sulfate (LiDS), and 5 mM dithiothreitol (DTT) (Invitrogen). Non-ionic lysis solution consisted of 0.5% NP-40 or Triton X-100 in 1X PBS, pH 7.4 (Gibco). 10X serial dilutions of cell lysate were prepared by diluting 10 µL of cell lysate into 90 µL of lysis solution.

mRNA from cell lysate solutions was purified using oligo$(dT)_{25}$ beads (Dynabeads mRNA Direct kit, Invitrogen). For each reaction, 50 µL of 2.8µm diameter oligo$(dT)_{25}$ Dynabeads (10^7 beads/mL) was transferred into a 1 mL DNAse- and RNase-free microcentrifuge tube (Axygen) and placed on a magnetic tube rack (LifeSep1.5S, Bangs Labs) for 1 minute (Figure 3.4). The superparamagnetic Dynabeads formed a tight pellet that adhered to the sidewall of the microcentrifuge tube adjacent to the magnet, allowing the supernatant to be removed by pipet. Beads were re-suspended in 100 µL of alkaline lysis solution. The magnetic wash step was repeated and the beads were re-suspended in cell lysate solution. Cell lysate was incubated with oligo$(dT)_{25}$ Dynabeads for 5 minutes. Following incubation, beads were concentrated by magnet and washed in 100 µL of solution consisting of 10 mM Tris-HCl, pH 7.5, 0.15 M LiCl, 1 mM EDTA, and 0.1% LiDS (Wash buffer A). This wash step was repeated to remove all LiDS using a solution of 10 mM Tris-HCl, pH 7.5, 0.15 M LiCl, 1 mM EDTA (Wash buffer B).

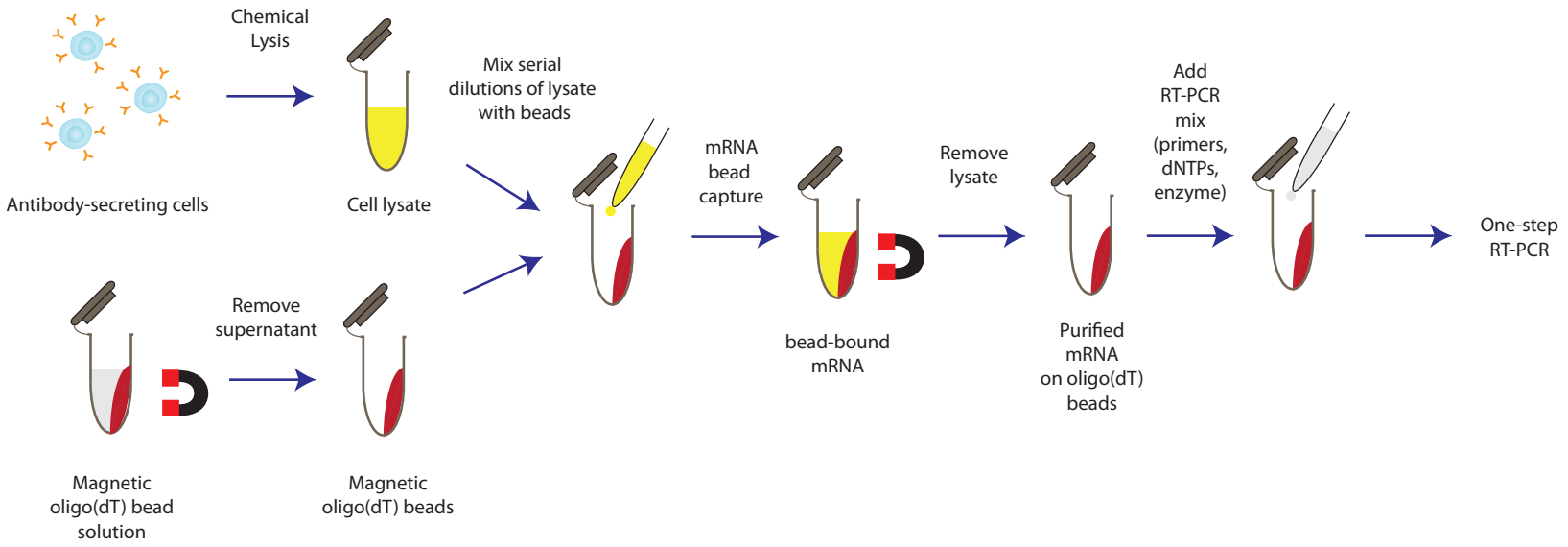

Figure 3.5 RT-PCR experiment for amplifying genes from antibody-secreting cells. Cells are enumerated using a haemocytometer. The protocol is repeated with serial dilutions of cell lysate in order to determine the detection limit of RT-PCR reactions for mouse β-actin and antibody heavy and light chain genes.

As LiDS is a strong protein denaturant, it must be removed prior to subsequent RT-PCR reactions. Finally, the bead solution was placed on the magnetic tube rack, the supernatant was decanted, and beads were re-suspended in RT-PCR reaction mix.

3.3.3 RT-PCR Reaction Mix and Cycling Conditions

RT-PCR primers were ordered in dried lyophilized form from IDT Technologies. A 100μM stock solution of each individual primer was prepared in RT-PCR-grade (i.e. DNase-free and RNase-free) water (Qiagen). Two distinct primer sets for mouse antibody genes were tested: a highly degenerate primer set (Appendix A.1)[134] and a low-degeneracy nested PCR primer set (Appendix A.2). Working solutions of 5' and 3' primers were prepared by mixing individual primers in equal amounts such that each primer was at 8μM concentration. As a control, commercial PCR primers were ordered for amplifying the mouse β-actin gene (514bp), similar in size to the antibody heavy and light chain genes (Stratagene). The sense and anti-sense primer sequences directed against the mouse β-actin gene were TGTGATGGTGGGAATGGGTCAG and TTTGATGTCACGCACGATTTCC, respectively.

RT-PCR reactions were performed in 0.2mL PCR reaction tubes on a 96-well PTC-100 benchtop thermal cycler (MJ research). Each RT-PCR reaction was performed in a 50 μL reaction volume prepared using the Qiagen One-step RT-PCR kit. For single-plex PCR reactions of heavy or light (kappa) chain genes, the reaction mix consisted of 21 μL RT-PCR grade water, 10 μL 5X reaction buffer, 7.5 μL 5' primer mix, 7.5 μL 3' primer mix, 2 μL enzyme mix containing both RT and DNA polymerase enzyme, and 2 μL dNTP. For multiplex RT-PCR reactions, the 50 μL reaction volume was maintained by

using only 6μL of water with 7.5 μL of both forward and both reverse primer mixes. The final concentration of each primer in the PCR reaction was 600 nM.

One-step RT-PCR amplification was performed in order to minimize sample losses and potential contamination during transfer steps from RT to PCR reactions (Table 3.2). As the RT enzyme may be active at room temperature, all RT-PCR samples were prepared on ice and transferred directly to the thermal cycler at 50°C for 30 min for reverse transcription. The subsequent 15 min hold at 95°C simultaneously denatures the RT enzyme while activating the hot-start DNA polymerase. Each PCR cycle consisted of three temperature steps: a denaturation step at 94°C, a primer annealing step (45-65°C), and a DNA extension step at 72°C. A variety of primer annealing temperatures were tested, ranging from 45 to 65°C. For touchdown PCR experiments, the annealing temperature during the first PCR cycle was set 5°C higher than the primer melting temperature (e.g. 55°C for a T_m = 50°C) and progressively reduced by 1°C each cycle for the first 10 cycles.

Table 3.2 One-step RT-PCR cycling protocol.

Step	Temperature (°C)	Hold Time	# of cycles
Reverse transcription (RT)	50	30 min	1
Hot-start Activation	95	15 min	1
Denaturation	94	30 sec	40
Anneal	55	30 sec	40
Extension	72	1 min	40
Final extension	72	10 min	1

The annealing temperature was then held constant for the remaining 40 PCR cycles. A final extension step at 72°C for 10 min was used to complete the PCR reaction for any partially amplified products. For nested PCR reactions, 3.5 µL reaction product from the 1st round of PCR was mixed with 50 µL reaction mix containing the same reaction mixture as the 1st round but with the nested primers. The cycling protocol for 2nd round of nested PCR reactions was identical to the 1st round, except that the initial RT step was omitted.

3.3.4 Analysis, Purification, and Sequencing of RT-PCR Products

RT-PCR amplification products were analyzed by DNA gel electrophoresis. 1% agarose gels were prepared by dissolving 0.5 g of agarose (Sigma) in 50 mL of 1X TAE buffer containing 0.5 µL of 10,000X SYBRSafe concentrated solution (Invitrogen). The size of the PCR products was compared against a 1 kb Plus ladder (Invitrogen) and fluorescence images were taken with the Alpha Imaging gel imaging system (Alpha Innotech). Melting curve analysis was also performed on RT-PCR products by adding SYBRSafe DNA dye at 10X concentration and measuring the sample fluorescence at every 0.5°C over a range of approximately 60-100°C using the Chromo4 Opticon thermal cycler (Bio-Rad).

For sequencing, DNA samples were extracted from the gels by a scalpel and purified using spin columns as per the Qiagen MinElute kit. Samples were eluted from the spin columns in low TE buffer and stored in a -20°C freezer. DNA samples and associated primers were submitted to the Nucleic Acid Protein Service Unit (NAPS, http://www.msl.ubc.ca/services/naps) for standard Sanger sequencing.

3.3.5 Microfluidic Single-Cell Sorting, Lysis, and Recovery

Prototype microfluidic devices were designed and fabricated with 8 chambers, approximately ~1 nL in volume, each with an independent valve to control reagent flow through the chamber (Figure 3.6). In order to trap large particles (e.g. cells, beads), all chambers contains a partially closing sieve valve that are controlled in parallel. The device consists of 9 inlets controlled by a multiplexing valve structure to enable the injection of different solutions through the device and into a single output port.

In a typical experiment, a solution containing mouse hybridoma cells (10^5-10^6 cells/mL) was injected into the device and into the channel upstream of the microfluidic chambers with the sieve valves closed. Single cells were sorted into chambers by briefly opening each chamber valve when a cell approached the chamber inlet as observed under a brightfield microscope. Cells were typically trapped at the chamber interface where the height of the chamber reduced from ~12-14 μm to ~3 μm, several times smaller than the ~10-15 μm diameter hybridoma cells (Figure 3.6C). The remaining cells in the channel were then flushed into the outlet using 1X PBS solution. Subsequently, a solution of 2.8 μm diameter oligo(dT) beads was injected into the device and several hundred beads were stacked against the sieve valve in each chamber. An alkaline lysis solution (1% LiDS) was injected into each chamber to lyse cells and capture poly(A) tailed-mRNA on the downstream stack of oligo(dT) beads. After flushing lysis solution out of the device using 1X PBS solution, the sieve valves were opened and beads from each chamber were sequentially eluted to the output port. Samples were recovered either by: 1) removal of the stainless steel pin and Tygon tubing connected to the output port; or, 2) manual pipetting of solution out of the outlet

port using a gel-loading pipet tip. Recovered samples were pipetted directly into 50µL of RT-PCR reaction mix and transferred to a benchtop thermal cycler for amplification according to one of the protocols described above (see section 3.4.3).

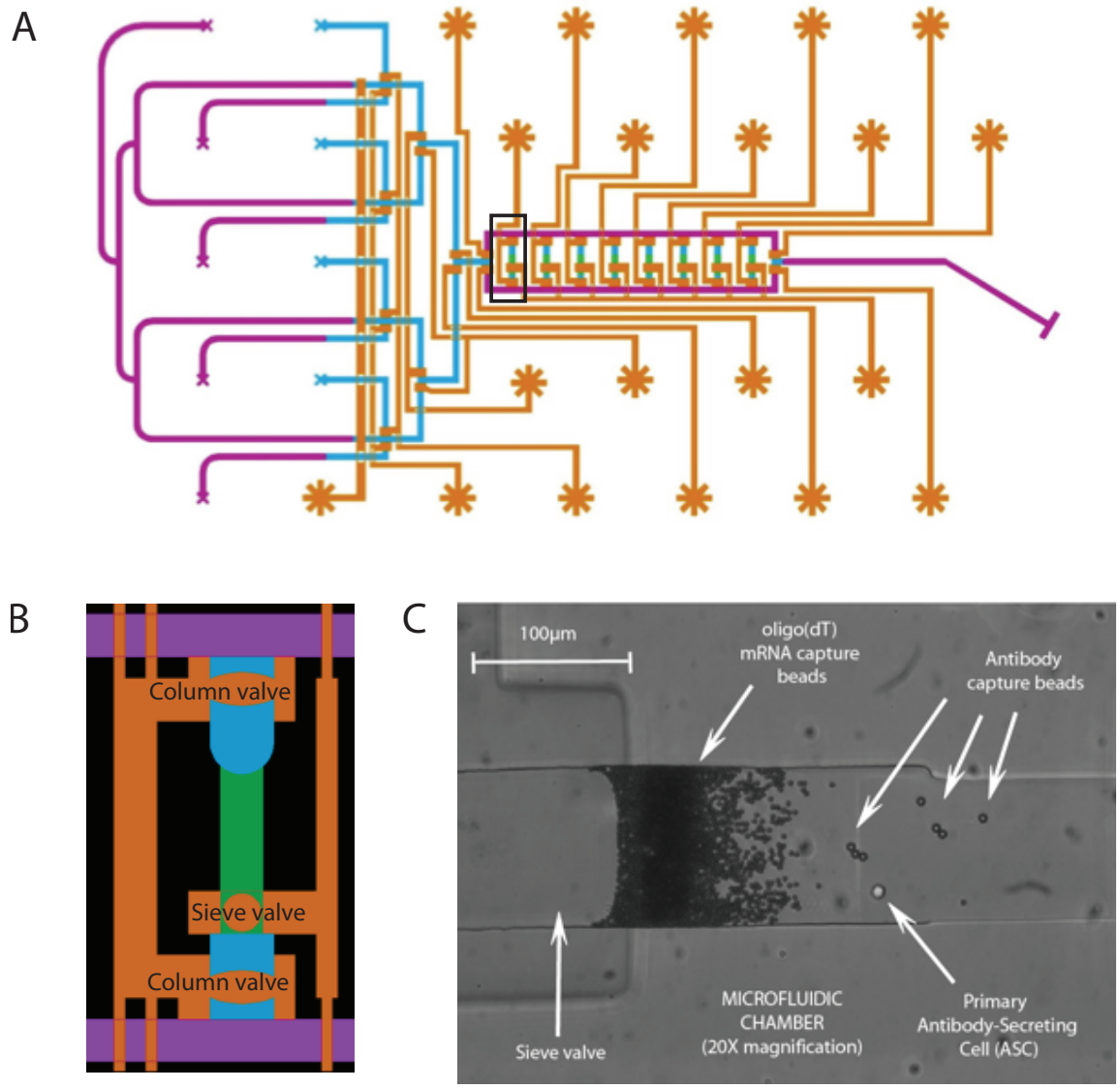

Figure 3.6 Microfluidic device for sorting, lysis, and mRNA bead capture from single cells. (A) Schematic of microfluidic device containing 9 reagent inlets (left), 8 chambers (one cell per chamber) and one fluidic outlet (right). (B) (expanded view of boxed region in A) Each chamber contains a partially closing sieve valve used to trap cells and beads. Cells are lysed in the chamber to release cellular mRNA that is captured on oligo(dT) beads. Beads are sequentially eluted from each chamber and recovered from the output port for single-cell RT-PCR amplification. (C) Brightfield microscope image of single chamber containing a stack of oligo(dT) beads, an antibody-secreting cell, and antibody-capture beads. Microscope image is rotated 90° counter-clockwise from the schematic drawings in (A) and (B).

3.4 Results

3.4.1 RT-PCR Optimization for Single-Cell Amplification of Mouse Heavy and Light Chain Antibody Genes

The sensitivity of a highly degenerate primer set (Appendix A.1) for RT-PCR amplification of antibody heavy and light chain genes was tested using serial ten-fold dilutions of a mouse hybridoma cell lysate (Figure 3.7). Heavy and light chain genes were successfully amplified from initial template concentrations ranging from tens to thousands of cell equivalents; however, no PCR products were detected from template concentrations less than or equal to a single cell (Figure 3.7). Successful RT-PCR amplification of mouse β-actin genes from 0.1 to 1 cell equivalents of mRNA suggested that loss of template during purification was not responsible for unsuccessful amplification of antibody gene products at low template concentrations.

The poor amplification of antibody genes at low template concentrations may be the result of poor primer binding to template and/or amplification of competing, non-specific products. DNA melting curve analysis was performed in order to detect non-specific products in RT-PCR samples.[136] Based on the known gene sequence for the mouse β-actin as well as the antibody heavy and light chain genes from the selected mouse hybridoma cells (e.g. D1.3 and HyHEL-5), the theoretical melting temperatures of all amplicons were estimated to be within the range of 82-85°C.[137,138] Compared to the β-actin RT-PCR reactions, amplification of antibody heavy and light chain genes generated significantly greater levels of non-specific products with melting temperatures less than 80°C (Figure 3.7B and C). At template concentrations of 0.1-1

cell eq., these non-specific products were present even though antibody genes were not successfully amplified.

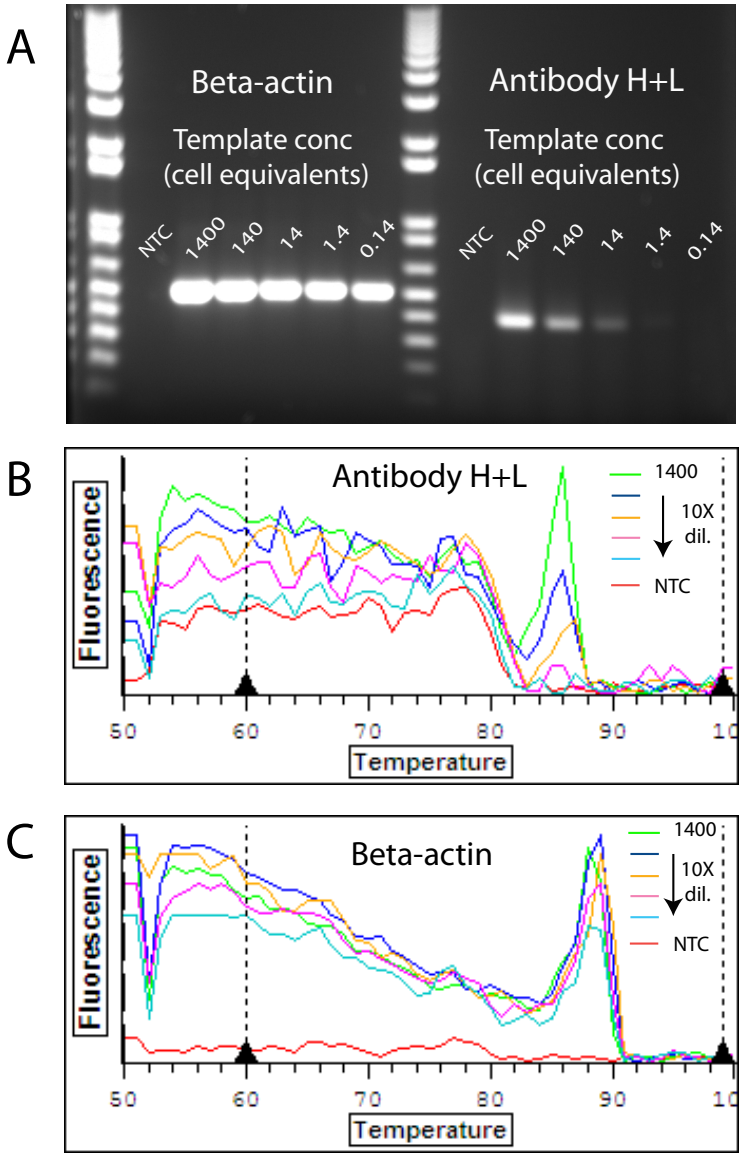

Figure 3.7 RT-PCR of mouse β-actin and antibody heavy and light chain genes using purified mRNA from different concentrations of D1.3 hybridoma cell lysate. (A) RT-PCR products visualized on a 1% DNA agarose gel with a 100bp ladder. The β-actin gene product appears as a single band with ~500 bp in size. Multiplex PCR of both heavy and light chain reactions also appear as a single ~400 bp band. Both heavy and light chain gene products were amplified as confirmed by excising, purifying, and sequencing the DNA products. DNA melting curve analysis for both mouse β-actin (B) and multiplexed heavy and light chain RT-PCR reactions (C). Plotted is the change in fluorescence intensity (dI/dT) at each temperature. The large fluorescence signal change at ~52°C coincides with the primer melting temperature.

To increase specificity of antibody heavy and light chain RT-PCR reactions, a range of primer concentrations was tested. Whereas low primer concentrations may produce insufficient template amplification, high primer concentrations can result in mis-priming and non-specific amplification.[139] For typical RT-PCR reactions, gene-specific primer concentrations range from 50 to 200 nM.[139] However, the optimal primer concentration for RT-PCR reactions using degenerate primers is reaction-specific because, in each reaction, many primers will not bind to the template, while primers that bind may have variable affinities due to possible base mismatches. RT-PCR amplification of antibody heavy and light chain genes was successful over a broad range of primer concentrations ranging from 160 nM to 1.2 μM (Figure 3.8). RT-PCR reactions with lower primer concentrations (i.e. 160 nM) resulted in both a reduction in the amount of both specific amplicons and primer dimers compared to reactions using a higher primer concentration (600 nM). Thus, reduction in primer concentration did not appear to be a robust strategy for improving RT-PCR sensitivity of antibody genes using this highly degenerate primer set.

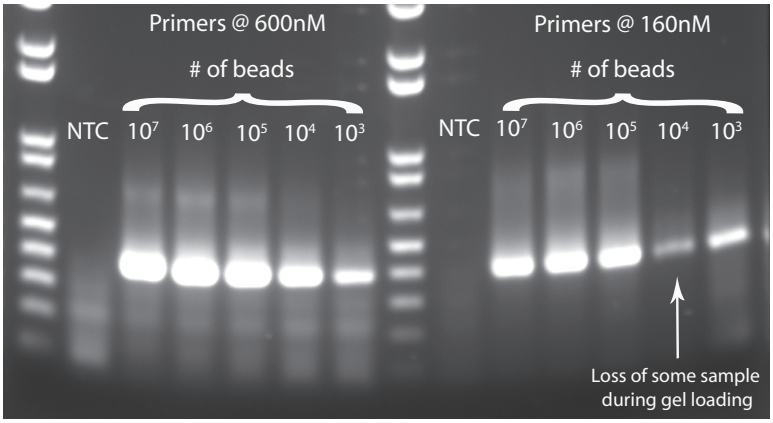

Figure 3.8 Multiplex RT-PCR of mouse heavy and light chain genes of mRNA purified from ~10^6 D1.3 hybridoma cells using highly degenerate primers at two different concentrations (160 nM and 600 nM). Lower primer concentrations resulted in reduced amplification of both specific amplicons and non-specific primer dimers. Shown is a 1% DNA agarose gel with 100 bp ladder.

Annealing temperatures also affect reaction specificity, as increases in temperature reduce the likelihood of base mismatches during primer-template binding; however, increases in annealing temperature may also come at the expense of reduced amplification efficiency. A range of annealing temperatures from 45°C to 65°C flanking the primer melting temperature (T_m ~ 50°C) was tested using "touchdown" PCR. Touchdown PCR can improve amplification specificity by using high annealing temperatures during early PCR cycles to increase primer binding stringency, thus selecting for target template amplification over the formation of non-specific products.[140,141] Once template concentration has increased after the initial PCR cycles, target template can outcompete non-specific template for primer binding, thus enabling gradual reduction of annealing temperature in later PCR cycles in order to improve amplification efficiency. The annealing temperature for the first PCR cycle was varied between 50°C to 65°C, followed by progressively lower temperatures (1°C lower per cycle) for the next 10 PCR cycles, and then a constant annealing temperature for the final 40 PCR cycles. However, changes to annealing temperatures did not improve amplification efficiency at low target template concentrations, nor reduce non-specific amplification (Figure 3.9). The lack of improvement in RT-PCR sensitivity when altering both primer concentrations and annealing temperatures suggested that these highly degenerate primers may not be suitable for amplification of antibody genes from single cells.

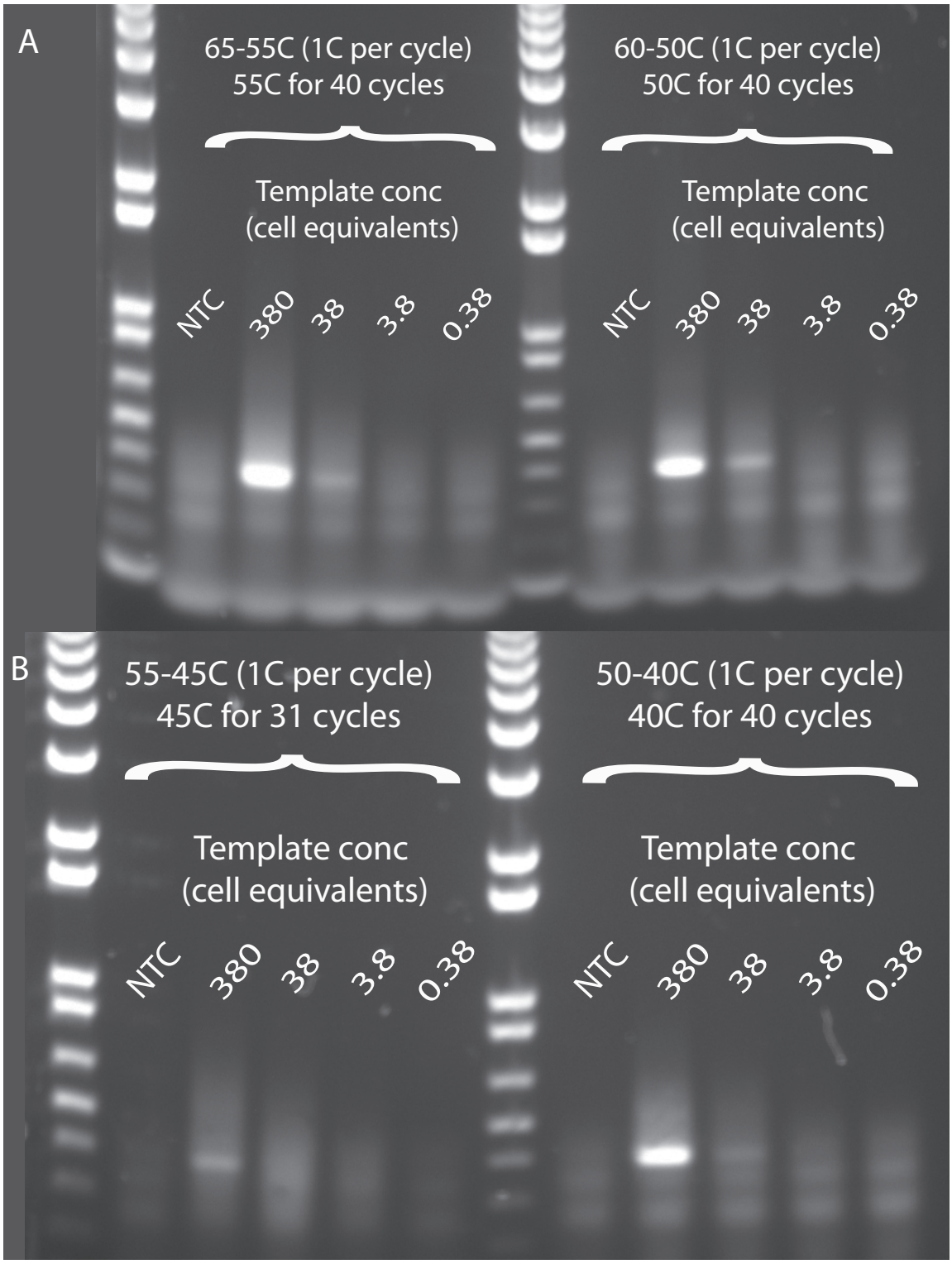

Figure 3.9 Multiplex RT-PCR of mouse antibody genes at different annealing temperatures. 4 different touchdown PCR protocols were tested with annealing temperatures varying from (A) 65°C-55°C and 60°C-50°C to (B) 55°C-45°C and 50°C-40°C. Amplification was successful using template concentrations greater than ~100 cell equivalents, with significant non-specific amplification observed in all reactions. Shown is a 1% DNA agarose gel with 100bp ladder.

The RT-PCR sensitivity of a low degeneracy nested primer set[58] (Appendix A.2) was directly compared to that of the above-described highly degenerate primers. RT-PCR was performed on dilutions of purified mRNA from multiple different mouse hybridoma cell-lines (D1.3, HyHEL-5, and CD1d) in order to estimate amplification performance across different cells. Notably, mouse antibody genes were successfully amplified from all cells at all tested template concentrations, including concentrations as low as 0.1 cell equivalents, (Figure 3.10) using only the 1st round primers from the low degeneracy set. These results demonstrate that primer design is critical for successful amplification of antibody genes from single cells, and that primers with reduced degeneracy may be less prone to nonspecific amplification than high degeneracy primers.

Despite successful RT-PCR amplification of all three hybridoma cell-lines using the 1st round low degeneracy primers, only a single PCR product was visible on the DNA gel from multiplex PCR reactions of the CD1d hybridoma (Figure 3.10). Extraction of this product from the gel and DNA sequencing confirmed that this product corresponded to an antibody light (kappa) chain, indicating a failure of the heavy chain RT-PCR reaction (Figure 3.10C). In an attempt to improve heavy-chain amplification efficiencies, single-plex RT-PCR reactions were carried out by purifying mRNA on oligo(dT) beads from both mouse D1.3 and CD1d hybridoma cells, and splitting the beads into two equal parts for amplification using heavy and light chain primers, respectively (Figure 3.11).

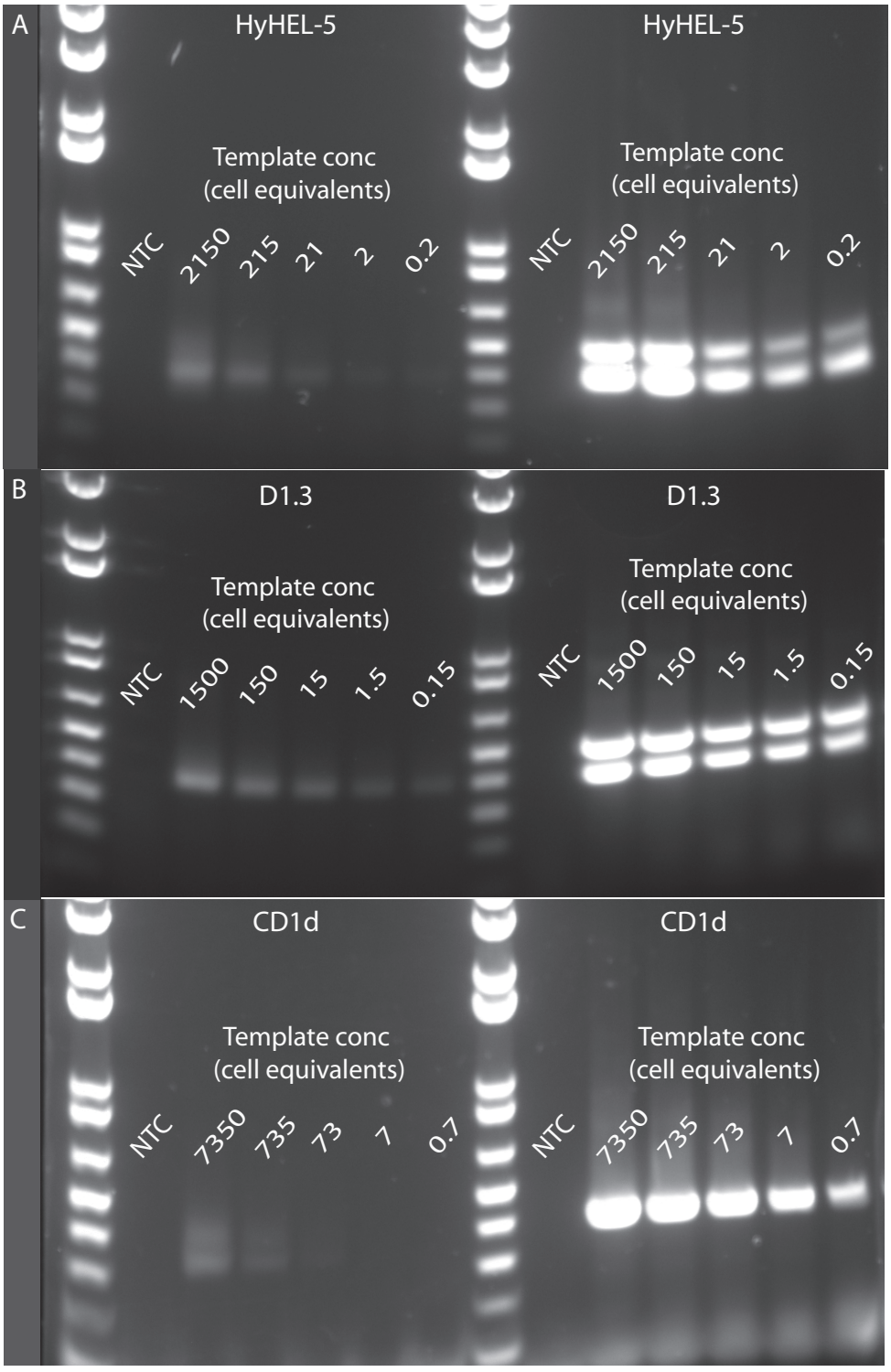

Figure 3.10 Multiplex RT-PCR of mouse antibody genes on serial dilutions of oligo(dT) bead-purified RNA from HyHEL-5 (A), D1.3 (B), and CD1d (C) mouse hybridoma cells using a highly degenerate primer set[134] (left) and 1st round primers from a low degeneracy primer set[58] (right) at 600nM concentration. Single-cell RT-PCR sensitivity using low degeneracy primers obtained for all three hybridoma cells. Shown is a 1% DNA agarose gel with 100bp ladder.

Successful amplification of both antibody genes from both cell-lines indicated that heavy and light chain amplification reactions can compete in multiplex reactions (Figure 3.10) and, thus, should be performed independently.

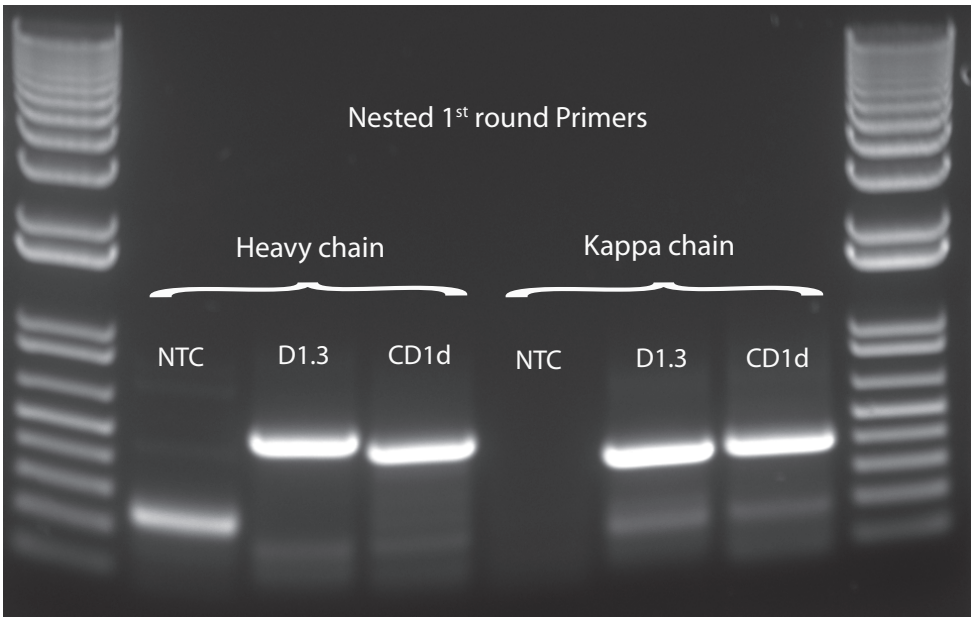

Figure 3.11 Single-plex RT-PCR of mouse antibody genes from mouse hybridoma cells using 1st round primers from a low degeneracy primer set[58]. mRNA from 3.5×10^5 D1.3 cells and 6×10^5 CD1d cells was purified using oligo(dT) beads. The beads were then split into two equal parts and mixed with RT-PCR reaction mix containing primers at a concentration of 600nM for heavy and light chain amplification, respectively. Shown is a 1% DNA agarose gel with 100bp ladder.

Measurements of template concentrations based on cell equivalents are imprecise; that is, it is unclear whether mouse hybridoma cells contain comparable amounts of antibody-encoding mRNA as primary antibody-secreting cells (ASCs) harvested from immunized animals. Thus, in the absence of an absolute measure of template concentration, single-plex RT-PCR reactions were performed on serial dilutions of purified mRNA from primary ASCs (i.e. CD138+ splenocytes) harvested from mice immunized with the model antigen hen egg lysozyme (see Chapter 4 for

methods). ASCs were sorted into RT-PCR tubes by fluorescent-activated cell sorting (FACS) and chemically lysed. Serial ten-fold dilutions of cell lysate were prepared and mRNA was purified from each dilution using oligo(dT) beads. The beads were split into two equal parts for amplification with low degeneracy heavy and light chain primers (Appendix A.2), respectively. Importantly, RT-PCR amplification of both heavy and light chain genes was successful down to single-cell template concentrations (Figure 3.12). Whereas robust amplification of kappa chain genes occurred at template concentrations of 0.1 cell equivalents, heavy chain reactions were successful at a minimum template concentration of 1 cell equivalent. Heavy chain reactions produced significant amounts of both large (~600 bp) and small (~250 bp) non-specific products, though the larger products were outcompeted by specific amplicons when using high initial template concentrations (i.e. 100 cell equivalents, Figure 3.12). Although the amount of specific amplification of heavy chain genes was modest compared to light chain genes at single-cell template concentrations, the established RT-PCR protocols should be suitable for amplification of both heavy and light chain genes from single ASCs selected by microfluidic screening. The following section describes methods to sort single ASCs in microfluidic devices in a manner compatible with detection of secreted antibodies (Chapter 4) and subsequently lyse and recover selected cells for RT-PCR amplification of antibody genes.

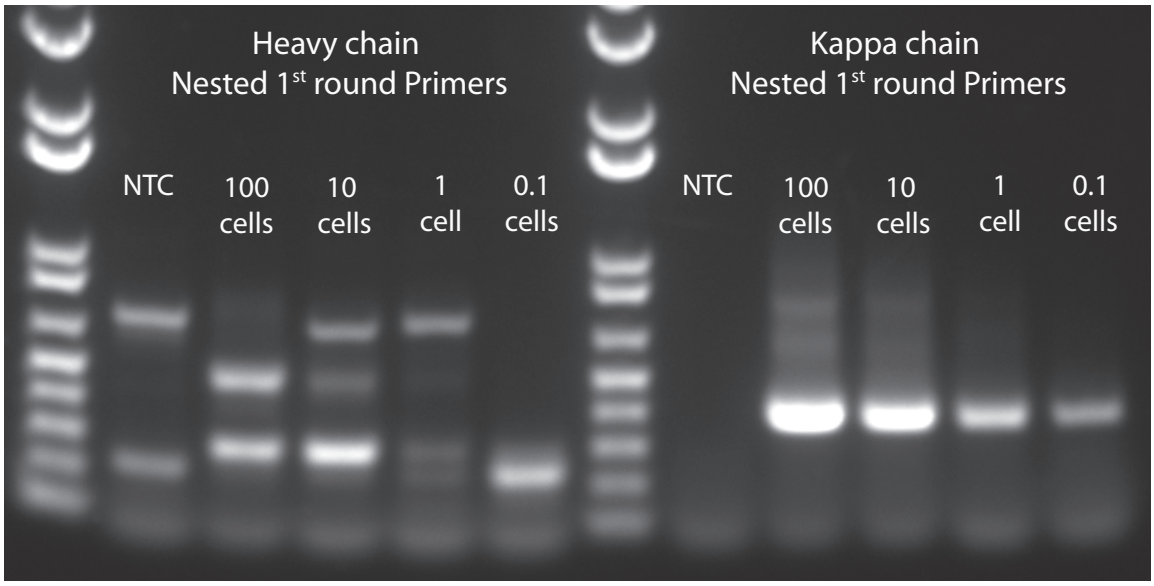

Figure 3.12 Single-plex RT-PCR of mouse antibody genes from primary antibody-secreting cells (ASCs) harvested from mice immunized with hen egg lysozyme (HEL). Cells were sorted by fluorescence-activated cell sorting (FACS). ASCs were lysed and the mRNA from serial dilutions of cell lysate was purified using oligo(dT) beads. The beads were then split into two equal parts and mixed with RT-PCR reaction mix containing low degeneracy primers[58] at 600nM for heavy and light chain amplification, respectively. Amplification in the heavy chain NTC reaction was due to reagent contamination, which was removed when using fresh primer solutions and RT-PCR reagents (data not shown). Shown is a 1% DNA agarose gel with 100bp ladder.

3.4.2 Microfluidic Single-Cell Sorting, Lysis, and Recovery

Single hybridoma cells were sorted into ~1 nL microfluidic chambers containing oligo(dT) beads trapped with a sieve valve (Figure 3.6 and Section 3.4.5). Cells were lysed using a harsh alkaline lysis solution (1% LiDS) in order to purify cellular mRNA on the oligo(dT) beads. With several hundred beads per chamber and an estimated binding capacity of 10^6 mRNA molecules per bead, the total bead binding capacity greatly exceeded the number of mRNA molecules in single mammalian cells (10^5-10^6).[142–144] Thus, all cellular mRNA should be captured on the bead stack, with the remaining cellular components (DNA, proteins, carbohydrates, and lipids) washed out of the device.

Beads loaded with cellular mRNA were sequentially eluted from each chamber and recovered by removal and replacement of the stainless steel pin and Tygon tubing connected to the output port. This solution was mixed with reaction mix (e.g. primers, dNTPs, and enzyme) and placed on a thermal cycler for RT-PCR amplification. As samples from all microfluidic chambers were eluted through a common outlet port, a test for cross-contamination between samples was performed by alternating elution of chambers with and without hybridoma cells. Amplification of antibody genes from all samples confirmed significant contamination between samples, which was not removed by washing the output port both with 1X PBS and 10% bleach solution following elution of each chamber (Figure 3.13). This cross-contamination was caused by a large dead-volume in the outlet port (diameter ~ 500 μm) that is not adequately flushed by the much smaller feed channel (100 μm wide × 100 μm high).

An alternative method of recovering samples from the device was therefore developed. Devices were fabricated with a large elution port (diameter ~ 1.2 mm) such that solution could be extracted by manual pipetting out of the outlet port using a gel-loading pipet tip. With this new device design, very little contamination was observed between eluted samples when the output port was thoroughly flushed by repeated pipetting of a 1X PBS solution and a new pipet tip was used between each eluted sample (Figure 3.14).

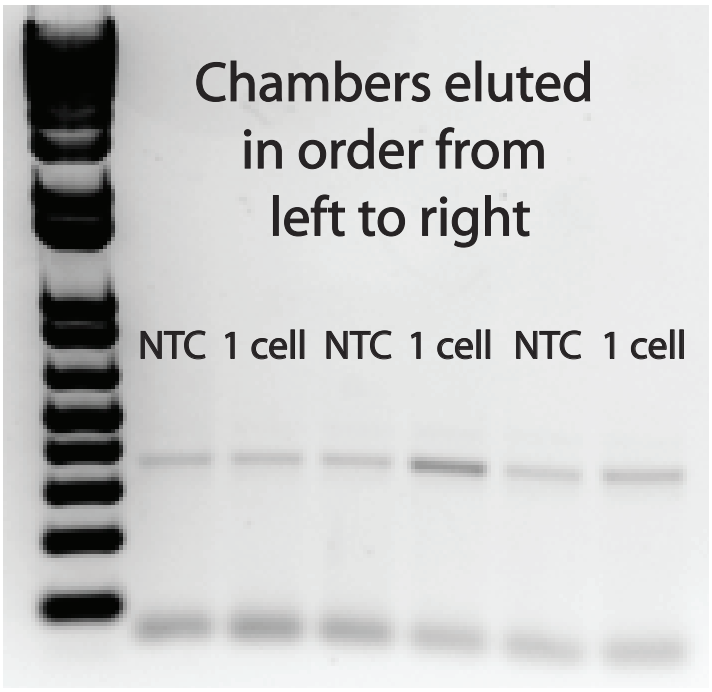

Figure 3.13 RT-PCR of mouse antibody genes from mRNA purified on oligo(dT) beads from single HyHEL-5 hybridoma cells sorted in a microfluidic device. Beads from chambers with a single cell ("1 cell") and without cells ("NTC") were alternately eluted and recovered from the output port in a stainless steel pin and Tygon tubing. The output port was washed with 1X PBS and 10% bleach in between each sample elution. Significant cross-contamination occurred between samples. Shown is a 1% DNA agarose gel with 100 bp ladder. Pixel intensities are inverted to highlight amplified products.

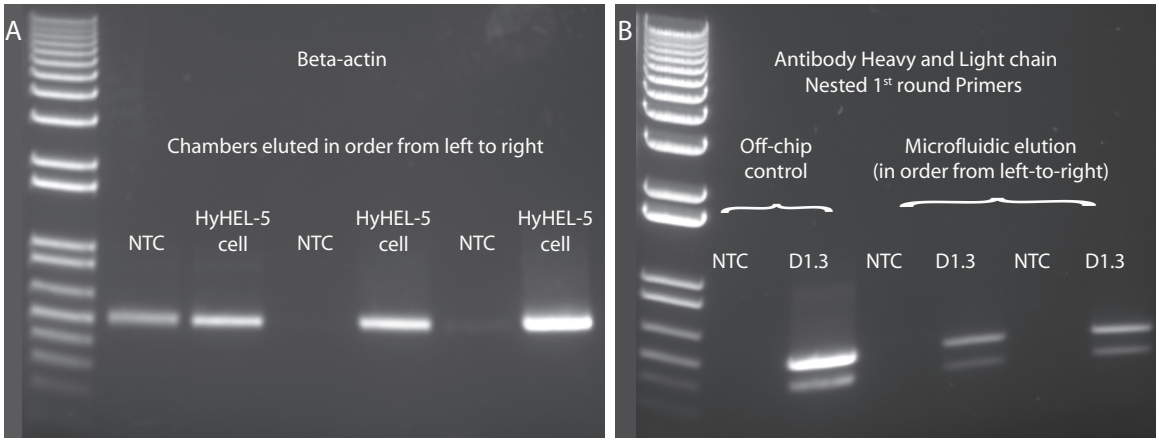

Figure 3.14 RT-PCR of mouse β-actin (A) and antibody heavy and light chain genes (B) from mRNA purified on oligo(dT) beads from single HyHEL-5 hybridoma cells sorted and recovered from a microfluidic device. Beads from chambers with a single cell ("HyHEL-5 cell" or "D1.3") and without cells ("NTC") were alternately eluted and recovered by manual pipetting with a new gel-loading tip for each sample. Cross-contamination between samples occurred if the output port was insufficiently washed with 1X PBS in between each sample elution. Shown is a 1% DNA agarose gel with 100 bp ladder.

The above-described method for microfluidic single-cell sorting, lysis, mRNA purification and recovery is a robust method for RT-PCR amplification of expressed genes from single cells. However, the chemical lysis step in this method may preclude its integrated use with methods to screen secreted antibodies from these same cells as described in Chapter 2. Alkaline lysis solutions containing sodium or lithium dodecyl sulfate (SDS or LiDS) are powerful protein denaturants;[145] thus, while facilitating purification of cellular mRNA, these solutions may also denature secreted antibodies present on antibody-capture beads adjacent to the cell in the microfluidic chamber (Figure 3.6C). Denaturation of secreted antibodies will, therefore, restrict screening of secreted antibody function to be performed prior to cell lysis and recovery. In attempt to circumvent this limitation, single cells were eluted from microfluidic chambers without lysis or mRNA bead purification. Cells were recovered from the device output port by manual pipetting with a gel-loading tip and transferred directly to RT-PCR reaction mix. In this manner, successful amplification of both heavy and light chain genes was performed (Figure 3.15). Interestingly, no cell lysis step was required, suggesting that cells lyse in RT-PCR reaction mix solution. Moreover, PCR primers for heavy and light chain genes successfully primed the reverse transcription reaction without dedicated RT primers, such as oligo(dT) or random hexamers. A further benefit of this approach is the fact that mRNA is retained within the cell during elution and recovery, reducing the chances of cross-contamination if a small number of oligo(dT) beads is left behind in the output port during pipet recovery (Figure 3.14). Indeed, no cross-contamination between samples was observed after alternating elution of

microfluidic chambers containing cells or no cells (Figure 3.15). Most importantly, microfluidic single-cell sorting and recovery followed by optimized RT-PCR amplification (e.g. using low degeneracy primers) resulted in >90% success rates for amplifying antibody genes from single cells from three different mouse hybridoma cell-lines (D1.3, HyHEL-5, and CD1d).

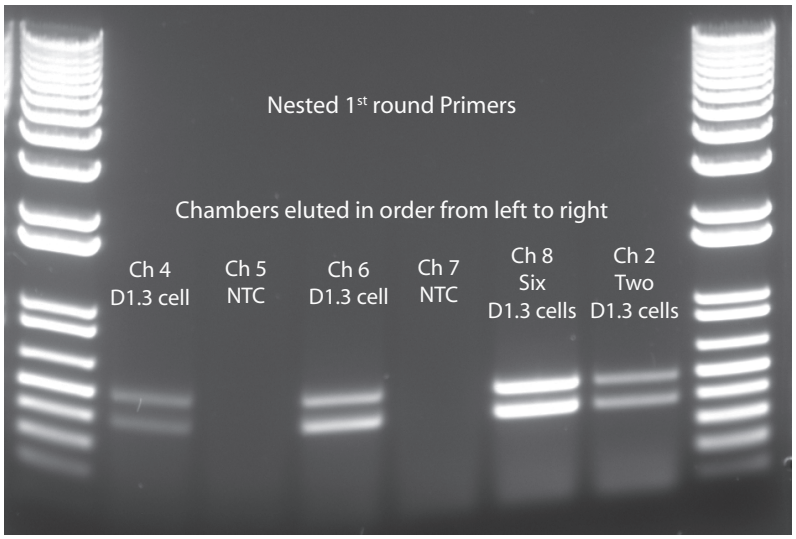

Figure 3.15 RT-PCR of antibody heavy and light chain genes from D1.3 hybridoma cells sorted and recovered from a microfluidic device without on-chip cell lysis. Chambers with and without cells were alternately eluted and recovered by manual pipetting with a new gel-loading tip for each sample. Samples were directly transferred to RT-PCR reaction mix without dedicated RT primers. Antibody heavy and light chain genes were successfully amplified from eluted samples from chambers containing single D1.3 cells as well as two chambers loaded with multiple cells (2 and 6 cells, respectively). No cross-contamination between samples was observed. RT-PCR performed using low degeneracy primers[58] at 600nM concentration. Shown is a 1% DNA agarose gel with 100bp ladder.

3.5 Conclusions

This chapter described optimized methods for RT-PCR amplification of antibody heavy and light chain genes from low template concentrations. Single-cell RT-PCR sensitivity was confirmed using low degeneracy primers to amplify genes from mouse hybridoma cells as well as primary antibody-secreting cells harvested

from immunized mice. Future experiments harnessing microfluidic single-cell RT-PCR and high-density digital PCR may enable absolute quantification of antibody-encoding mRNA in single cells.[75,81]

Optimized RT-PCR protocols were coupled with microfluidic devices for sorting, lysis, and recovery of single cells. Successful amplification of antibody genes was performed from single mouse hybridoma cells both with and without on-chip chemical lysis and mRNA bead purification. Moreover, single-cell RT-PCR amplification of antibody genes was successfully performed without dedicated RT primers in the reaction mix, indicating that gene-specific PCR primers can prime the reverse transcription reaction. Notably, microfluidic single-cell sorting and recovery followed by optimized RT-PCR amplification resulted in >90% success rates for amplifying antibody genes from single cells from three different mouse hybridoma cell-lines (D1.3, HyHEL-5, and CD1d).

The microfluidic device architecture for sorting and recovering single cells can be readily adapted to screen secreted antibodies from single antibody-secreting cells co-incubated with antibody-capture beads (Figure 3.13). The following chapter will describe the integration of a microfluidic fluorescence bead assay (developed in Chapter 2) and the optimized RT-PCR methods described in this chapter in order to perform screening and selection of novel monoclonal antibodies from single primary antibody-secreting cells (ASCs) from immunized animals. This approach can be extended to the amplification of single ASCs from other vertebrate species, such as rabbits and humans, using RT-PCR primers complementary to the unique antibody gene sequences present in each species.[19,50,58]

Chapter 4: Rapid, High-Throughput Screening and Selection of High Affinity Monoclonal Antibodies from Single Antibody-Secreting Cells

This chapter describes the development of a novel pipeline (Figure 4.1) for screening and selection of high affinity antigen-specific monoclonal antibodies (mAbs) from single primary antibody-secreting cells (ASCs). Animals are first immunized with a target antigen. ASCs are then harvested from the immunized animals and purified by labeling known plasma cell surface markers to perform fluorescence-activated cell sorting (FACS). Following purification, ASCs are loaded into a microfluidic device and loaded as single cells into an array of microfluidic chambers (volume ~1 nL). By concentration enhancement (see Chapter 1, Figure 1.11), single ASCs secrete sufficient numbers of mAbs within 1 hour for measurements of antibody-antigen binding kinetics and affinities using the microfluidic fluorescence bead assay described in Chapter 2. ASCs producing antigen-specific mAbs are sequentially recovered from the device and subjected to single-cell RT-PCR to amplify their antibody heavy and light chain genes using methods described in Chapter 3. Antibody genes for high-affinity mAbs were then cloned into expression vectors for recombinant production in mammalian cell lines.

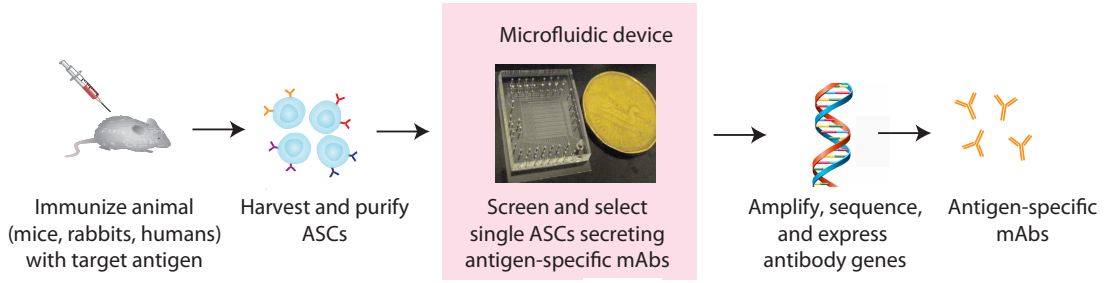

Figure 4.1 Microfluidic screening and selection of mAbs from single cells.

This technology was validated through the selection of nearly 200 high-affinity mouse mAbs to the model antigen hen egg lysozyme (HEL) by screening fewer than 1000 ASCs harvested from HEL-immunized mice. Over 80% of these mAbs bound HEL with equilibrium dissociation constants (K_d) less than or equal to 1 nM and on-rate constants (k_{on}) greater than 10^6 $M^{-1}s^{-1}$. Microfluidic single-cell screening yielded a 10X greater number of high-affinity antigen-specific mAbs compared to recently described single-cell micro-well screening approaches (Chapter 1, Figure 1.12) and conventional hybridoma technology (Chapter 1, Figure 1.6), without requiring time-consuming clonal expansion and sub-cloning steps required in the latter process.[51,90114114,146] As described below, this microfluidics-based pipeline for screening mAbs from single cells offers the potential both to select antigen-specific mAbs with desired binding kinetics and affinities, and to improve our understanding of affinity maturation and immune-dominance in the vertebrate adaptive immune system.

4.1 Experimental Methods

4.1.1 Mouse Immunization, Harvesting and Purification of ASCs

BALB/c and C57JBL/6 strain mice (6-wk to 1-year old) were given intra-peritoneal (IP) injections of HEL emulsified in Freund's incomplete adjuvant and were boosted every 2 weeks (2-10 injections). Mice were sacrificed 1 week after a final subcutaneous booster injection with HEL in Alum and single-cell suspensions from the dissected spleen were prepared using a cell strainer. Mouse splenocytes were then stained with fluorescently-labeled antibodies and sorted by fluorescent activated cell sorting (FACS) to enrich for CD138+ cells, a known cell surface marker for mouse plasma cells.[58] An ELISPOT assay (Figure 4.2) was used to determine the frequency of IgG- and anti-HEL secreting ASCs in the FACS-enriched cell population. BALB/c mice yielded 50,000-150,000 CD138+ sorted into 500 μL of cell medium (Gibco RPMI 1640 medium with 10% fetal calf serum and 0.5% mercaptoethanol). The cells were spun down into a pellet by centrifugation at 1500rpm for 5min and 450 μL of cell medium was removed. The cells were re-suspended in the remaining ~50 μL to obtain a concentrated cell solution (>10^6 cells/mL), suitable for loading into microfluidic devices.

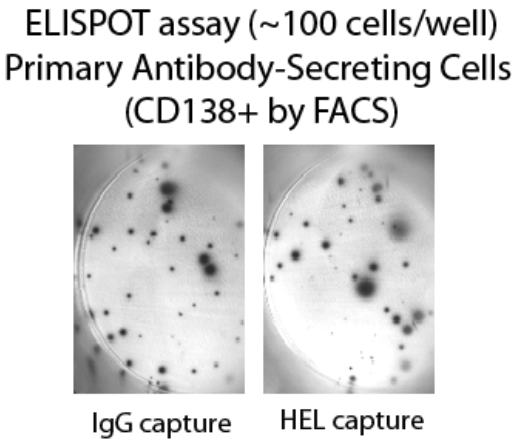

Figure 4.2 Representative results from ELISPOT assay to determine frequency of antigen-specific (i.e. anti-HEL) and IgG-secreting ASCs from FACS-enriched mouse splenocytes (Image prepared by Dr. Welson Wang, Biomedical Research Centre, UBC).

4.1.2 Reagent Preparation

Protein A-coated 5.5 μm diameter polystyrene beads (Bangs labs) were incubated with a 1mg/mL solution of Rabbit anti-mouse polyclonal antibodies (pAbs) purchased from Jackson Immunoresearch and used without further purification. All antibody and antigen solutions were prepared in PBS/BSA/Tween solution consisting of 1X PBS, pH 7.4 (Gibco) with 10mg/mL BSA (Sigma) and 0.5% Polyoxyethylene (20) sorbitan monolaurate (similar to Tween-20, EMD Biosciences). Lysozyme from chicken egg white (HEL) was purchased from Sigma. D1.3 and HyHEL-5 mouse hybridoma cell-lines were generously provided by Dr. Richard Willson (University of Houston). Fluorescent protein conjugates were prepared using Dylight488 and Dylight633 NHS esters (Pierce) and were purified using Slide-A-Lyzer™ dialysis cassettes (Pierce). The concentration of fluorescent conjugates was measured by spectrophotometry (Nanodrop). In order to minimize protein denaturation, fluorescent protein conjugates were labeled at a dye-to-protein ratio (D/P) of less ~5.

4.1.3 Microfluidic Device Design and Operation

A microfluidic device for screening antibody-secreting cells (ASCs) was designed and fabricated (Figure 4.3) using multilayer soft lithography.[86,87] The valves were designed in a push-down format such that flow channels could be directly bonded to thin (No. 1) coverglass for high-resolution optical imaging (see Chapter 2, section 2.3 for a complete description of fabrication methods). The device consists of an array of 112 discrete chambers (8 rows × 14 columns), 9 fluidic inlets for different reagents, and one common fluidic outlet. The outlet was used both for flushing reagents out of the device and for sample recovery. Reagent flow was directed into particular chambers by using a combination of a multiplexing valve structure[87] to select a particular row in the chamber array and a separate valve for each column of chambers. In addition to enabling reagent flow through a particular chamber, this valve architecture enabled fluid flow to be directed into an arbitrary set of chambers in a single row, all chambers in a particular column, or all chambers in the array. Dedicated valves upstream and downstream of the chamber array were also used to wash each row of the chamber array before delivery of a new reagent into the chambers.

The chambers were designed for reversible trapping of ASCs and antibody-capture beads (Figure 4.3B). A filter, consisting of an array of pillars spaced 2-3 μm apart, was used to trap cells and beads >5μm in diameter. The entry and exit regions of the chambers have rounded cross-sectional profiles with a height of 10-15 μm and a width of 150 μm; the rounded channel profiles enabled integration of valves to partition and isolate each chamber from adjoining chambers. The middle chamber regions have rectangular cross-section with a height of 2 - 4 μm aligned to a partially-closing sieve

valve[83] (see Chapter 2, Figure 2.2A for valve design) used to modulate the flow rate through each chamber. The total volume each of microfluidic chamber was approximately 1 nL (10^{-9} L).

At the start of the experiment, the sieve valves were closed in order to create high flow impedance and low flow rate through the chambers, thereby enabling cells and beads to be trapped upstream of the bead filter. By opening the sieve valve, the flow rate through the chamber was increased, causing the cells (but not the rigid beads) to deform and squeeze through the bead filter and into the fluidic outlet for manual recovery using a pipette. Recovered cells were then transferred to RT-PCR reaction mix for off-chip amplification of antibody genes. Antibody-capture beads retained in the microfluidic chambers were used for subsequent measurement of antibody-antigen binding kinetics. Importantly, the device and chamber architecture enabled recovery of cells without subjecting the chambers to cell lysis solutions, thus avoiding chemical denaturation of secreted antibodies and antigen on the capture beads.

Figure 4.4 shows a schematic of a single chamber on the device during a typical mAb screening experiment. At the start of the experiment, all chambers were first washed with 1X PBS buffer (Figure 4.4A). Next, ASCs in cell culture medium (~10^6 cells/mL) were loaded into each row of the chamber array at a low flow rate (~10 μL/hr). Single ASCs were loaded into each chamber by using a microscope to observe cells approaching a chamber; the corresponding column valve was then momentarily opened to direct reagent flow into the chamber (Figure 4.4B). In this manner, over 100 single cells were loaded into distinct chambers in 15-20 minutes. After cell loading into chambers, all remaining cells in channels upstream and downstream of the chambers

were washed out of the device. A solution of antibody-capture beads in cell medium was then loaded into the chamber array and beads were sequentially trapped against the bead filter in all 112 chambers (Figure 4.4C and D). Antibodies present in the cell medium were flushed out of the microfluidic chamber by the incoming bead solution, ensuring that the beads captured only antibodies secreted by adjacent single cells. There was no detectable cross-contamination of secreted mAbs between chambers, as evidenced by the lack of detectable antigen binding to beads in control chambers with no cells. In contrast, antigen bound to beads in all chambers (including those without cells) when beads were loaded into the device chambers either before or simultaneously with cells.

Cells and adjacent beads were co-incubated in each microfluidic chamber for 1 to 2 hours to allow for mAbs to be secreted and captured on beads at detectable concentrations (Figure 4.4E). After incubation, all chambers were washed with 1X PBS to remove mAbs free in solution (Figure 4.4F). All chambers were then flushed with a solution of fluorescently labeled antigen (e.g. HEL-Dylight488 or HA-Dylight488) for 5 to 10min (Figure 4.4G and H). The chambers were again washed for 5 minutes with 1X PBS prior to automated, high-resolution fluorescence imaging (Figure 4.4I).

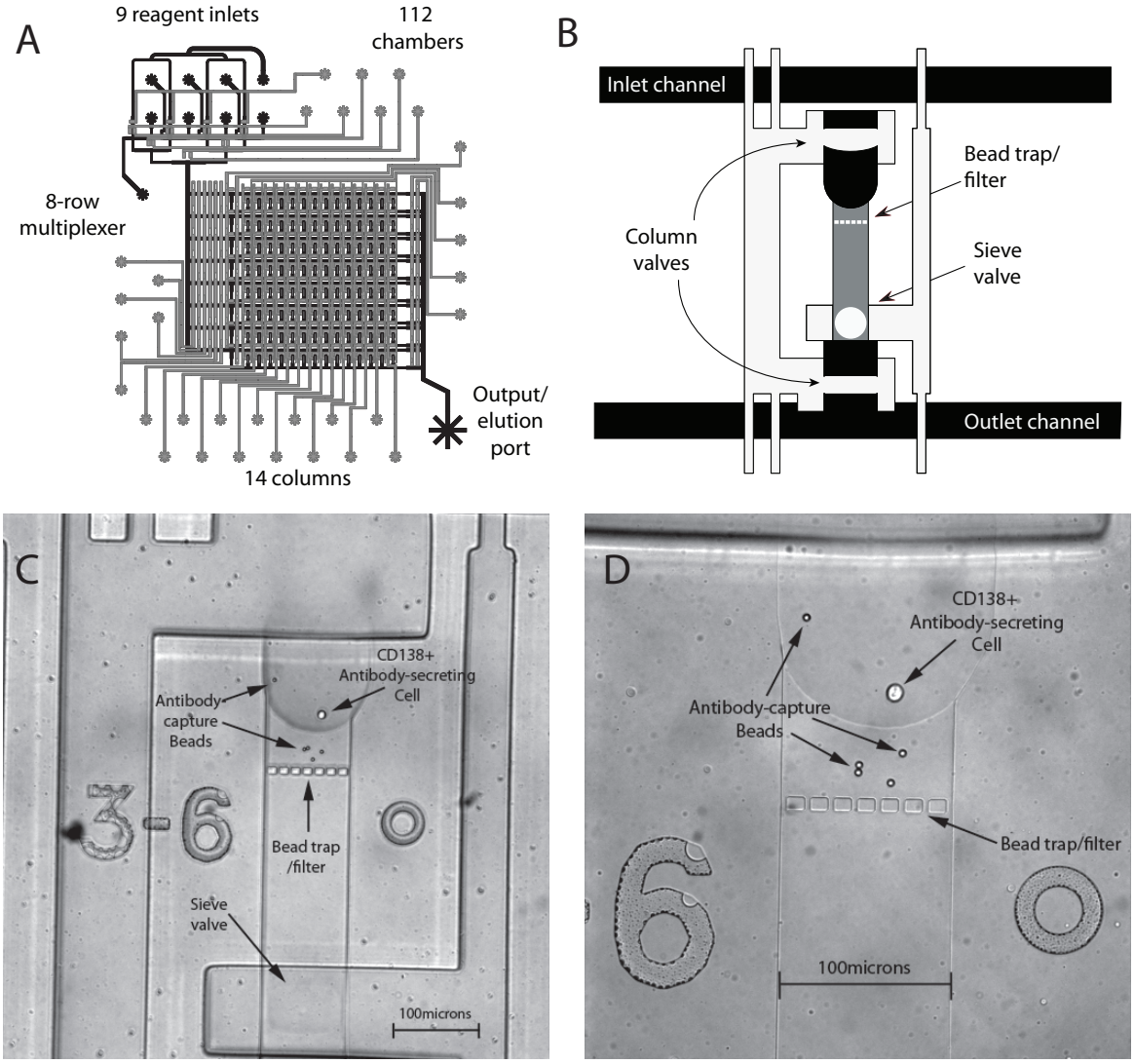

Figure 4.3 Microfluidic device for screening single antibody-secreting cells (ASCs). (A) Device schematic depicting 9 fluidic inlets, 1 fluidic outlet, and 112 chambers (8 rows × 14 columns) addressed using a row multiplexer and column valves. (B) Schematic of single microfluidic chamber (volume ~1 nL) containing a bead filter/trap and sieve valve to modulate flow rate through chamber. (C and D) Bright-field microscope images of sub-nanoliter microfluidic chambers containing single ASCs and antibody-capture beads at 20X (C) and 40X magnification (D).

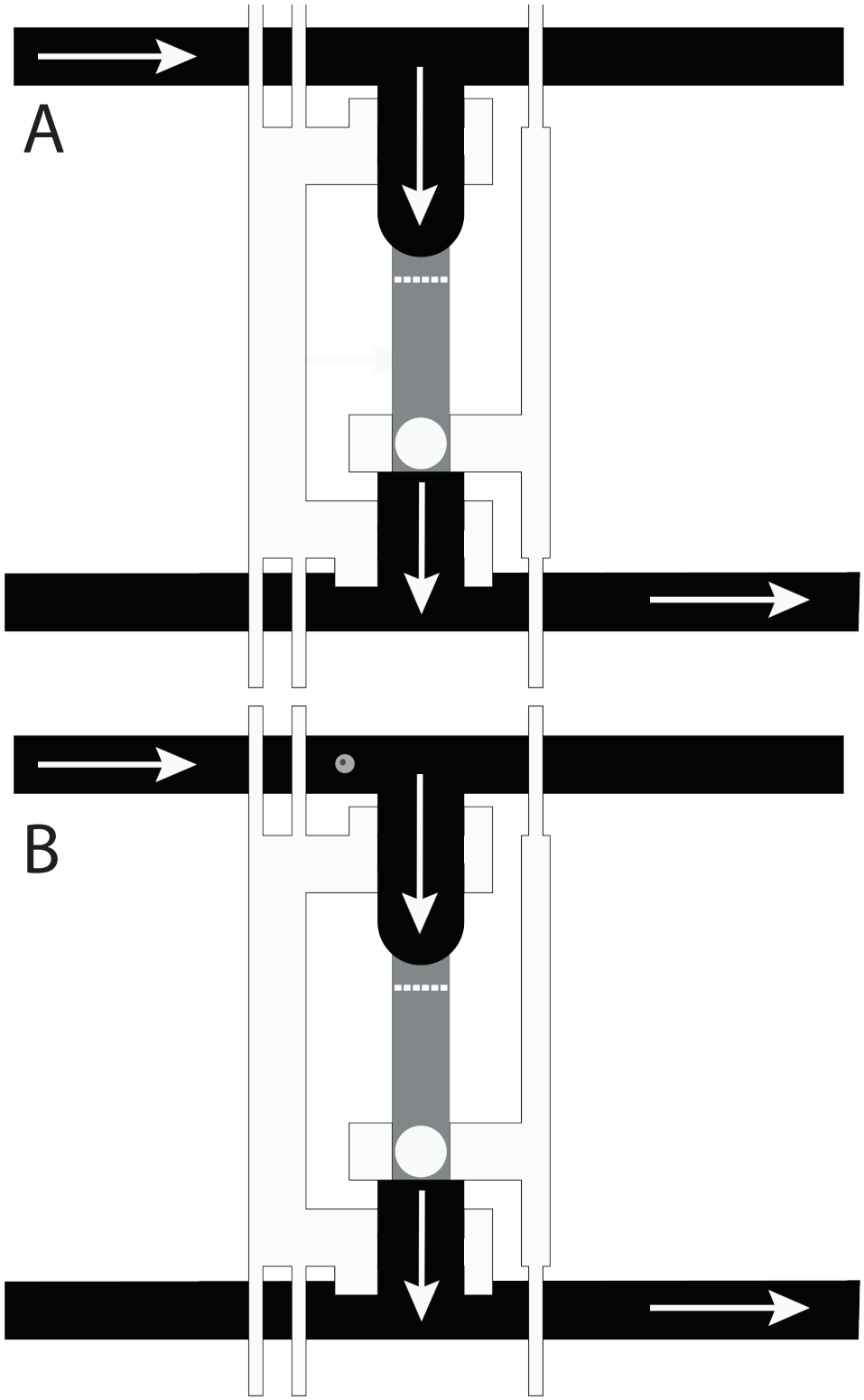

Figure 4.4 Schematic of microfluidic chamber while performing single-cell antibody screening and selection. See text for details. (Page 1 of 6).

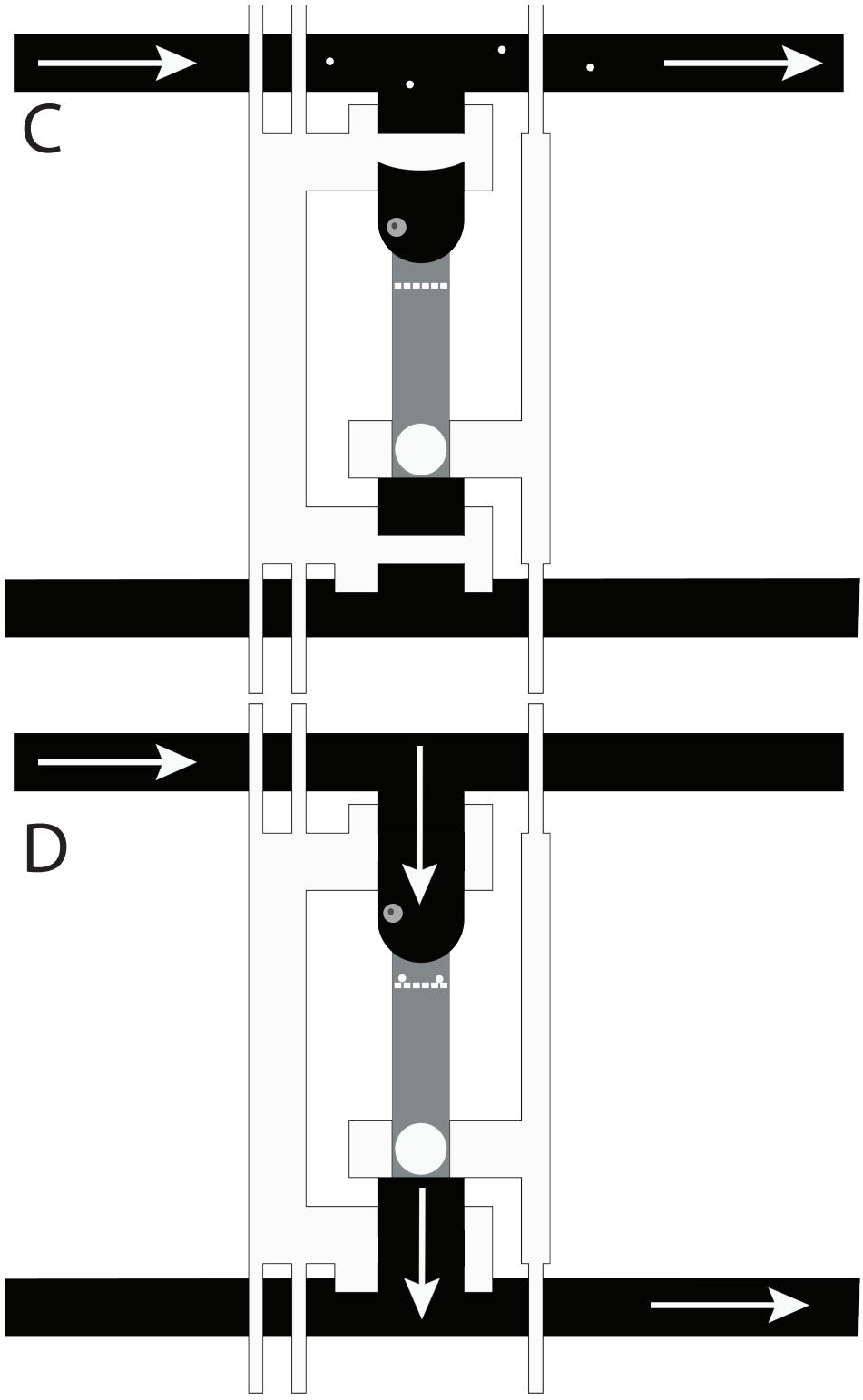

[Figure 4.4 con't - Schematic of microfluidic chamber while performing single-cell antibody screening and selection. See text for details. (Page 2 of 6).]

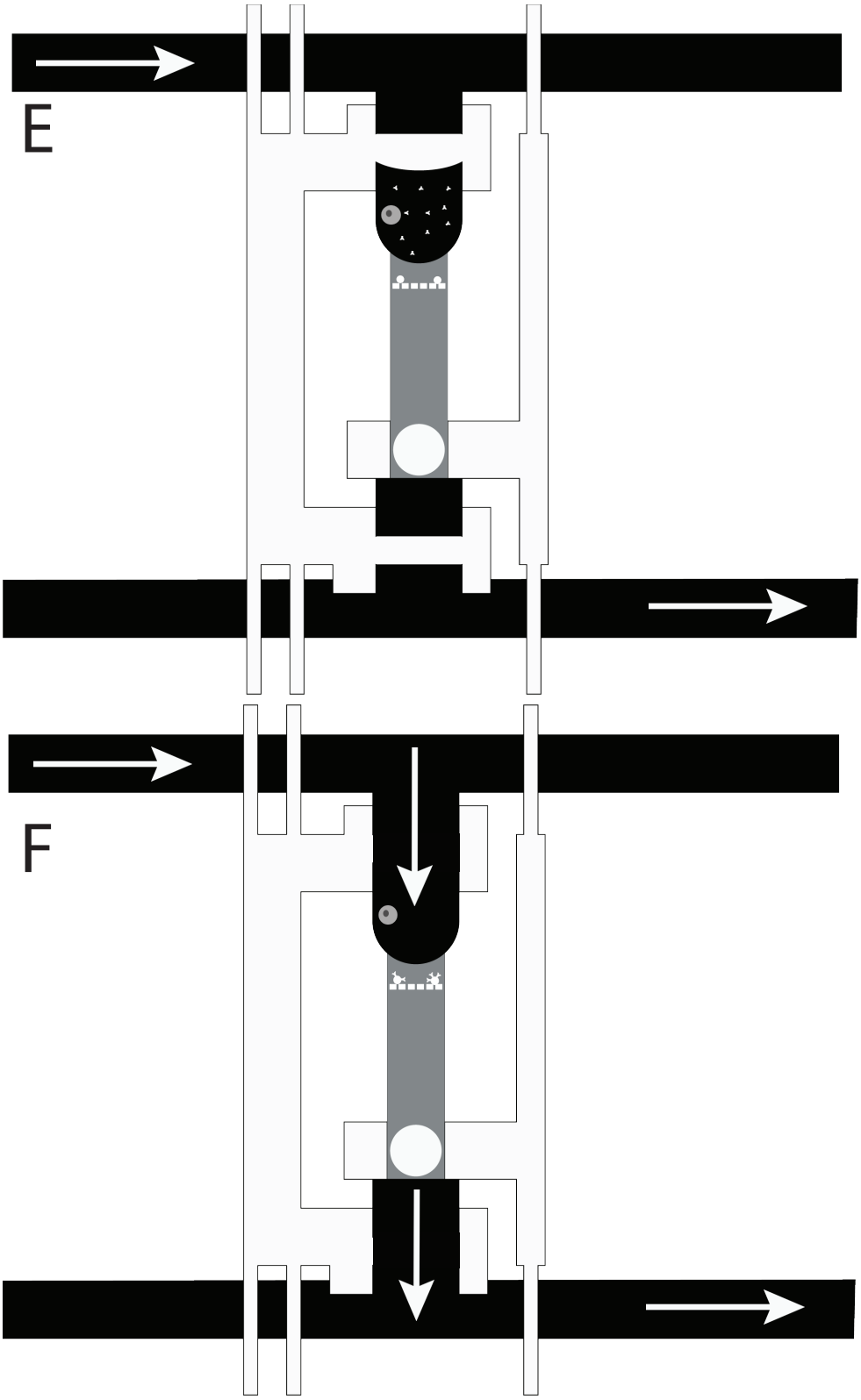

[Figure 4.4 con't - Schematic of microfluidic chamber while performing single-cell antibody screening and selection. See text for details. (Page 3 of 6).]

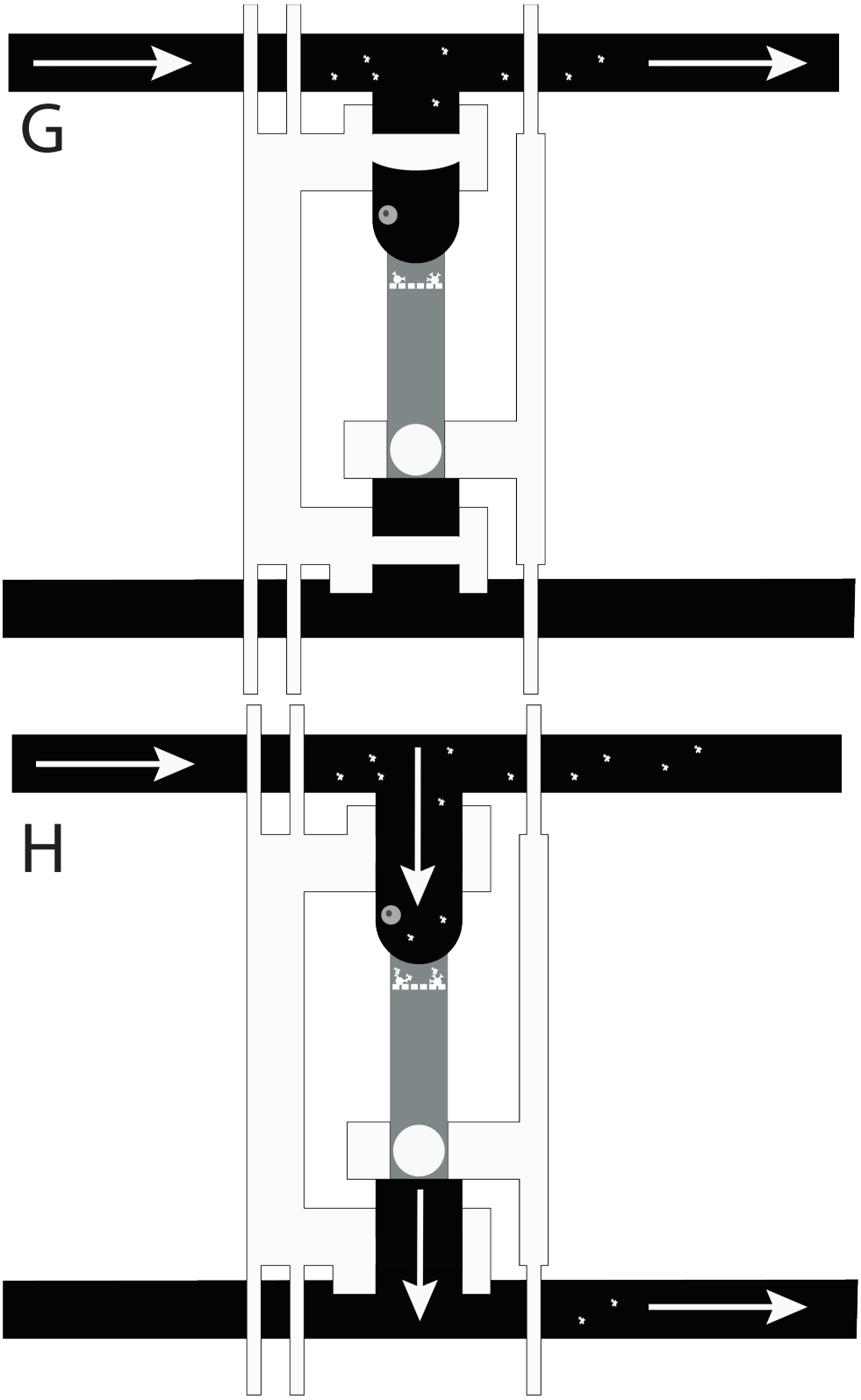

[Figure 4.4 con't - Schematic of microfluidic chamber while performing single-cell antibody screening and selection. See text for details. (Page 4 of 6).]

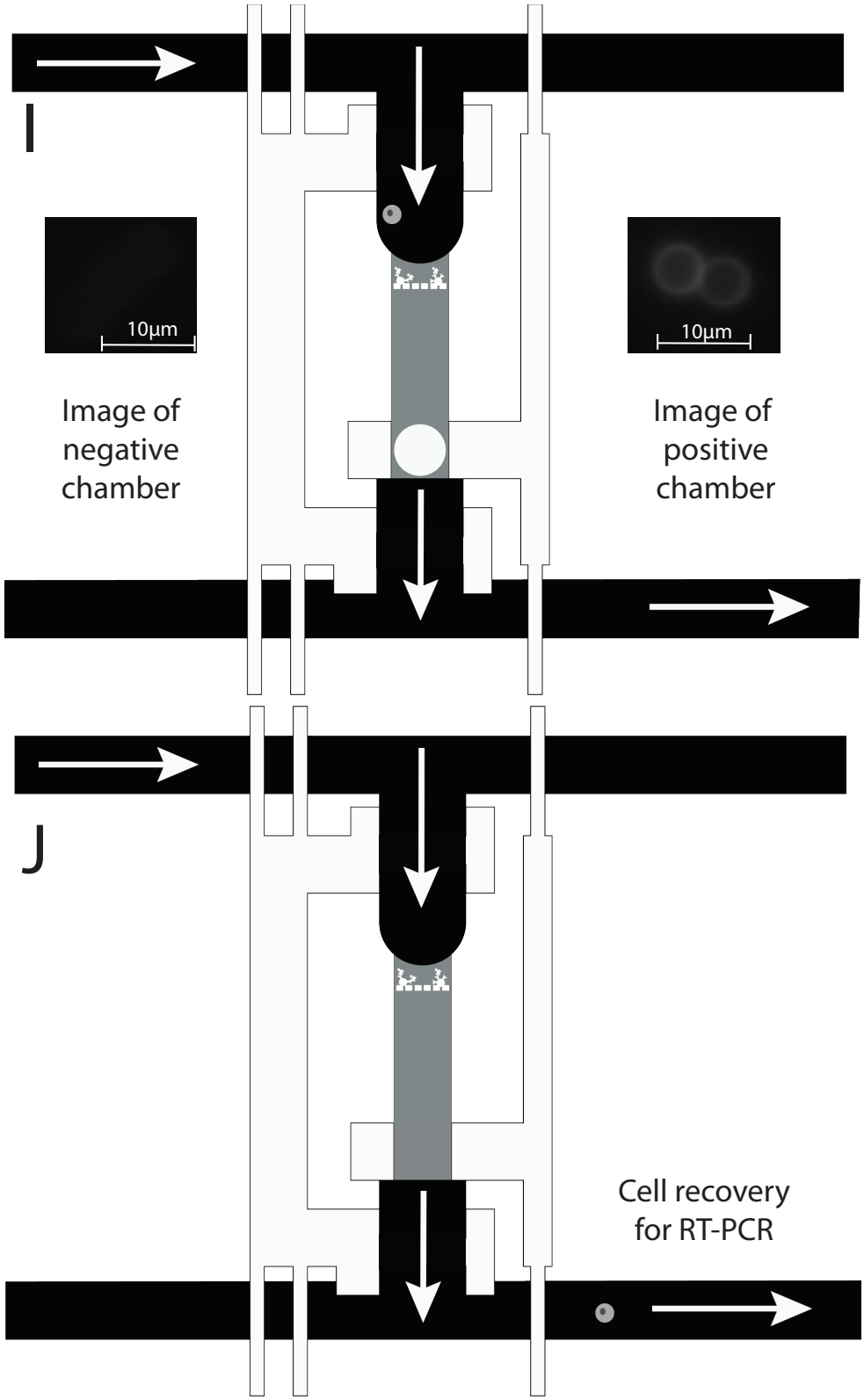

[Figure 4.4 con't - Schematic of microfluidic chamber while performing single-cell antibody screening and selection. See text for details. (Page 5 of 6).]

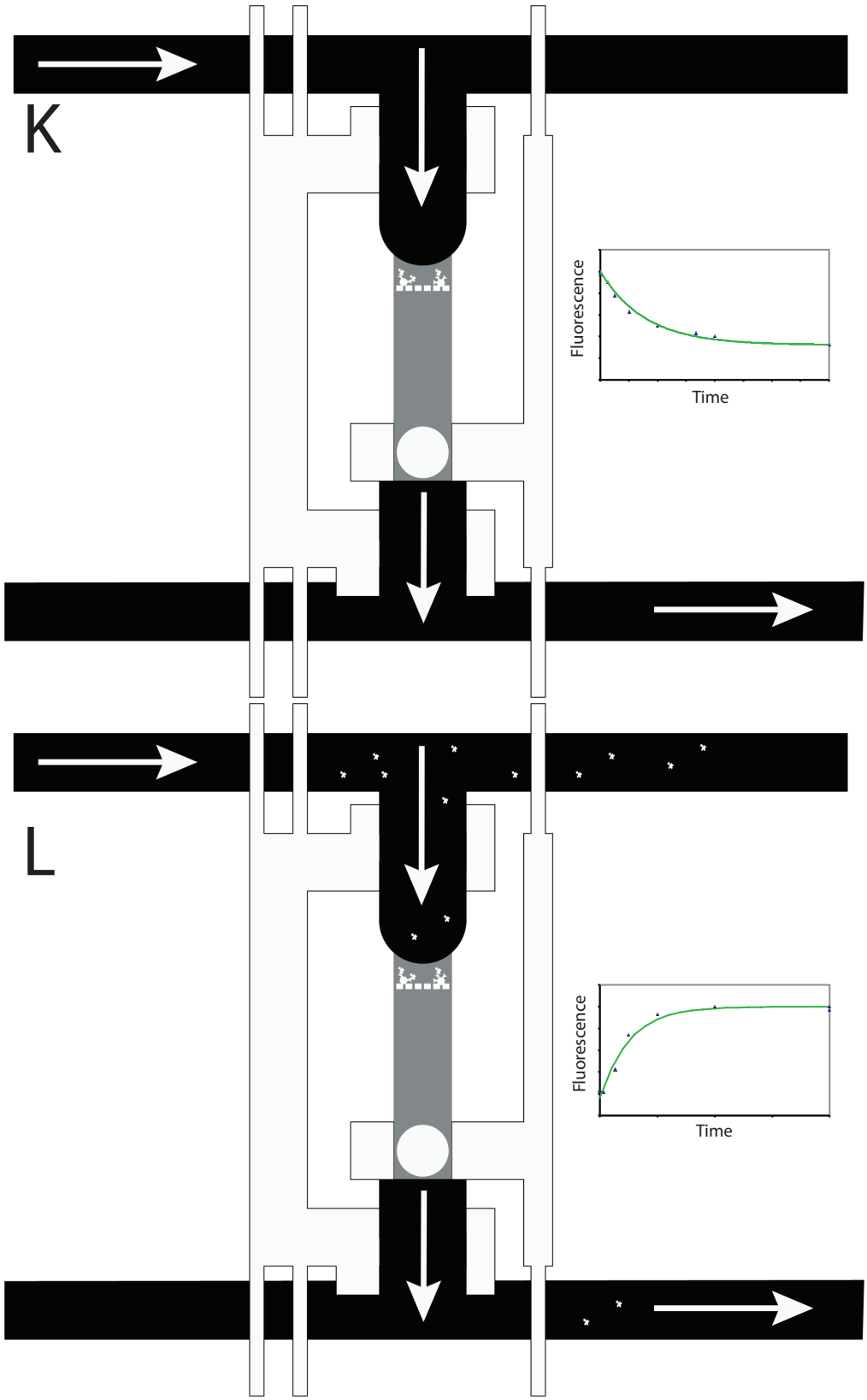

[Figure 4.4 con't - Schematic of microfluidic chamber while performing single-cell antibody screening and selection. See text for details. (Page 6 of 6).]

Bright-field and fluorescence images of all chambers were taken using a Nikon TE200 Eclipse inverted fluorescence microscope equipped with an automated xyz-microscope stage (Prior Scientific), a computer-controlled mechanical shutter (Ludl Electronic Products), a custom LED circuit for bright-field illumination, a 100X oil immersion objective (N.A. 1.30, Nikon Plan Fluor) and an EMCCD camera (Hamamatsu). Fluorescence images were taken using green (470/40 nm excitation, 535/30 nm emission) and red (600/60 nm excitation, 655 nm long-pass emission) fluorescence filter cubes (Chroma Technology). Custom LabView software was developed in order to automate hardware control and image acquisition (Appendix B.1). A custom autofocus algorithm was developed that consisted of taking a series of bright-field images at different focal (z-axis) positions and computing the variance in pixel intensity for each image. The image with maximum variance corresponded to the focal plane at the edge of the bead surface and, along with the known bead diameter, was used to locate the optimal focal position at the center of the beads, as confirmed by the distinctive bead diffraction pattern.

The maximum fluorescence intensity on the antigen-bound beads in each chamber was measured using custom LabView software (Appendix B.2). A fluorescence threshold was selected by computing the average plus two standard deviations of the maximal sorbate fluorescence intensity from multiple control chambers deliberately not loaded with a cell. Chambers with fluorescence intensity higher than this threshold were deemed positive for antigen-specific mAbs (95% confidence interval). Cells from each positive chamber were recovered from the device (i.e. ~1-1.5 hours after

incubation in microfluidic devices) in order to minimize the chances of cell death and mRNA degradation prior to RT-PCR amplification.

Selected cells from chambers deemed positive for antigen-specific mAbs were sequentially eluted in 1X PBS into the output port and manually recovered using a pipette with a gel-loading tip (Figure 4.4J). After each sample was recovered, the elution port was thoroughly washed by repeated pipetting of 1X PBS solution. Cells were directly transferred to 85 μL of Qiagen One-Step RT-PCR reaction mix containing 20 μL of RT-PCR buffer, 42 μL of RNase-free water, 4 μL of dNTPs, and 4 μL of RT and PCR enzymes. Each sample was then split into two equal parts, to which 7.5 μL of forward and reverse primer solutions (8 μM) were added for single-plex amplification of heavy and light chain genes, respectively. RT-PCR amplification was performed using previously-published low degeneracy primers that annealed to mouse V gene leader and constant region sequences[58] (see Appendix A.2 and Chapter 3 for list of primers and discussion of primer design). As roughly 90% of mouse mAbs utilize the kappa (Igκ) light chain, RT-PCR amplification was only performed using primers for the kappa light chain. A mixture of primers was used to amplify heavy chain genes encoding different antibody isotypes (e.g. IgA, IgM, IgG1, IgG2a, etc.). RT-PCR reaction mixes were then transferred to a bench-top thermal cycler for RT-PCR amplification (see Chapter 3, Table 3.2 for cycling protocols).

Following cell recovery, antibody-antigen binding kinetics and selectivity were measured on beads retained in the device using a microfluidic fluorescence bead assay (see Chapter 2). For kinetic measurements, chambers deemed positive for antigen-specific mAbs were first washed with 1X PBS and dissociation kinetics were measured

by time-lapse imaging (Figure 4.4K). Subsequently, each chamber was flushed with a solution of fluorescently labeled antigen (e.g. HEL-Dylight488 conjugate) and time-lapse images were taken to measure association kinetics (Figure 4.4L). Association kinetics were measured one chamber at a time to obtain sufficient time resolution; however, dissociation kinetics were simultaneously measured in multiple chambers (e.g. all chambers in a single column) using automated scanning. As secreted antibodies were irreversibly captured on beads for several days (see Chapter 2, Figure 2.7), measurements of antibody-antigen kinetics and selectivity could be performed for several days after initial mAb capture. Reported error represents the calculated standard deviation of multiple replicate measurements. Values measured only once are reported without error bars.

4.1.4 Sequencing of Antibody Heavy and Light Chain Genes and Recombinant Expression of Selected mAbs

After RT-PCR amplification, reaction products were analyzed by electrophoresis on 1% DNA agarose gels stained with 1X SYBR Safe DNA-binding dye. Amplicons were extracted from the gels by a scalpel and purified using spin columns as per the Qiagen MinElute kit. Samples were eluted from the spin columns in low TE buffer and stored in a -20°C freezer. DNA samples and associated primers were submitted to the Nucleic Acid Protein Service Unit (NAPS, http://www.msl.ubc.ca/services/naps) for standard Sanger sequencing. Each sample was sequenced using both forward 5' (leader region) and 3' reverse (constant region) primers. Heavy and light chain genes from selected anti-HEL mAbs were compared with mouse germline antibody sequences using IMGT

V-quest (http://www.imgt.org/IMGT_vquest/share/textes/). Common sequence differences found between germline genes and amplified genes sequenced using both 5' and 3' primers were labeled as somatic mutations. To ensure that assigned somatic mutations were not generated by polymerase errors during RT-PCR, heavy and light chain genes were amplified and sequenced in triplicate (Figure 4.5). A commercial vendor (Synogene, Inc., http://synogeneinc.com/) performed cloning and recombinant expression of selected mAbs. Briefly, heavy and light chain genes for selected mAbs were cloned into transfection vectors, expressed as whole IgG1 molecules in human embryonic kidney (HEK293) cells, and purified by Protein G affinity chromatography. Purified recombinant mAbs were tested for antigen reactivity using the microfluidic fluorescence bead assay.

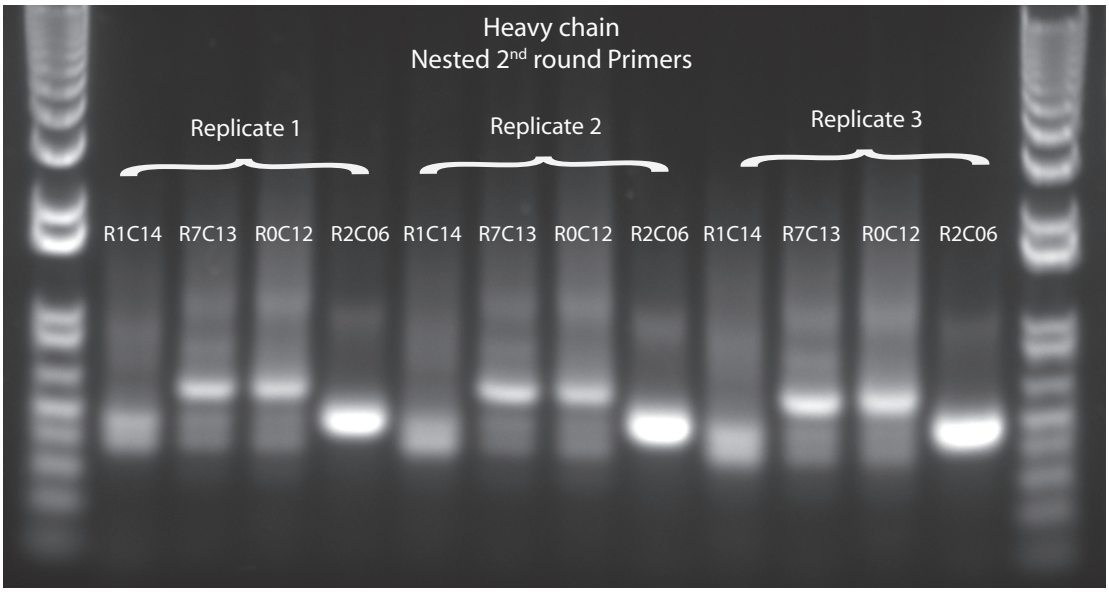

Figure 4.5 Heavy chain genes from four single-cell selected anti-HEL mouse mAbs amplified in triplicate by RT-PCR. All amplicons were extracted and purified for DNA sequencing. Comparison of DNA sequences of amplicons was performed to verify that assigned somatic mutations were not generated by polymerase errors during RT-PCR. RxCy nomenclature designates the row and column address for the microfluidic chamber from which the cells were recovered. Shown is a 1% DNA agarose gel with 100 bp ladder.

4.2 Results

4.2.1 Kinetic Screening and RT-PCR Amplification of Antibody Genes from Single Hybridoma Cells

Single cells from two distinct mouse hybridoma cells lines, D1.3 and HyHEL-5, were loaded into ~1 nL microfluidic chambers in a single device. Binding kinetics and affinities of cell-secreted mAbs measured from multiple single cells of each cell-line were precise to within 30% (Table 4.1), and were accurate when compared with binding data for purified mAbs (see Chapter 2, Table 2.1). Importantly, secreted antibodies were detected from all hybridoma cells loaded into microfluidic chambers. HyHEL-5 cells secreted mAbs that bound HEL with a ~50-fold higher affinity than mAbs secreted by D1.3 cells, as a result of ~5-fold faster association kinetics and ~10-fold slower dissociation kinetics.

Chambers containing D1.3, HyHEL-5 and no cells were sequentially eluted into a common output port on the device, recovered, and subjected to RT-PCR amplification (Figure 4.6). RT-PCR reactions performed on recovered samples from chambers containing cells always yielded amplified antibody genes, whereas no-cell control chambers did not yield any amplification products and DNA sequencing of amplicons confirmed that the correct heavy and light chain genes were amplified from chambers containing distinct hybridoma cells. These experiments therefore show that the described microfluidic device (Figure 4.3) enables highly efficient measurement of antibody-antigen binding kinetics and affinities and selective recovery of single hybridoma cells for robust RT-PCR amplification of antibody genes. These results also suggest that cells were stable

Table 4.1 Antibody-antigen binding kinetics and affinities from single D1.3 and HyHEL-5 hybridoma cells measured by a microfluidic fluorescence bead assay using a HEL-Dylight488 fluorescent conjugate. Results represent the average and standard deviation of replicate measurements performed on multiple distinct D1.3 (n = 30) and HyHEL-5 (n = 5) cells.

Hybridoma	k_{on} ($M^{-1}s^{-1}$)	k_{off} (s^{-1})	K_d (M)
D1.3	$(1.98 \pm 0.32) \times 10^{6}$	$(2.62 \pm 0.48) \times 10^{-3}$	$(1.33 \pm 0.32) \times 10^{-9}$
HyHEL-5	$(9.08 \pm 1.13) \times 10^{6}$	$(1.56 \pm 0.44) \times 10^{-4}$	$(1.71 \pm 0.53) \times 10^{-11}$

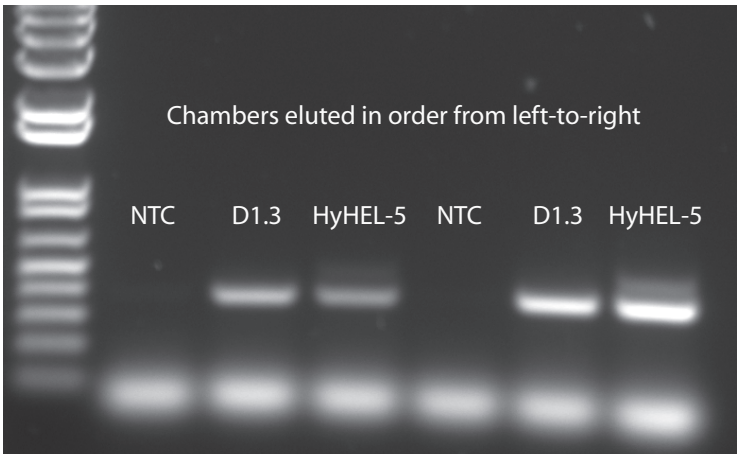

Figure 4.6 Multiplex RT-PCR amplification of antibody heavy and light chain genes from eluted chambers containing no cells (no-template control, NTC), a D1.3 cell, and HyHEL-5 cell. No amplification was observed from eluted chambers containing no cells. Amplified gene products were extracted and purified from the gel and sequenced to confirm that they correspond to the corresponding hybridoma cell-line. Shown is a 1% DNA agarose gel with 100 bp ladder.

4.2.2 Microfluidic Screening and Selection of mAbs from ASCs Purified from Mice Immunized with HEL

The complete microfluidic pipeline for selecting mAbs from single ASCs (Figure 4.1) was demonstrated from mice immunized with the model antigen hen egg lysozyme (HEL). Injection of BALB/c strain mice with HEL resulted in a large expansion of FACS-purified CD138+ mouse splenocytes (50,000 – 150,000 cells per spleen versus <10,000 cells per spleen from unimmunized mice). ELISPOT analyses confirmed that up to 50%

of CD138+ splenocytes secreted IgG antibodies, with roughly half of these cells secreting mAbs that bound HEL. In contrast to BALB/c mice, C57BL/6 strain mice immunized with HEL produced only 2,000-3,000 CD138+ mouse splenocytes, consistent with the fact that HEL fails to elicit the necessary T-cell help to generate a robust antibody response in this strain of mice.[147,148]

CD138+ splenocytes harvested from HEL-immunized BALB/c mice were screened in the microfluidic device for production of anti-HEL mAbs. By sequentially directing flow to each chamber using row and column valves, over 100 single cells were loaded into the chamber array. In contrast, using stochastic cell loading strategies, nearly two-thirds of chambers are typically left with either zero or >1 cells.[51,149] Cells and antibody-capture beads were incubated in the microfluidic chambers for 1 hour in order to ensure successful detection from all cells secreting anti-HEL mAbs. The detection limit of the fluorescence bead assay is ~8×10^4 mAb molecules (see Chapter 2, section 2.4.2); thus, the minimum antibody secretion rate required for detection after a 1-hour incubation is 20 mAb molecules per second assuming all secreted mAbs are captured on a single bead. In practice, both the antibody secretion rate and bead capture efficiency are unknown; however, ASCs are known to secrete thousands of mAb molecules per second under ideal conditions, suggesting that most (if not all) ASCs secreting anti-HEL mAbs would be detected after 1 hour incubation in the microfluidic device.[21,124,150] By comparison, mouse hybridoma cells secrete at least 200 mAbs/second when incubated in microfluidic devices under identical conditions (i.e. room temperature and identical cell culture medium, see Chapter 2, section 2.4.3).

Nearly 200 high-affinity anti-HEL mAbs (190) were identified by microfluidic single-cell screening of CD138+ splenocytes from six different HEL-immunized mice. On average, 30 ± 10% of chambers contained cells secreting anti-HEL mAbs, consistent with frequencies of antigen-specific ASCs measured by ELISPOT (Figure 4.7). The number of chambers containing cells secreting anti-HEL mAbs was increased by iterative re-loading of cells into the device. Specifically, after fluorescent scanning, cells were flushed out of all chambers negative for anti-HEL mAbs and these chambers were re-loaded with new cells. This process can be repeated multiple times to obtain more complete occupancy of chambers with cells secreting anti-HEL mAbs. In this manner, chambers were loaded with cells up to three times in a single experiment, yielding 70 anti-HEL mAbs (63% of chambers) in a single device.

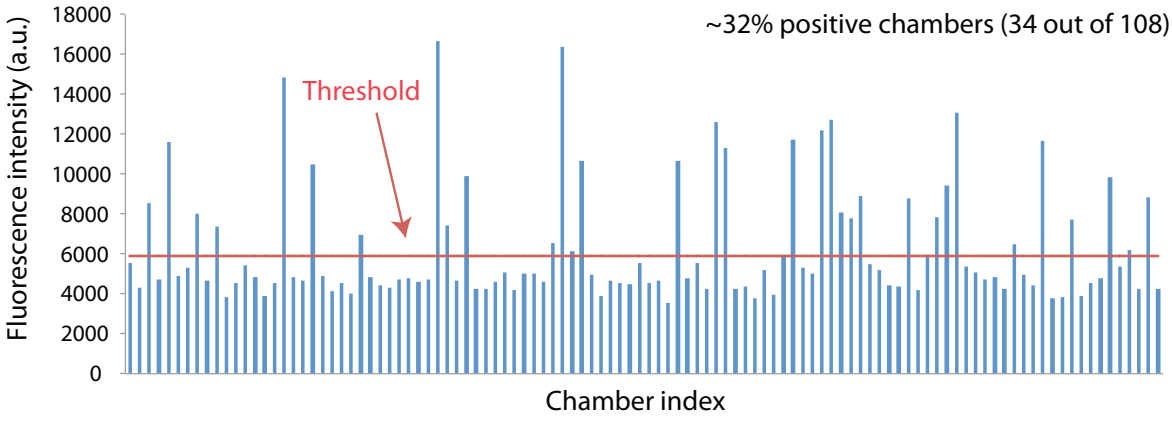

Figure 4.7 Identification of microfluidic chambers containing single cells secreting anti-HEL mAbs. After flushing chambers with fluorescently labeled antigen (i.e. 14.3nM HEL-Dylight488 conjugate), high-resolution fluorescence imaging of all chambers is performed. The maximum fluorescence bead intensity in each chamber is measured and a threshold is set equal to 2 standard deviations larger than the average fluorescence of no-cell control chambers (95% confidence interval).

A single device yielded a comparable number (~50) of antigen-specific mAbs to a single hybridoma fusion without the weeks of clonal expansion and sub-cloning required in the latter process. Indeed, the number of anti-HEL mAbs identified using the microfluidic single-cell screening (190) is approximately two-fold larger than all anti-HEL mAbs generated by hybridoma methods and previously reported reported in the literature.[114,146]

In addition, the microfluidic single-cell screening approach was found to identify antigen-specific mAbs from single ASCs with higher efficiency and throughput than recently described single-cell micro-well screening approaches.[51,90] Papa et al. identified 14 single cells secreting antigen-specific (i.e. anti-ovalbumin, anti-OVA) IgG mAbs out of 18,000 single cells harvested from antigen-immunized mice and stimulated in culture for 3 days prior to screening in micro-engraved wells.[90] Similarly, using micro-fabricated wells and a fluorescence immunospot assay (ISAAC), 27 single cells secreting anti-HEL mAbs were detected after screening 10,000 ASCs from HEL-immunized mice. The ~100-fold difference in measured frequency of ASCs secreting anti-HEL mAbs (0.27% of cells using ISAAC versus 30% in the microfluidic device) is attributed to increased sensitivity and a lower detection limit of the microfluidic fluorescence bead assay as compared with ISAAC.[51,112] Consistent with this notion, the ISAAC method detected as few as 15% of single hybridoma cells secreting high affinity ($K_d \sim 200$ pM) anti-HEL mAbs.[51] It is unlikely that the discrepancy in frequencies measured by microfluidic screening versus ISAAC is caused by differences in the purity of antigen-specific ASCs in the enriched cell fraction as both approaches screened

similar cell populations, namely CD138+ plasma cells from the spleen of HEL-immunized mice.

Anti-HEL mAbs were detected by microfluidic screening of CD138+ mouse splenocytes when stored for 36 hours post-harvest at 4°C in standard cell medium (i.e. Gibco RPMI 1640 medium with 10% fetal calf serum and 0.5% mercaptoethanol). A similar frequency of chambers containing antigen-specific ASCs were detected when comparing CD138+ mouse splenocytes screened either 4 hours or 36 hours post-harvest (30% of chambers versus 21%, respectively). As one round of microfluidic single-cell mAb screening can be performed in less than 4 hours, hundreds of antigen-specific mAbs can be identified from a single animal by using multiple devices to repeatedly screen ASCs stored for 1-2 days post-harvest. Corti et al. recently reported that ASCs can be maintained in culture for up to a week using cell medium supplemented with exogenous cytokines (e.g. IL-6) that promote plasma cell survival.[150] Thus, in principle, ASCs harvested and maintained in culture can be subjected to dozens of microfluidic antibody screens over several days in order select thousands of antigen-specific mAbs from a single animal.

4.2.3 Antibody-Antigen Binding Kinetics and Affinities of Novel Anti-HEL Mouse mAbs

Naturally-occurring antibodies are known to bind target antigens with affinities spanning up to five orders of magnitude (K_d values between 10 μM and 100 pM);[93] however, most mAbs used for research and therapeutic applications bind with moderate to high binding affinities (K_d < 10 nM).[151] Average K_d, k_{on} and k_{off} values for

anti-HEL mAbs selected using the microfluidic single-cell approach were 2.8nM, 3.4×10^{6} $M^{-1}s^{-1}$ and 5.3×10^{-3} s^{-1} (Table 4.2), respectively. Notably, over 80% and 90% of anti-HEL mAbs (60 to 65 out of 70) characterized in the microfluidic device had K_d values less than 10 nM and on-rate constants greater than 10^{6} $M^{-1}s^{-1}$, respectively (Figure 4.8). By contrast, in a sample of 23 hybridoma-generated anti-HEL mAbs, only 2 mAbs (<10%) were found to bind HEL with on-rate constants greater than 10^{6} $M^{-1}s^{-1}$.[114,152]

Microfluidic selection of anti-HEL mAbs was biased against K_d values greater than 10nM (i.e. low-affinity mAbs) by flushing the chamber array with a low concentration of fluorescent antigen (e.g. 214 ng/mL or 14.3 nM of HEL-Dylight488 conjugate) prior to imaging (see Chapter 2, equation 2.2). Similarly, by flushing chambers with a 14.3 nM concentration solution of HEL-Dylight488 conjugate for a short time period (e.g. 5 min), selection was biased against anti-HEL mAbs with on-rate constants less than 10^{6} $M^{-1}s^{-1}$ (see Chapter 2, equation 2.3). Thus, by carefully selecting the fluorescent antigen concentration and loading time, mAb selection was biased toward particular kinetic and equilibrium binding constants. Importantly, the above-reported frequency of antigen-specific ASCs (~30%) is likely an underestimate as it accounts only for cells secreting moderate to high-affinity anti-HEL mAbs (K_d < 10 nM). Goldbaum et al. reported that approximately 20% of hybridoma-generated anti-HEL mouse mAbs bound HEL with equilibrium dissociation constants (K_d) ranging from 10 nM to ~100 nM.[114] Thus, accurate frequencies of antigen-specific ASCs can be determined by using microfluidic single-cell screening with high antigen concentrations

(e.g. ~100 nM) for longer periods of time (e.g. 1 hour) to detect both low and high affinity anti-HEL mAbs.

Foote and Milstein proposed that clonal selection of B cells is influenced by both kinetic and equilibrium binding properties, with a premium placed on B cells expressing mAbs that bind target antigens rapidly (i.e. high k_{on}).[20] For this reason, it is often assumed that k_{off} values are highly correlated to equilibrium K_d values, with on-rate constants confined to a narrow range of values.[153] In sharp contrast to this assumption, no correlation was observed between K_d, k_{on} and k_{off} values for anti-HEL mAbs selected using the microfluidic single-cell approach (Figure 4.9) Selected anti-HEL mAbs exhibited equilibrium and kinetic rate constants both spanning ~2 orders of magnitude, with K_d values ranging from ~100 pM - 10 nM, k_{on} values ranging from ~10^5-10^7 $M^{-1}s^{-1}$, and k_{off} values ranging from ~5×10^{-4}-10^{-2} s^{-1} (Table 4.2). Furthermore, this large diversity of kinetic (on-rate and off-rate) and equilibrium dissociation constants was observed in mAbs from multiple different HEL-immunized mice (Table 4.3). Collectively, anti-HEL mouse mAbs selected by microfluidic screening and hybridoma methods exhibit a 2 to 3 order of magnitude range in k_{on} (10^4 - 10^7 $M^{-1}s^{-1}$), k_{off} (10^{-2} - 10^{-4} s^{-1}) and K_d (10^7 - 10^{10} M) values,[114] demonstrating that affinity maturation can significantly alter both on-rate and off-rate kinetics.

The highest-affinity anti-HEL mAbs selected by microfluidic single-cell screening exhibited K_d values as low as ~100 pM, consistent with the theoretical affinity "ceiling" resulting from physiological constraints of the adaptive immune system.[93] The maximum on-rate constants of antibody-antigen interactions are governed by the diffusion limit and stringent geometric requirements for antibody-antigen binding.[93,96]

For antibody interactions with small molecule haptens, on-rate constants as large as 10^8 $M^{-1}s^{-1}$ have been observed.[20,93,154] As protein molecules are approximately ten-fold larger in size than hapten molecules and, thus, have ten-fold smaller diffusion constants,[118,155] diffusion-limited on-rate constants of antibody interactions with protein antigens would be approximately 10^7 $M^{-1}s^{-1}$ (see Chapter 2, equations 2.5 and 2.6). Indeed, three microfluidic-selected mAbs bound HEL with k_{on} values ranging from 1×10^7 $M^{-1}s^{-1}$ – 2.5×10^7 $M^{-1}s^{-1}$, comparable to the fastest binding anti-HEL mAbs previously generated by hybridoma methods (HyHEL-5 and HyHEL-10).[156]

As cellular endocytosis typically occurs on the time scale of several minutes, it has been postulated that the clonal selection process cannot discriminate between B cells producing antibodies that bind antigen with interaction half-lives greater than one hour (i.e. $k_{off} < 10^{-4}$ s^{-1}).[93] Consistent with this notion, the smallest off-rate constant observed amongst all selected anti-HEL mAbs was 5.7×10^{-4} s^{-1}, corresponding to a half-life of ~20 min for the antibody-antigen complex. Of the 200 - 300 anti-HEL mouse mAbs generated by both microfluidic single-cell screening and the hybridoma method, less than a handful of mAbs bind HEL with an off-rate constant less than 10^{-4} s^{-1}.[105,114] The rarity of such mAbs is consistent with the fact that B cells can stochastically generate mAbs with very low off-rate constants, but that the adaptive immune system does not positively select these cells over other B cells producing high-affinity mAbs with $k_{off} > 10^{-4}$ s^{-1}.[93]

Table 4.2 Measured antibody-antigen binding kinetics and affinities from over 70 anti-HEL mAbs selected using the microfluidic single-cell screening approach.

	k_{on} ($M^{-1}s^{-1}$)	k_{off} (s^{-1})	K_d (M)
Average	3.4×10^{6}	5.3×10^{-3}	2.8×10^{-9}
Maximum	2.5×10^{7}	3.0×10^{-2}	1.7×10^{-8}
Minimum	2.7×10^{5}	5.7×10^{-4}	1.4×10^{-10}
Fold-variation (Max/Min)	93	51	120

Table 4.3 Range of kinetic and equilibrium rate constants for anti-HEL mAbs selected using the microfluidic single-cell screening approach from three different HEL-immunized BALB/c mice.

	k_{on} ($M^{-1}s^{-1}$)		k_{off} (s^{-1})		K_d (M)	
Mouse	**Max**	**Min**	**Max**	**Min**	**Max**	**Min**
M1	6.9×10^{6}	1.7×10^{6}	4.0×10^{-3}	5.8×10^{-4}	7.8×10^{-10}	1.4×10^{-10}
M2	2.5×10^{7}	5.5×10^{5}	3.0×10^{-2}	7.8×10^{-4}	2.9×10^{-9}	7.8×10^{-10}
M3	7.7×10^{6}	2.7×10^{5}	2.3×10^{-2}	9.5×10^{-4}	1.7×10^{-8}	2.7×10^{-9}

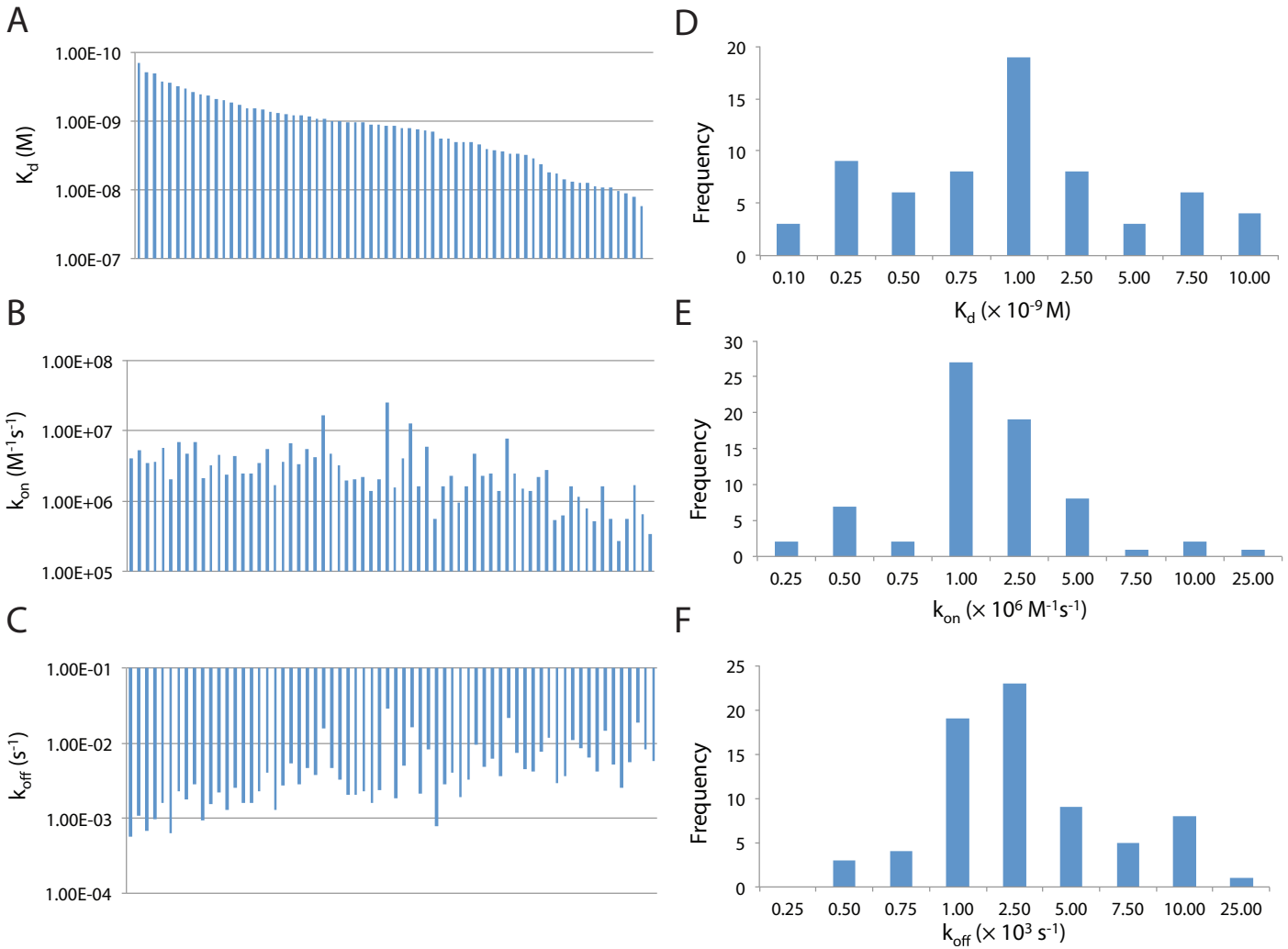

Figure 4.8 Measured binding kinetics and affinities from ~70 anti-HEL mAbs selected by microfluidic single-cell screening. Equilibrium dissociation constants (A), on-rate constants (B), and off-rate constants (C) plotted in rank order of affinity, as well as histograms of these binding constants (D-F).

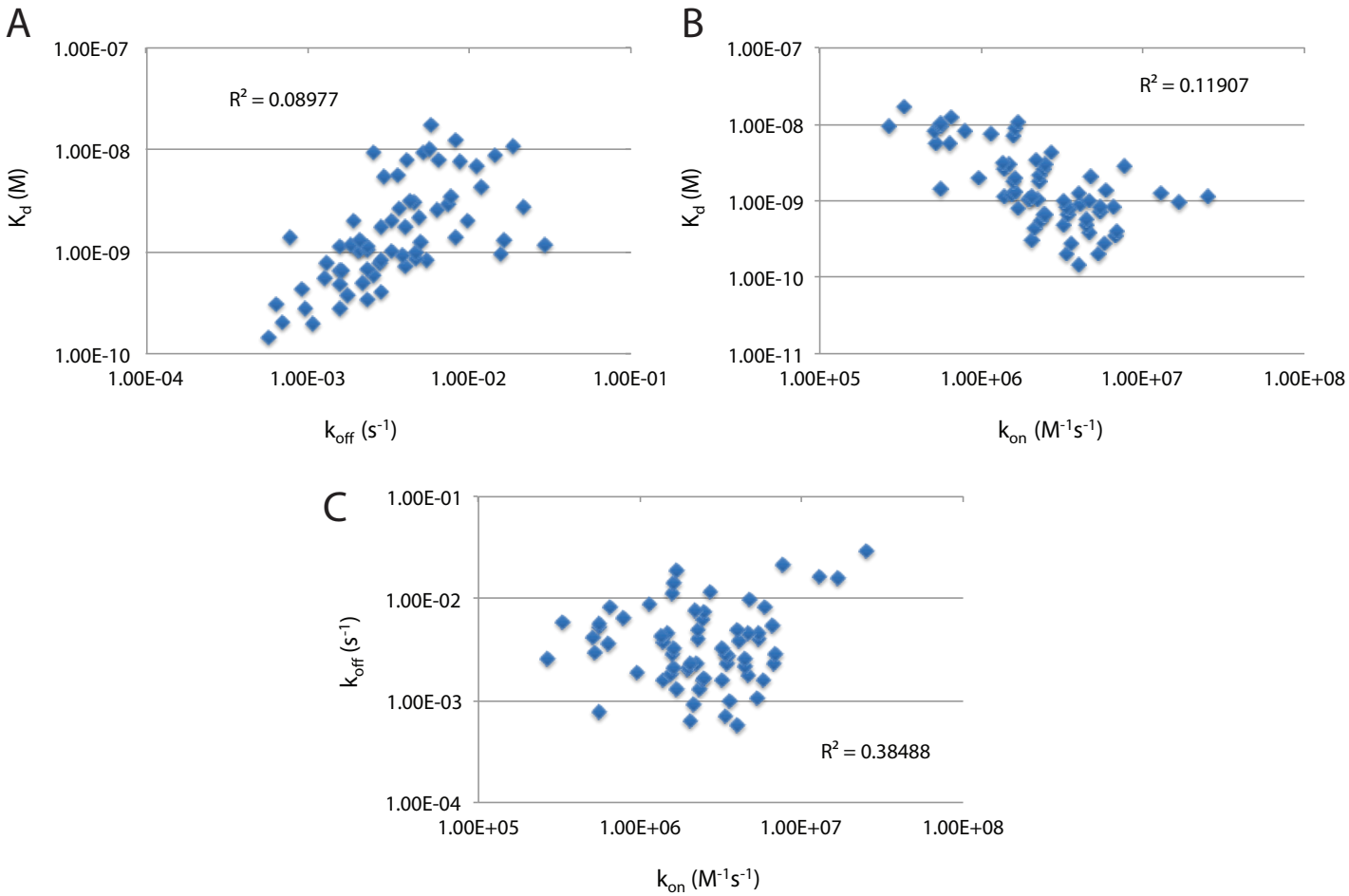

Figure 4.9 No correlation observed between equilibrium and kinetic binding rate constants for over 70 anti-HEL mAbs selected by microfluidic single-cell screening. R^2 values correspond to linear regression of the plotted data.

4.2.4 Analysis of Heavy and Light Chain Genes from Novel Anti-HEL Mouse mAbs

ASCs secreting anti-HEL mAbs were selectively recovered from microfluidic devices in order to perform single-cell RT-PCR amplification of heavy and light chain genes (Figure 4.10). In total, 75 ASCs secreting anti-HEL mAbs were selectively recovered from microfluidic devices and subjected to RT-PCR for both heavy and light chain genes. These reactions yielded 48 Igκ and 24 IgH genes, corresponding to RT-PCR success rates of 64% and 32%, respectively. Both heavy and light chain genes were amplified for 18 anti-HEL mAbs (24% of recovered ASCs). These RT-PCR success rates were comparable to previously reported success rates (20-40%) for amplification of antibody genes from single mouse B cells in RT-PCR tubes.[58]

VDJ gene usage was analyzed for heavy and light chain genes from selected anti-HEL mAbs. Kappa chains were encoded by 22 unique V_κ genes, representing 9 out of the 16 distinct mouse Igκ gene families[58] (Figure 4.11). Heavy chain gene usage was considerably less diverse than kappa chain gene usage, with 14 unique V_H genes amplified, representing only 4 out of 16 out of mouse IgH gene families[58]. A large fraction of amplified heavy chain genes (35%) belonged to the V_H1 gene family, consistent with a previous report that this gene family accounted for nearly 75% of heavy chain genes produced in mouse B cells.[58] The diversity (D) and junction (J) regions of selected anti-HEL mAbs were encoded by 4 out of 10 D gene families, and all four J_H and J_κ gene families, respectively.

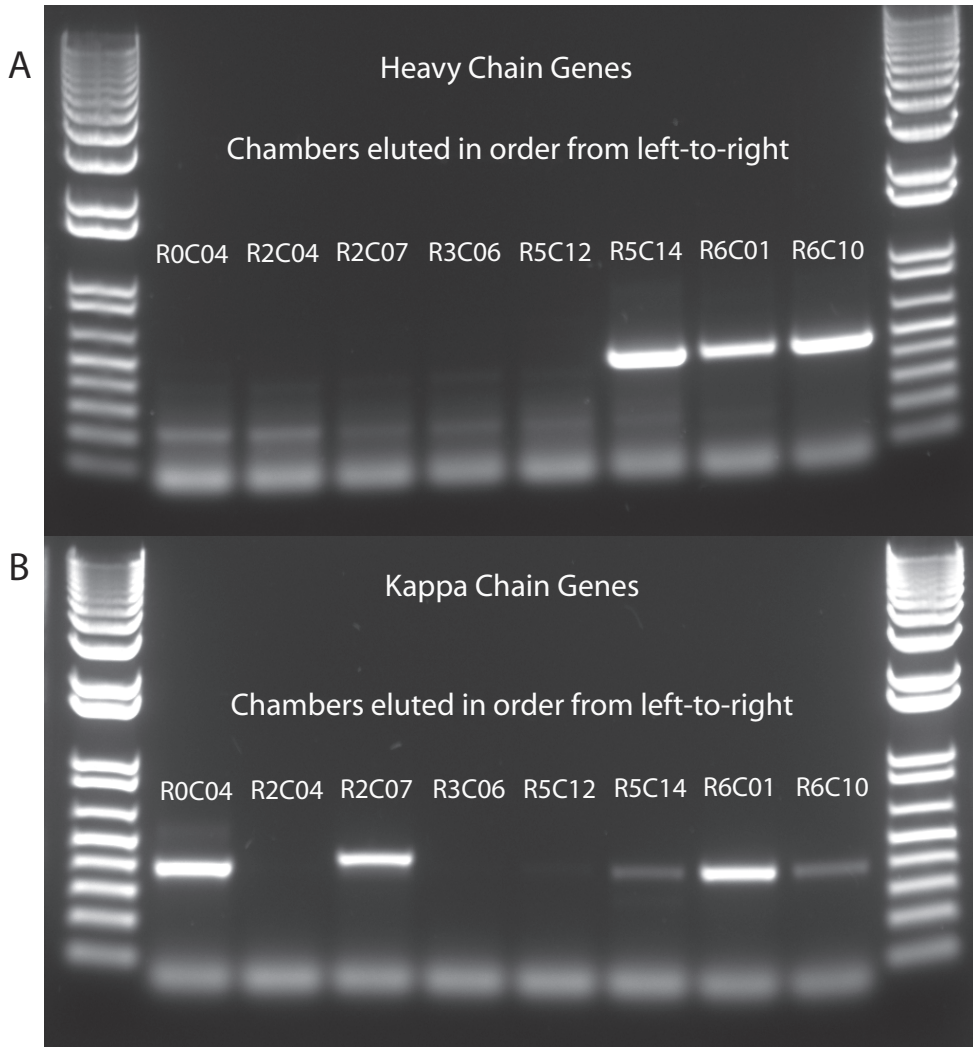

Figure 4.10 Single-cell RT-PCR amplification of antibody heavy and light chain genes from ASCs secreting anti-HEL mAbs. Cells are sequentially recovered from the microfluidic device (left-to-right). RxCy nomenclature designates the row and column address for the microfluidic chamber from which the cells were recovered. Shown is a 1% DNA agarose gel with 100 bp ladder.

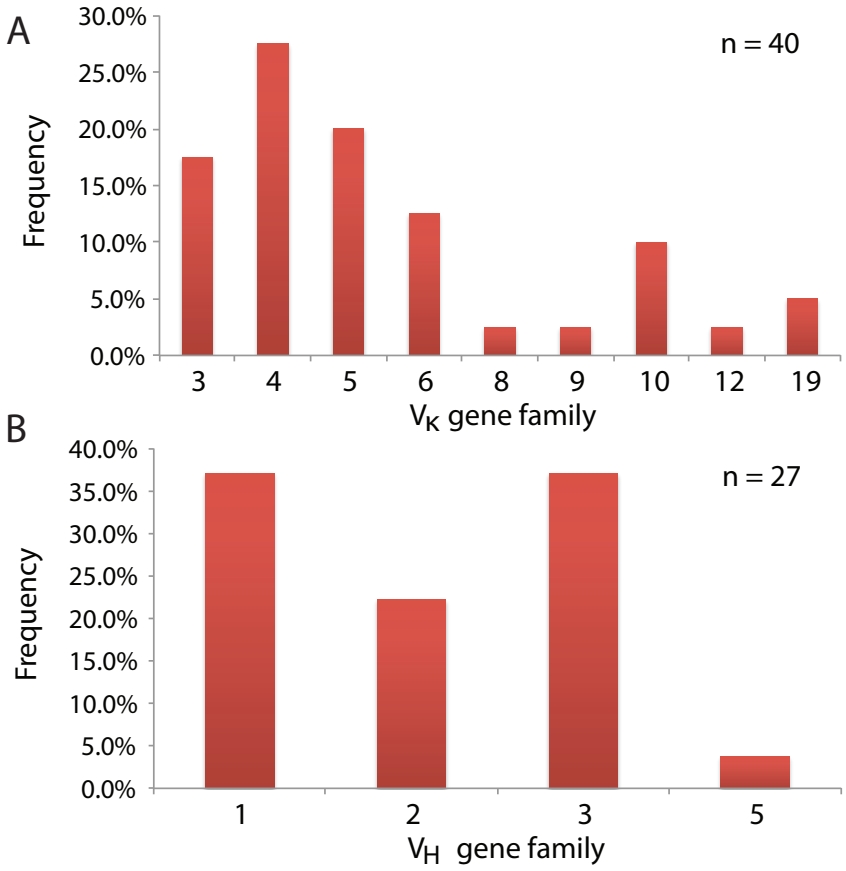

Figure 4.11 Light (A) and heavy (B) chain gene usage for anti-HEL mouse mAbs selected by microfluidic single-cell screening.

Although selected anti-HEL mAbs were encoded by a greater diversity of kappa chain genes, heavy chain genes were more highly mutated than kappa chain genes. The mean homologies of kappa and heavy chain sequences to their respective germline genes were 96.7% and 93.2%, corresponding to approximately 9 and 20 somatic DNA mutations per gene, respectively. These mutations produced an average of 2.6 and 7.3 amino acid substitutions per kappa and heavy chain, respectively. Whereas the most heavily mutated heavy chain contained 15 amino acid substitutions, the most heavily mutated kappa chain contained only 5 substitutions. Surprisingly, 20% of all amino acid substitutions involved serine substitutions to asparigine (N), arginine (R), or glycine

(G). It is unclear whether somatic mutation favoured serine substitutions or whether these substitutions are functionally significant for facilitating mAb binding to the HEL protein. Serine substitutions have previously been used to to modulate the hydrophobicity of the antibody binding pocket.[157]

Interestingly, no correlation was observed between the degree of mutation of antibody heavy and kappa chains and the binding kinetics or affinities of the corresponding anti-HEL mAbs (Table 4.4). As a corollary, multiple high-affinity anti-HEL mAbs consisted of heavy or light chains completely homologous to germ-line sequences. Similarly, comparing two anti-HEL mAbs previously generated by hybridoma methods (HyHEL-8 and HyHEL-10), HyHEL-8 mAb binds HEL with a 5-fold lower affinity than HyHEL-10 despite being encoded by the same kappa and heavy chain genes and having more than twice the number of amino acid substitutions (17 versus 7, respectively).[152] It thus appears that HEL-immunized BALB/c mice generate several different (near) germ-line-encoded antibodies that bind antigen with high affinity. This observation is consistent with past studies that found that the average avidity of anti-HEL mAbs did not increase during the immune response in HEL-immunized mice, and that affinities and association rate constants of anti-HEL mAbs were independent of the number of immunizations and immunization dosages.[114,146]

Table 4.4 Binding kinetics, affinities, VDJ gene usage and number of amino acid (AA) substitutions in kappa and heavy chain gene sequences for select subset of selected anti-HEL mAbs. (n/a = not amplified, i.e. the corresponding kappa or light chain gene did not amplify by RT-PCR). [continued on next page]

mAb	k_{on} ($\times 10^{6}$ $M^{-1}s^{-1}$)	k_{off} ($\times 10^{-3}$ s^{-1})	K_d ($\times 10^{-9}$ M)	V_k gene	J_k gene	AA (Kappa)	AA (total)
M3_R03C04	3.6	1.0	0.3	IGKV5-48*01	IGKJ1*01	2	-
M3_R06C03	2.1	0.6	0.3	IGKV3-2*01	IGKJ2*01	0	-
M1_R05C14	3.8	2.8	0.7	IGKV5-43*01	IGKJ2*01	3	10
M1_R06C01	3.6	2.9	0.8	IGKV5-39*01	IGKJ2*01	1	8
M2_R00C03	4.4	3.8	0.9	n/a	n/a	-	-
M2_R07C08	2.4	2.3	1.0	IGKV4-74*01	IGKJ1*01	3	13
M2_R07C06	6.5	8.3	1.3	IGKV4-74*01	IGKJ1*01	4	19
M2_R01C08	0.6	0.8	1.3	IGKV3-12*01	IGKJ2*01	5	10
M2_R06C08	2.6	4.9	1.9	IGKV19-93*01	IGKJ2*01	4	10
M1_R06C10	1.8	4.5	2.5	IGKV5-43*01	IGKJ2*01	1	7
M1_R00C04	1.7	4.3	2.6	IGKV10-96*01	IGKJ4*01	2	9
M1_R02C07	3.0	1.9	6.3	IGKV8-21*01	IGKJ1*01	3	-

Table 4.4 [continued from previous page] – For clarity, information on binding kinetics, affinities, and total AA substitutions is repeated on both pages.

mAb	k_{on} ($\times 10^{6}$ $M^{-1}s^{-1}$)	k_{off} ($\times 10^{-3}$ s^{-1})	K_d ($\times 10^{-9}$ M)	V_H gene	D_H gene	J_H gene	AA (Heavy)	AA (total)
M3_R03C04	3.6	1.0	0.3	n/a	n/a	n/a	-	-
M3_R06C03	2.1	0.6	0.3	IGHV3-8*02	-	IGHJ4*01	-	-
M1_R05C14	3.8	2.8	0.7	IGHV3-8*02	IGHD4-1*01	IGHJ2*01	7	10
M1_R06C01	3.6	2.9	0.8	IGHV2-9-1*01	IGHD4-1*02	IGHJ4*01	7	8
M2_R00C03	4.4	3.8	0.9	IGHV3-8*02	-	IGHJ3*01	3	-
M2_R07C08	2.4	2.3	1.0	IGHV3-8*02	-	IGHJ3*01	10	13
M2_R07C06	6.5	8.3	1.3	IGHV1S81*02	-	IGHJ1*01	15	19
M2_R01C08	0.6	0.8	1.3	IGHV3-8*02	-	IGHJ3*01	5	10
M2_R06C08	2.6	4.9	1.9	IGHV3-8*02	-	IGHJ3*01	6	10
M1_R06C10	1.8	4.5	2.5	IGHV3-8*02	IGHD4-1*02	IGHJ2*01	6	7
M1_R00C04	1.7	4.3	2.6	IGHV1S130*01	IGHD2-4*01	IGHJ4*01	7	9
M1_R02C07	3.0	1.9	6.3	n/a	n/a	n/a	-	-

Several V_H and V_κ genes encoded multiple distinct anti-HEL mAbs. Most notably, the V_H3-8 gene accounted for 80% of sequences assigned to the V_H3 gene family and nearly 30% (8 out of 27) of all amplified heavy chain genes. In contrast, the entire V_H3 gene family accounted for only ~5% of heavy chains amplified from hundreds of B cells harvested from unimmunized mice.[58] Similarly, multiple selected anti-HEL mAbs contained light chains encoded by the V_κ3-2, V_κ4-61, V_κ4-74, V_κ5-39, V_κ5-43, V_κ10-96, and V_κ19-93 genes. Of these, the V_κ5-43 encoded light chains for the greatest number of distinct anti-HEL mAbs (5). Anti-HEL mAbs with the V_H3-8 heavy chain were paired with kappa chains encoded by five different V_κ gene families, whereas anti-HEL mAbs encoded by the V_κ5-43 light chain gene were paired with heavy chains encoded by three different heavy chain genes (V_H1-9, V_H3-8, and V_H5-4).

Interestingly, the V_H3-8 and V_κ5-43 genes also encode multiple anti-HEL mAbs previously generated by hybridoma methods (Table 4.5). The V_H3-8 and V_κ5-43 genes encode respective heavy and light chains for the HyHEL-10, HyHEL-8, HyHEL-26, and HyHEL-63 anti-HEL mAbs.[152] The V_κ5-43 gene encodes an additional two hybridoma-generated anti-HEL mAbs (D44.1 and F10.6.6) paired with a heavy chain encoded by the V_H1-9 gene (Table 4.5). The significant over-representation of anti-HEL mAbs encoded by one or both of the V_κ5-43 and V_H3-8 genes suggests that the corresponding heavy and light chains serve as structurally complementary scaffolds to the HEL protein, thus yielding high-affinity anti-HEL mAbs.

Anti-HEL mAbs encoded by identical V_κ5-43 and V_H3-8 genes displayed a diverse range of binding kinetics and affinities despite being 90-95% homologous in amino acid sequence (Figure 4.12 and Table 4.6). For example, the HyHEL-10 and HyHEL-26 mAbs

bind HEL with a 10-fold difference in binding affinity, despite the fact that HyHEL-26 contains identical amino acid residues to HyHEL-10 at all but one position (in the kappa chain CDR1 region) known to contact HEL at the HyHEL-10/HEL binding interface (Figure 4.12).[152] Similarly, the M1_R05C14 and M1_R06C10 mAbs, which are also encoded by the V_H3-8 and V_κ5-43 genes, bind HEL with a 3-fold difference in binding affinity, while having only four total amino acid differences in both heavy and light chain CDR regions. The existence of multiple amino acid substitutions in the 1st and 2nd heavy chain framework regions of otherwise homologous anti-HEL mAbs with distinct binding affinities and kinetics (Figure 4.12 and Table 4.5) indicates that residues at these positions may either be present at the antibody-antigen contact interface or induce functionally-significant changes to the antibody structural scaffold.[117] Taken together, these observations are consistent with the fact that relatively few amino acid substitutions can significantly alter antibody-antigen binding kinetics, affinities, and specificities.[114,152] Indeed, a single amino acid substitution can theoretically alter antibody-antigen binding affinity by up to 3 orders of magnitude if it abolishes or generates a new hydrogen bond at the binding interface.[114]

Many amino acid substitutions in both framework and CDR regions were found to be common between anti-HEL mAbs encoded by identical V_κ and V_H genes (Figure 4.12). For example, the glycine (G) to aspartic acid (D) substitution observed at position 37 (IMGT) in H-CDR1 of HyHEL-10, HyHEL-8, and HyHEL-26 mAbs was observed in half (4 out of 8) of newly selected anti-HEL mAbs encoded by the V_H3-8 gene. Similarly, the serine (S) to glycine (G) conversion at position 36 (IMGT) in the K-CDR1 of HyHEL-10 and HyHEL-8 mAbs was conserved in 2 out of 4 newly selected mAbs encoded by the

V_κ5-43 gene. Interestingly, identical somatic mutations even in highly homologous antibodies had significantly different effects on mAb binding affinity. Of the newly selected high-affinity anti-HEL mAbs encoded by the V_H3-8 gene, half (4 out of 8) contained the germ-line alanine (A) residue at position 103 in the H-CDR3 region, whereas the other half contained a mutated aspartic acid (D) residue also found in the HyHEL-10 mAb (Figure 4.12). Reversion of the D to A amino acid substitution in the HyHEL-10 mAb was previously shown to reduce its binding affinity for HEL by nearly 4 orders of magnitude (9000-fold).[158] In contrast, newly selected mAbs containing the alanine germ-line residue were capable of binding HEL with sub-nanomolar binding affinities; for instance, the M3_R06C03 mAb binds HEL with K_d equal to ~300 pM (Table 4.5). Thus, mAbs encoded by identical V_κ and V_H genes may contain similar heavy and kappa chain scaffolds, but likely have functionally distinct binding epitopes governed by context-specific somatic mutations unique to each mAb.

As the heavy chain CDR3 (H-CDR3) region is the site for VDJ recombination, this region typically contains the greatest sequence diversity in the antibody molecule.[159] Consistent with this fact, the H-CDR3 region contained the greatest sequence diversity in all anti-HEL mAbs encoded by the V_H3-8 gene (Figure 4.12). The highest affinity anti-HEL mAb selected by microfluidic single-cell screening contained an identical CDR3 region to the high-affinity HyHEL-10 mAb. In contrast, the CDR3 sequences most divergent from the HyHEL-10 mAb were found in the lowest affinity anti-HEL mAbs (HyHEL-26 and D44.1) and the X25 mAb, which is encoded by the same V_κ and V_H genes but binds the hapten dinitrophenyl (DNP) and not HEL. The X25 mAb contains germ-

line residues in all CDR regions other than H-CDR3, implicating sequence differences in the H-CDR3 region as a primary determinant for mAb binding specificity.[152,159]

The discovery of nearly identical mAbs generated from different HEL-immunized mice was a particularly surprising result. Of the eight different mAbs containing V_H3-8-encoded heavy chains generated from three different mice, six mAbs were recombined with an identical D allele (IGHD4-1*01) and either the IGKJ2*01 or IGKJ3*01 J allele (Table 4.6). Anti-HEL mAbs with identical VDJ usage were generated by multiple independent recombination events in different ASCs, as confirmed by analysis of nucleotide sequences in the heavy chain junction region of these mAbs. VDJ recombination is imprecise due to addition or deletion of untemplated nucleotides to the junctional N regions by terminal deoxyribonucleotidyl transferase (TdT) and exonuclease enzymes, respectively; thus, the junction sequence serves as a unique signature of a particular recombination event.[2] All four anti-HEL mAbs from a single mouse (M2) were derived from a single recombination event, whereas four additional anti-HEL mAbs were generated by four distinct recombination events in two different mice (M1 and M3) (Table 4.6). Of these, two mAbs (M1_R05C14 and M1_R06C10) derived from independent heavy chain recombination events in a single mouse were paired with the identical kappa chain (V_κ5-43) as multiple hybridoma-generated anti-HEL mAbs (HyHEL-10, HyHEL-8, HyHEL-26, and HyHEL-63) (Table 4.5). The fact that these mAbs were generated by different methods in distinct mice many decades apart indicates that the mouse antibody immune response to HEL exhibits preferential V gene usage, VDJ recombination and heavy/light chain pairing.

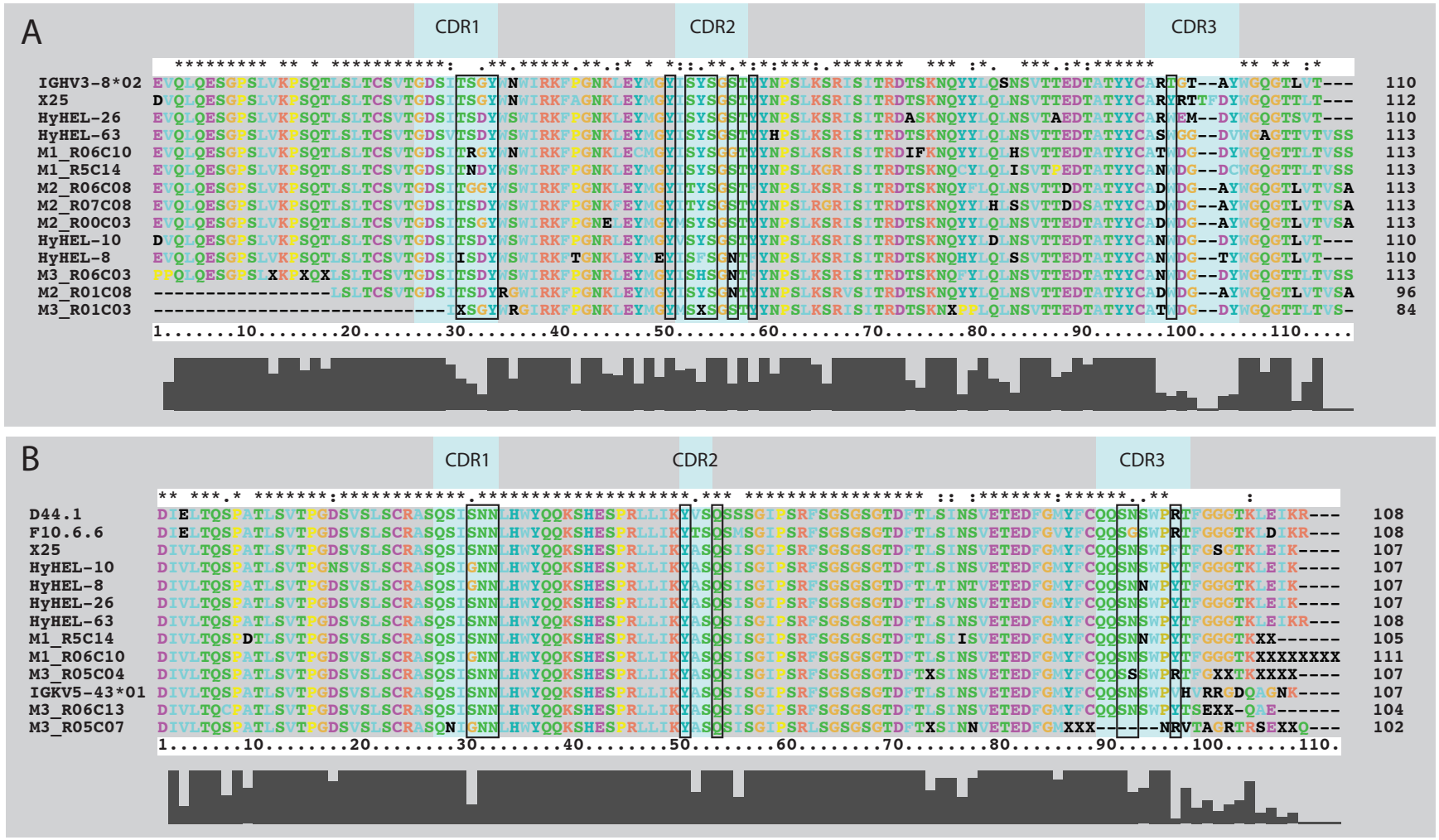

Figure 4.12 Amino acid sequences of anti-HEL mAbs encoded by IgHV3-8 heavy (A) and IgK5-43 kappa (B) chain genes. HyHEL-10, HyHEL-26, HyHEL-8, HyHEL-63, F10.6.6, and D44.1 are hybridoma-generated anti-HEL mAbs, whereas X25 is an anti-DNP mAb. Boxed residues are those that contact HEL in the HyHEL-10/HEL complex. Sequences are aligned and clustered using ClustalX. Truncated heavy chain sequences (i.e. M2_R01C08 and M3_R01C03) were not used for clustering. CDR regions are highlighted by shaded boxes.

Table 4.5 Binding kinetics, affinities, VDJ gene usage and CDR sequences for anti-HEL mAbs encoded by the V_κ5-43 and V_H3-8 genes. (n/a = not amplified, n/r = not reported). mAbs are listed in order of binding affinity to HEL (highest affinity at the top). mAbs marked with an asterisk are encoded by both V_κ5-43 kappa and V_H3-8 heavy chains. The heavy chain diversity (D) region of some mAbs was not identified. [continued on next page]

mAbs	k_{on} ($M^{-1}s^{-1}$)	k_{off} (s^{-1})	K_d (M)	V_k gene	J_k gene	K-CDR1	K-CDR2	K-CDR3
Germline	-	-	-	IGKV5-43*01	IGKJ2*01	QSISNN	YAS	QQSNSWPVH
F10.6.6	7.2E+06	7.0E-04	1.0E-10	IGKV5-43*01	IGKJ1*01	QSISNN	YTS	QQSGSWPRT
HyHEL-10*	2.3E+05	5.2E-05	2.2E-10	IGKV5-43*01	IGKJ2*01	QSIGNN	YAS	QQSNSWPYT
M3_R06C03	2.1E+06	6.4E-04	3.0E-10	IGK3-2*01	IGKJ2*01	ESVDNYGISF	AAS	QQSKEVPYT
M3_R01C03	2.2E+06	9.3E-04	4.2E-10	n/a	n/a	-	-	-
M1_R05C14*	3.8E+06	2.8E-03	7.4E-10	IGKV5-43*01	IGKJ2*01	QSISNN	YAS	QQSNNWPYT
M2_R00C03	4.4E+06	3.8E-03	8.7E-10	n/a	n/a	-	-	-
M2_R07C08	2.4E+06	2.3E-03	9.7E-10	IGKV4-74*01	IGKJ1*01	SSVSSSF	STS	HQYHRSPPT
HyHEL-8*	1.9E+05	2.2E-04	1.1E-09	IGKV5-43*01	IGKJ2*01	QSIGNN	YAS	QQSNNWPYT
M2_R01C08	6.1E+05	7.8E-04	1.3E-09	IGKV3-12*01	IGKJ2*01	KSVSTSGYSY	LVS	QHIRELT
M2_R06C08	2.6E+06	4.9E-03	1.9E-09	IGKV19-93*01	IGKJ2*01	QDINKY	YTS	IQYDNXPYTF
M1_R06C10*	1.8E+06	4.5E-03	2.5E-09	IGKV5-43*01	IGKJ2*01	QSIGNN	YAS	QQSNSWPYT
HyHEL-26*	1.7E+05	4.9E-04	2.9E-09	IGKV5-43*01	IGKJ2*01	QSISNN	YAS	QQSNSWPYT
D44.1	4.2E+04	2.9E-03	1.4E-07	IGKV5-43*01	IGKJ1*01	QSISNN	YVS	QQSNSWPRT

Table 4.5 [continued from previous page] – For clarity, information on binding kinetics and affinities is repeated on both pages. All hybridoma-generated mAbs from the HyHEL series have ~10-fold lower on- and off-rate constants compared to the microfluidic-selected anti-HEL mAbs; it is possible that this discrepancy resulted from methodological differences (e.g. previous measurements were performed by SPR using Fab fragments whereas measurements in this study were performed using the microfluidic bead assay and full-length IgG mAbs).

mAbs	k_{on} ($M^{-1}s^{-1}$)	k_{off} (s^{-1})	K_d (M)	VH gene	DH gene	JH gene	H-CDR1	H-CDR2	HCDR3
Germline	-	-	-	IGHV3-8*02		IGHJ3*01	GDSITSGY	ISYSGST	ARTGTAY
F10.6.6	7.2E+06	7.0E-04	1.0E-10	IGHV1-9*01		IGHJ2*01	GYTFTTYW	ILPGSDST	ARGDGFYVY
HyHEL-10*	2.3E+05	5.2E-05	2.2E-10	IGHV3-8*02		IGHJ3*01	GDSITSDY	VSYSGST	ANWDGDY
M3_R06C03	2.1E+06	6.4E-04	3.0E-10	IGHV3-8*02	IGHD1-1*01	IGHJ4*01	GDSITSDY	ISHSGNT	ANWDGDY
M3_R01C03	2.2E+06	9.3E-04	4.2E-10	IGHV3-8*02	IGHD3-3*01	IGHJ2*01	IXSGY	MSXSGST	ATWDGDY
M1_R05C14*	3.8E+06	2.8E-03	7.4E-10	IGHV3-8*02	IGHD4-1*01	IGHJ2*01	GDSITNDY	ISYSGST	ANWDGDC
M2_R00C03	4.4E+06	3.8E-03	8.7E-10	IGHV3-8*02	IGHD4-1*01	IGHJ3*01	GDSITSGY	MSYSGST	ADWDGAY
M2_R07C08	2.4E+06	2.3E-03	9.7E-10	IGHV3-8*02	IGHD4-1*01	IGHJ3*01	GDSITSDY	ITYSGST	ADWDGAY
HyHEL-8*	1.9E+05	2.2E-04	1.1E-09	IGHV3-8*02		IGHJ3*01	GDSIISDY	ISFSGNT	ANWDGTY
M2_R01C08	6.1E+05	7.8E-04	1.3E-09	IGHV3-8*02	IGHD4-1*01	IGHJ3*01	GDSITSDY	ISYSGNT	ADWDGAY
M2_R06C08	2.6E+06	4.9E-03	1.9E-09	IGHV3-8*02	IGHD4-1*01	IGHJ3*01	GDSITGGY	ITYSGST	ADWDGAY
M1_R06C10*	1.8E+06	4.5E-03	2.5E-09	IGHV3-8*02	IGHD4-1*01	IGHJ2*01	GDSITRGY	ISYSGGT	ATWDGDY
HyHEL-26*	1.7E+05	4.9E-04	2.9E-09	IGHV3-8*02		IGHJ4*01	GDSITSDY	ISYSGST	ARWEMDY
D44.1	4.2E+04	2.9E-03	1.4E-07	IGHV1-9*01		IGHJ2*01	GYTFSTYW	ILPGSGST	ARGDGNYGY

Table 4.6 Nucleotide sequences of the heavy chain junction region for anti-HEL mAbs encoded by the V_H3-8 gene. mAbs marked with an asterisk also utilize the same kappa chain gene (V_κ5-43).

mAb	N1-REGION	P5'D	D-REGION	P3'D	N2-REGION	P5'J	5'J-REGION
M1_R06C10*	c	-	ctgggac	-	ggg	-	gactactgg
M1_R05C14*	-	-	actgggac	-	ggg	-	gactgctgg
M2_R06C08	gg	-	actgggac	-	gg	-	tgcttactgg
M2_R00C03	gg	-	actgggac	-	gg	-	tgcttactgg
M2_R07C08	gg	-	actgggac	-	gg	-	tgcttactgg
M2_R01C08	gg	-	actgggac	-	gg	-	tgcttactgg
M3_R06C03	-	-	attgggatgg	-	c	-	gactactgg
M3_R01C03	-	-	cttgggatg	-	gc	-	gactactgg

4.2.5 Cloning and Expression of Novel Anti-HEL Mouse mAbs

To validate the microfluidic single-cell antibody selection method, a single high-affinity anti-HEL mAb was commercially produced by cloning and recombinant expression as a full-length mouse IgG antibody. The recombinant mAb was tested for binding to HEL using the microfluidic fluorescence bead assay. The cloned mAbs bound HEL with similar binding kinetics and affinities as observed when selected from mouse ASCs (Table 4.7 and Figure 4.13). Although recombinant production of additional mAbs is required to quantify overall success rates, this experiment demonstrates that, in principle, mAbs selected from the microfluidic platform retain their antigen specificity, binding kinetics, and affinities when produced by standard recombinant methods.

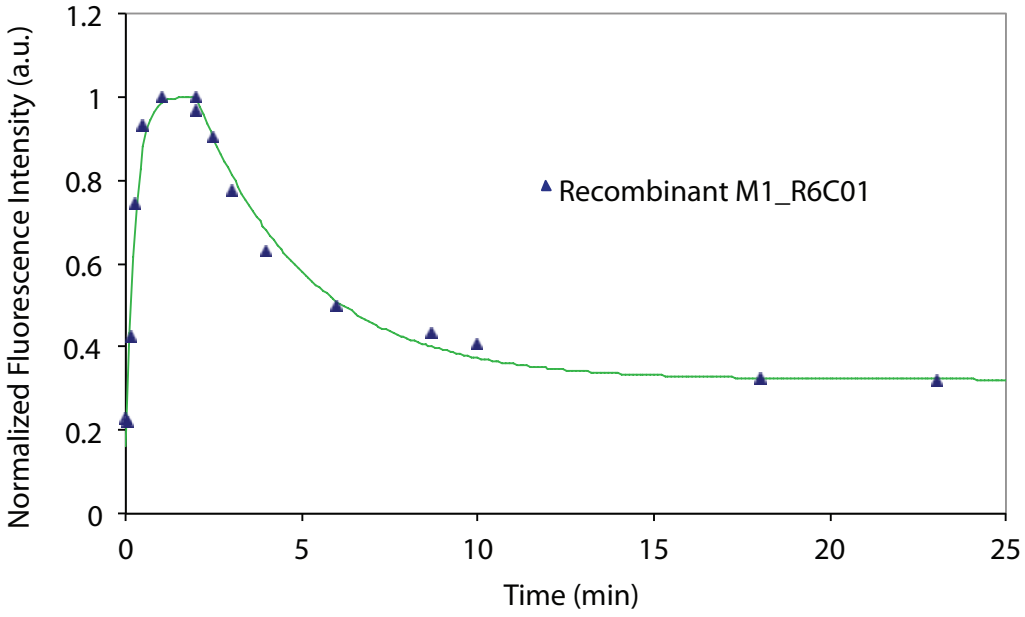

Figure 4.13 Sample association and dissociation curves of recombinant M1_R6C01 mAb binding to HEL-Dylight488 fluorescent conjugate (14.3 nM concentration) measured using the microfluidic fluorescence bead assay. Solid line represents experimental fit using mass-action equations (Chapter 2, equations 2.7a-c)

Table 4.7 Comparison of binding kinetics of M1_R06C01 anti-HEL mouse mAb selected from single ASC and produced by recombinant expression in mammalian cells. Reported error represents the calculated standard deviation of multiple replicate measurements. Values measured only once are reported without error bars.

mAb	k_{on} ($M^{-1}s^{-1}$)	k_{off} (s^{-1})	K_d (M)
M1_R06C01	3.6×10^{6}	2.9×10^{-3}	7.9×10^{-10}
Recombinant M1_R06C01	$(4.5 \pm 1.3)\times10^{6}$	$(4.6 \pm 0.7)\times10^{-3}$	$(1.0 \pm 0.3)\times10^{-9}$

4.3 Conclusions

The microfluidic single-cell screening method described in this chapter provides a rapid and high-throughput route for screening, selection and production of high affinity antigen-specific monoclonal antibodies (mAbs). The technology facilitates selection of mAbs based on both kinetic and equilibrium binding parameters, which may be particularly useful for the selection of therapeutic mAbs that bind their target antigens with K_d values less than 10 nM.[12] Selection of mAbs based on kinetic off-rate constants (i.e., very long interaction half-lives) may also produce therapeutic mAbs that can be administered less frequently or in smaller dosages, thus reducing both the cost and side effects of administering these therapies. Methods for laboratory-directed evolution of antibodies (e.g. phage display, yeast display, etc.) typically select binding candidates libraries based on an equilibrium binding or kinetic dissociation-based screen.[160] As a result, laboratory-evolved variants of mAbs often have a large diversity of off-rate constants (e.g. 3- to 4-orders of magnitude) but a relatively small range of on-rate constants (e.g. 10-fold).[102,153] Thus, the microfluidic single-cell-screening method may be uniquely suited to on-rate selection of mAbs by screening the large diversity of on-rate constants produced by the natural immune system. On-rate selection may be

particularly useful for anti-viral therapies, in which mAbs with large association rate constants may serve as entry inhibitors for potent virus neutralization.[100]

Selection of mouse anti-HEL mAbs selected by both the microfluidic single-cell screening and hybridoma methods revealed several interesting features of the adaptive immune system. Firstly, no correlation was observed between the numbers of somatic coding mutations and binding kinetics and affinities of associated anti-HEL mAbs, consistent with the idea that affinity maturation increases the number and diversity of mAbs rather than an increase in the average affinity of antigen-specific mAbs.[146] Analysis of gene sequences of anti-HEL mAbs also revealed that both repertoire drift (i.e. point mutations to antibody genes) and repertoire shift (i.e. different V gene usage) are capable of generating large diversity in antigen-antibody binding kinetics and affinities. For example, the D44.1 and F10.6.6 mAbs vary by 3 orders of magnitude in HEL-binding affinity (102 pM versus 144 nM) despite differing by a total of only 5 amino acid residues in both heavy and light chain CDR regions. Similarly, a single amino acid substitution between the HyHEL-10 mAb and its nearest germ-line sequence altered binding of HyHEL-10 to HEL by nearly 4 orders of magnitude (i.e. 9000-fold).[158] This diversity in binding affinities exceeds the range of binding affinities of all microfluidic-selected anti-HEL mAbs encoded by one to two dozen unique V_κ and V_H genes, respectively. By contrast, based on the mouse immune response to the 2-phenyl-oxazolone (phOx) hapten, Foote and Milstein concluded that repertoire drift resulted in more modest (<10-fold) changes to antibody-antigen binding kinetics and affinities when compared to repertoire shift.[20] Thus, it appears that the relative importance of repertoire drift and shift in generating mAbs with diverse binding kinetics and affinities

may vary in the immune response to different antigens. The relative improvement in antibody on- and off-rate constants by affinity maturation may also vary in the immune response to different antigens.[93]

Early reports of antibody V gene usage indicated that fetal mice preferentially use particular V gene segment based on particular chromosomal organization, but that this preferential usage is lost throughout development.[161] Thus, V gene segment usage in antibodies produced by adult mice is dependent on the strain-specific V gene family size.[161] By sequencing the entire antibody repertoire in both immature and adult zebrafish, Quake and coworkers have also identified a "stereotyped" development, in which particular VDJ usage is highly enriched between different individuals.[162] However, these studies have not shed light on whether stereotyped antibody repertoires tend to bias antigen-specific immune responses to particular V gene segments.

Anti-HEL mAbs selected by microfluidic single cell screening and hybridoma methods from distinct mice many decades apart displayed an unprecedented level of stereotypy, consisting of preferential V gene usage, VDJ recombination and heavy/light chain pairing. Epitope mapping studies and crystallographic structures of mouse mAbs in complex with the HEL protein suggest that the stereotyped anti-HEL mAb response is functionally significant.[146,163] Crystal structures of multiple mAbs in contact with HEL indicate that both heavy and light chain amino acid residues make contact with HEL at the binding interface.[152,163] Preferential heavy/light chain pairing among anti-HEL mAbs may thus reflect positive selection in the adaptive immune system for mAbs heavy and light chains that jointly form effective HEL-binding domains.

Stereotypy in the anti-HEL mAb response also appears to be caused by particular (immunodominant) regions of the HEL protein. Smith-Gill and coworkers previously reported that anti-HEL mouse mAbs can be sub-divided into three "complementation groups" that bind three non-overlapping regions on the HEL protein.[146] These complementation groups were functionally defined by competitive binding experiments, where mAbs from different complementation groups simultaneously bound different regions of the HEL protein, while co-binding of mAbs from the same complementation group was inhibited (Figure 4.14). Using this approach, D1.3, HyHEL-5, and HyHEL-10 mAbs were identified as representative members of the three different complementation groups and anti-HEL mAbs encoded by identical heavy and light chain genes were found to belong to the same complementation group.[146] Thus, the enrichment of anti-HEL mAbs with identical V gene usage, VDJ recombination and heavy/light chain pairing as the HyHEL-10 mAb suggest that these mAbs all bind to an immunodominant region of the HEL protein. Several anti-HEL mAbs selected by microfluidic single-cell screening were encoded by only one of the V_κ5-43 and V_H3-8 genes (Table 4.5). In addition, one selected anti-HEL mAb was encoded by the same V_H gene as D1.3 (V_H2-6-7), while another mAb was encoded by the same V_κ gene as HyHEL-5 (V_κ4-59). Competitive binding experiments of these mAbs will be required to investigate whether the complementation group of a particular mAb can be predicted solely based on only heavy or light chain gene usage.

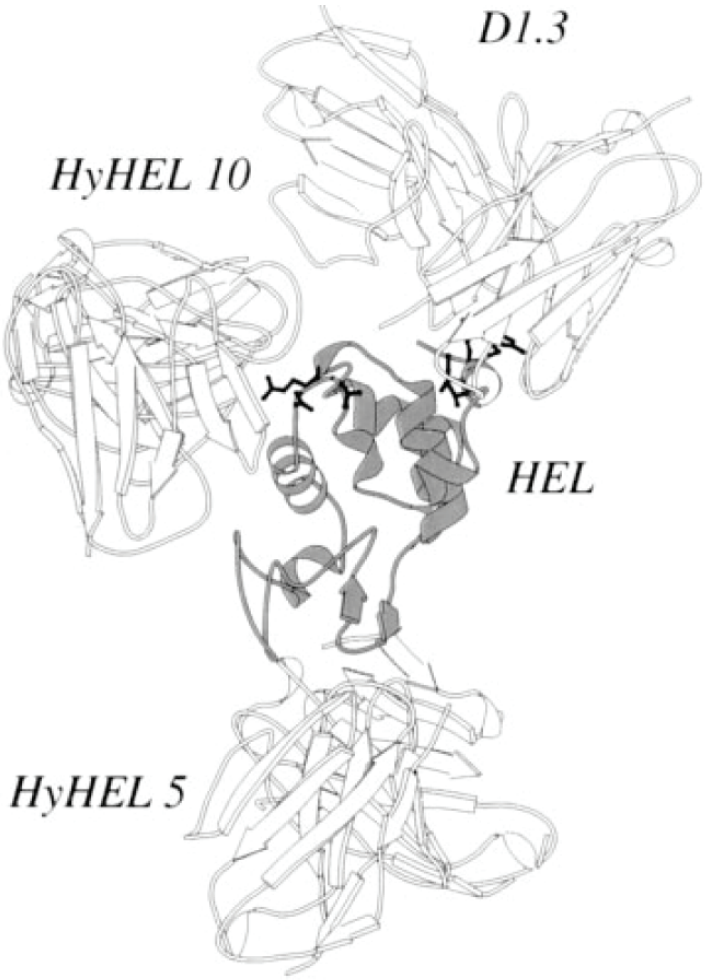

Figure 4.14 The HEL protein can be sub-divided into three non-overlapping regions that bind to distinct ("complementation") groups of mAbs.[146] D1.3, HyHEL-5, and HyHEL-10 are representative members of the three different complementation groups. Image reproduced from Batista et al (Cell Press, 1998).[115]

Though not typically observed across multiple distinct animals, restricted V gene usage has also been previously reported in the mouse antibody response to haptens phOx and phosphorylcholine, the amyloid β peptide, polysaccharides, as well as the human antibody response to infectious bacteria [e.g. haemophilus influenza] and viruses [e.g. human immunodeficiency virus (HIV), influenza virus, cytomegalovirus (CMV)].[20,164–170] Thus, antibody stereotypy may be a common feature of the antigen-specific adaptive immune response in both mice and humans. Antibody stereotypy may

have clinical and therapeutic implications for the human adaptive immune response to natural pathogens. For example, recent studies of antibodies produced by humans in response to the 2009 pandemic H1N1 influenza virus infection or vaccination have revealed an abundance of mAbs that bind to a conserved "stem" region of the viral hemagglutinin (HA) protein and, hence, broadly cross-react with HA proteins from multiple influenza sub-types (e.g. H1, H3, H5).[49,171,172] These broadly cross-reacting mAbs are reportedly enriched for heavy chains encoded by the V_H1-69 gene, which has also been found in human mAbs against other viruses, such as HIV and Hepatitis C virus (HCV).[169,172] It remains to be seen whether other V genes and heavy/light chain pairs are preferentially enriched in broadly cross-reacting anti-influenza mAbs. Microfluidic screening of mAbs from multiple infected humans could shed light on whether broadly cross-reacting mAbs are produced by all infected humans. If not, it will be interesting to study whether individuals with antibody repertoires deviating from a stereotyped response exhibit different clinical outcomes in response to a common antigenic challenge.

As described in Chapter 5, microfluidic single-cell screening can be adapted to the selection of mAbs based on other functional binding properties (e.g. selectivity, viral neutralization, etc.) from several different animal species (e.g. rabbits, humans). This chapter will also describe approaches to increase the number of ASCs that can be analyzed in a single microfluidic device, as well as methods to increase the success rate of single-cell RT-PCR reactions.

Chapter 5: Conclusions and Future Work

The previous chapters describe the development of a microfluidic platform for screening and selection of high affinity monoclonal antibodies (mAbs) from single antibody-secreting cells (ASCs). This technology was used to precisely measure the binding kinetics of antigen and antibodies secreted by single ASCs (Chapter 2), to recover and amplify heavy and light chain genes from single ASCs (Chapter 3), and to screen and select novel high affinity antigen-specific mAbs from primary ASCs harvested from immunized animals (Chapter 4). As a validation of the technology, nearly 200 high affinity mouse mAbs to the model antigen hen egg lysozyme, representing a 10-fold increase in the number of high affinity anti-HEL mouse mAbs previously generated using recent micro-well technologies and conventional hybridoma methods. The microfluidic mAb selection technology has also provided interesting insights into affinity maturation, as well as stereotypy and immuno-dominance in the adaptive immune system. Specifically, the binding constants and gene sequences of anti-HEL mAbs selected by microfluidic screening support the hypothesis that affinity maturation acts to increase the number and diversity of antigen-specific mAbs, rather than increase the average affinity of individual antibodies.[146] Anti-HEL mouse mAbs selected using both microfluidic and hybridoma methods also revealed an unexpected level of convergent evolution across different mice, consisting of preferential V gene usage, VDJ recombination, and heavy-light chain pairing. The mAbs enriched in these "stereotyped" antibody responses are generated in response to immunodominant epitopes in the HEL protein.

This chapter focuses on future extensions of the microfluidic single cell antibody screening technology and can be divided into three sections: selection of mAbs based on multiple different functional properties (e.g. antigen binding affinity, kinetics, selectivity, viral neutralization, etc.), increasing the capacity to screen larger numbers of single ASCs, and selection of mAbs from different animal species and cell types.

5.1 Selection of mAbs for Multiple Functional Binding Properties

Although the present thesis focused on screening mAbs based on their antigen binding kinetics and affinities, antibodies may also be selected for other important functional binding properties, such as specificity or cross-reactivity to antigenic variants, binding to particular antigenic epitopes, viral neutralization, and inhibition of cell growth and signaling.[49,146,173,174] Antibodies with these properties can be selected by integrating a variety of different high-resolution optical assays with the microfluidic mAb selection technology. For example, mAbs that bind one or more antigenic variants can be selected by flushing bead-captured mAbs with antigenic variants each labeled with a spectrally unique fluorophore. Subsequently, microfluidic chambers can be fluorescence imaged with multiple filter cubes corresponding to each labeled fluorophore. In principle, optical multiplexing can be performed using five to ten distinct fluorophores, though more sophisticated multiplexing strategies using both wavelength- and intensity-multiplexing with quantum dots[175] may facilitate screening of a large number of antigenic variants in this manner.

Selection of mAbs that bind particular epitopes may also be performed by competitive binding assays using cell-secreted mAbs and previously-generated mAbs

known to bind particular antigenic epitopes.[146,172,176] This may be particularly useful for biasing antibody selection against immunodominant epitopes. For instance, this approach may facilitate selection of mAbs to the conserved "stem" region of the influenza hemagglutinin (HA) protein rather than the "head" region that appears to be the dominant target of antibodies produced in response to seasonal influenza vaccines.[171,177] This approach may therefore enable the selection of mAbs that broadly cross-react with different influenza viral strains.[49]

Optical assays for antibody viral neutralization may also be integrated with microfluidic single cell antibody screening. For example, single ASCs can be pre-incubated with pseudo-typed viruses containing fluorescent transgene reporters (e.g. GFP) prior to mixing of virus with a reporter cell-line.[178,179] Fluorescence measurements of the reporter cell-line can then be used to screen whether cell-secreted mAbs altered viral transduction efficiencies. Similarly, cell-secreted mAbs can be pre-incubated with influenza viruses prior to mixing with red blood cells in order to select mAbs that inhibit bind and inhibit hemagglutination (i.e. the hemagglutination inhibition assay).[172,180]

A variety of optical cell growth and signaling assays can be used to identify therapeutic mAbs for the treatment of different cancers (breast, colorectal) and immunological disorders (rheumatoid arthritis, lupus).[41] For instance, the therapeutic antibody Herceptin is known to inhibit *in vitro* proliferation of human breast cancer cells.[174] Thus, antibody-secreting cells can be co-incubated with breast cancer cells in microfluidic chambers in order to select mAbs that similarly inhibit cancer cell proliferation. Humira, a clinically approved antibody for the treatment of rheumatoid

arthritis, is known to target the inflammatory cytokine tumor necrosis factor alpha (TNF-α). Tay et al. recently used a microfluidic fluorescence imaging assay to study the effects of *in vitro* TNF-α stimulation in an engineered mouse fibroblast (3T3) cell-line.[181] By extension, co-incubation of ASCs with this reporter cell-line may facilitate selection of mAbs that inhibit TNF-α cell signaling. Screening of mAbs based on aggregation properties and solution stability may also be facilitated by microfluidic methods.

5.2 Increasing Capacity to Screen Larger Numbers of ASCs

By conventional wisdom, high affinity antibodies are rare, suggesting that higher quality antigen-specific mAbs will identified by screening more single cells. Despite only screening ~0.1% of the total CD138+ splenocytes harvested from HEL-immunized mice (i.e. ~100 out of over 100,000 cells per spleen), most of the characterized mAbs (>80%) had K_d values less than or equal to 1 nM, with the highest affinities reaching ~100 pM (Chapter 4, Table 4.2). However, selection of rare mAbs with exceptionally low dissociation rates ($k_{off} < 10^{-4}$ s^{-1}) and equilibrium dissociation constants less than the 100 pM affinity ceiling may require improvements to the capacity of the of the microfluidic system to screen larger number of ASCs. Indeed, using a combination of ELISA analysis on binned cell populations and the SLAM approach (Chapter 1, Figure 1.8), Babcook and coworkers screened a large number of B cells to identify mAbs that bound antigen (i.e. human IL-8) with picomolar affinities.[50,182]

The current microfluidic architecture is limited to analyzing up to 1000 cells per device, due to practical limitations imposed by individual addressability in two-

dimensional microfluidic chamber arrays.[87] Further increases in cell capacity can be obtained by integrating the developed microfluidic technology with upstream assays of binned cell populations. For example, up to 100 ASCs can be FACS-sorted into individual wells and the cell supernatant from each well can be screened for antigen-specific mAbs using enzyme-linked immunosorbent assays (ELISA). Selected wells containing antigen-specific antibodies can be subsequently screened at the single-cell level using the developed microfluidic technology. In this manner, hundreds of thousands of ASCs can be screened using only ten 96- or 384-well plates and an optional number of microfluidic devices depending upon the number of selected wells. Alternatively, larger number of ASCs may be screened by integrating highly sensitive bead-based detection with previously reported micro-well or droplet-based methods capable of encapsulating tens to hundreds of thousands of cells, thus eliminating the need for addressable microfluidic chamber arrays.[14,51,91,92] One embodiment of this approach involves the co-encapsulation of single ASCs with multi-functionalized beads capable of capturing both secreted antibodies and antibody-encoding mRNA (Figure 5.1). By co-incubating cells and beads in droplets and subsequent cell lysis by merging droplets containing mild detergent (e.g. 0.5% NP-40), both secreted mAbs and antibody-encoding mRNA from single ASCs can be captured on the bead surface. Subsequent recovery and FACS-sorting of beads from the droplet emulsion can be used to enrich beads containing antigen-specific mAbs. Finally, RT-PCR amplification of sorted beads can be used to amplify the heavy and light chain genes for subsequent cloning and expression of selected mAbs.

Importantly, the throughput of all single cell antibody-screening methods, including the described microfluidic technology, is constrained by low amplification efficiencies of heavy and light chain genes from single cells. RT-PCR amplification successfully identified approximately 20% of paired heavy and light chain genes from selected ASCs both in this work (see Chapter 4, section 4.2.4) and other state-of-the-art studies.[58] Improved primer design may lead to significantly higher amplification efficiencies at low template concentrations, as found when comparing two different primer design strategies (Chapter 3). Alternative amplification strategies, such as 5'-RACE and single-cell whole transcriptome amplification (WTA), obviate the need for design of primers to the antibody variable region, but it is presently unclear whether these methods will result in higher success rates than single-cell RT-PCR amplification.[183,184] Recent advances in microfluidic technologies have facilitated robust RT-PCR amplification of mRNA transcripts from single cells with sensitivity down to single molecules.[75,81] Thus, integration of single-cell RT-PCR amplification and recovery into microfluidic devices may yield significantly greater numbers of heavy and light chain genes from selected ASCs.[79]

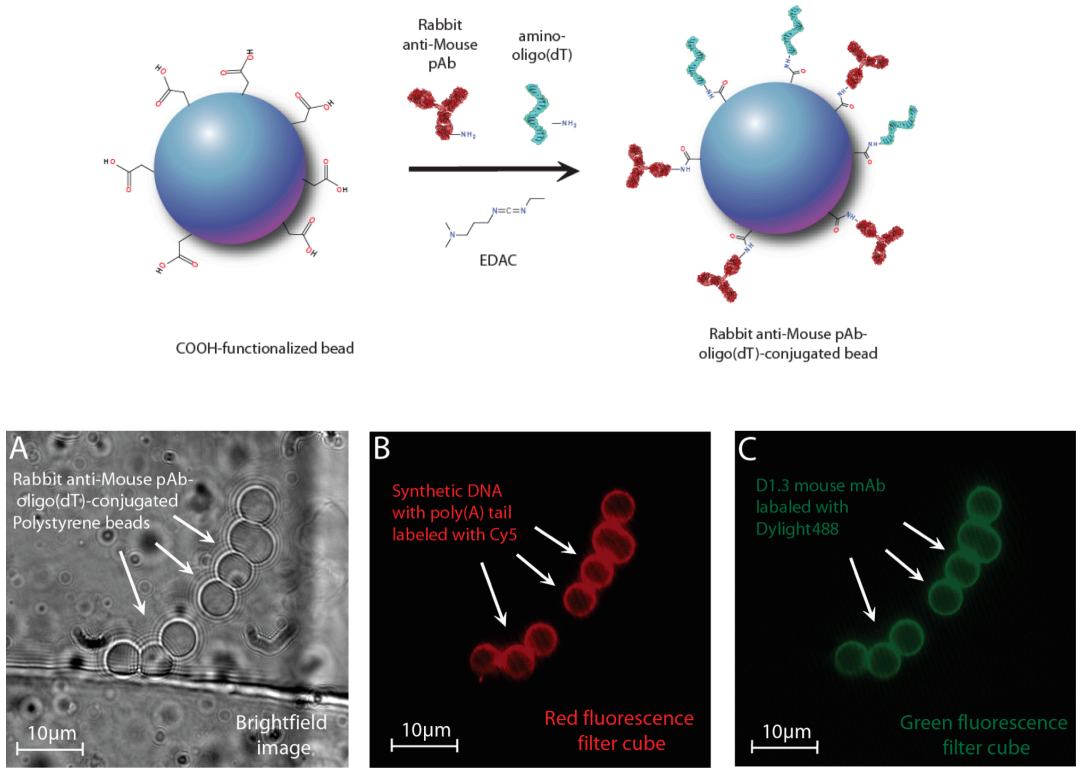

Figure 5.1 Bi-functionalized beads for the simultaneous capture of mAbs and antibody-encoding mRNA from single cells. (Top) Scheme for chemical conjugation of secondary mAbs and oigo(dT) to beads using carbodiimide chemistry. (Bottom) Microscope images of bi-functionalized beads trapped by a microfluidic sieve valve (A). Captured on the bead surface are fluorescently labeled synthetic DNA (B) and fluorescently labeled mouse mAbs (C). (Bottom) Measurement of binding kinetics of antigen and single cell-secreted antibodies on bi-functionalized beads as described in Chapter 2. Figure adapted from US Patent Application 2012/0015347 A1.[185] [continued on next page]

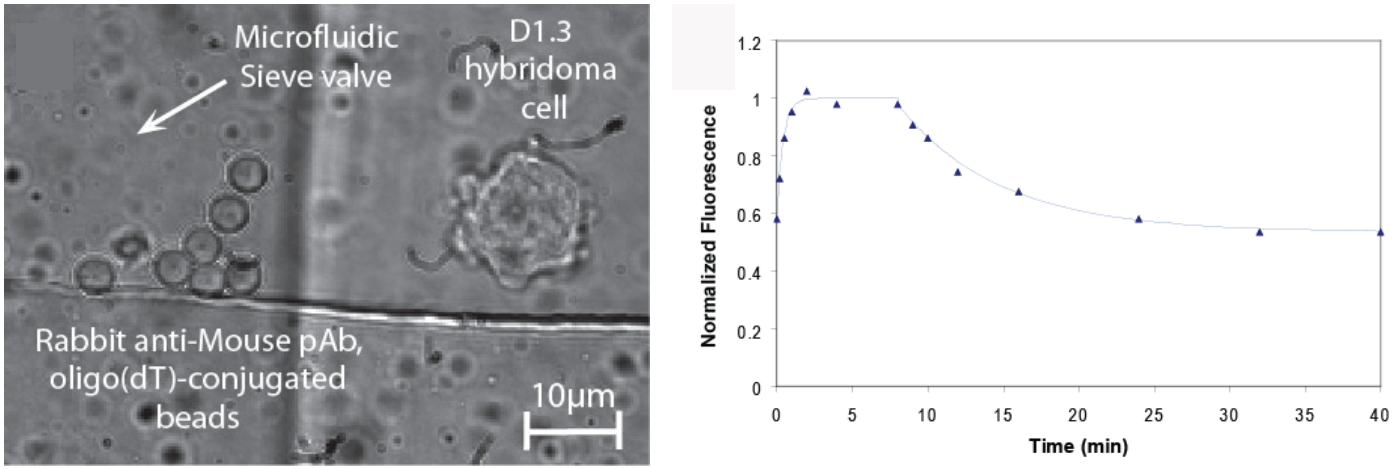

Figure 5.1 [continued from previous page] Microscope image of hybridoma cell adjacent to antibody capture beads in microfluidic device (left) and measurement of binding kinetics of antigen and single cell-secreted antibodies on bi-functionalized beads as described in Chapter 2 (right). Figure adapted from US Patent Application 2012/0015347 A1.[185]

5.3 Selection of mAbs from Other Animal Species (e.g. Humans, Rabbits, etc.) and Cell Types

As microfluidic single cell antibody screening circumvents the need for hybridoma generation by fusion with a partner cancer cell-line, the technology can select mAbs from many different species, including humans and rabbits. Human ASCs can be readily purified based on CD19 and CD38 cell-surface markers, and several different primer designs have been previously reported for single-cell RT-PCR amplification of both human and rabbit heavy and light chains genes.[19,23,50,172] Thus, in addition to facilitating selection of research-grade mouse mAbs, the microfluidic technology can be used to select fully human therapeutic mAbs that bind target antigen with high affinity.

Extension of the microfluidic technology for mAb selection from species other than mice and humans will require advances in the identification of cell-surface markers to purify and enrich ASCs from immunized animals.[31,50] As described above, the current microfluidic architecture is limited to screening several hundred cells from a single animal; thus, successful mAb selection using this approach requires that antigen-specific ASCs comprise >1% of the purified cell populations. Increases in the capacity to screen larger numbers of ASCs screened will reduce the necessary level of enrichment for screening ASCs from all species, as well as facilitate the selection of rare mAbs. Interestingly, even though up to 70% of enriched human ASCs secrete anti-influenza mAbs, Corti et al. screened 100,000 plasma cells in order to select a single mAb that cross-reacts with all influenza strains.[23,49]

In addition to screening antibody-secreting cells (ASCs) harvested from immunized animals, the microfluidic technology can be extended to selection of antibodies from memory B cells and sub-cloning of hybridoma and recombinant cell-lines, such as Chinese hamster ovary (CHO) cells and human embryonic kidney (HEK) cells transfected with expression vectors (e.g. phage, viruses) for production of full-length antibodies (e.g. IgG) or antibody fragments (e.g. scFv, Fab, Fv, bispecific antibodies, minibodies, antibody-drug conjugates ADCs, etc.).[28,45,50,186,187] Memory B cells can be induced *in vitro* to secrete antibodies by immortalization with Epstein-Barr virus (EBV) and/or stimulation with toll-like receptor (TLR) agonists (i.e. CpG oligonucleotides). The induced memory B cells can thus be screened in a manner analogous to antibody-secreting cells. In contrast to selecting cells secreting antibodies with desired antigen-binding kinetics or specificity, time-course measurements of the amount of bead-captured antibodies (see Figure 2.12) can be used to select clones that produce large amounts of antibody for recombinant production. Finally, the microfluidic technology can be used to select recombinant cells and other cell types (e.g. T-cells) producing bio-molecules, such as T-cell receptors (TCRs), cytokines, recombinant proteins, carbohydrates, lipids, and small molecules.

5.4 Other Insights into the Adaptive Immune System

Application of the developed microfluidic technology for selecting anti-HEL mAbs yielded interesting insights into "convergent evolution" of antibodies in mice; that is, anti-HEL mAbs are preferentially encoded by particular V genes, VDJ recombination, and heavy-light chain pairing in response to immunodominant epitopes

on the HEL protein. Future extensions of this approach may assist in vaccine design by assigning enriched antibody populations to immunodominant epitopes in common human pathogens, such as human immunodeficiency virus (HIV), influenza virus, and human cytomegalovirus (CMV).[169,170,172] Moreover, microfluidic selection can provide both functional and sequence information for antigen-specific mAbs that can be used to query fully-sequenced antibody repertoires in order to obtain more global insights into antigen-specific antibody "stereotypy".[18,162] This approach may facilitate the diagnostic and/or prognostic identification of antibodies that are over- or under-expressed in particular states of human health, including bacterial and viral infections, autoimmune disorders (e.g. systemic lupus erythematosus, rheumatoid arthritis, cystic fibrosis, multiple sclerosis, Crohn's disease, etc.), allergic responses, osteoporosis, cancer (e.g. breast, colorectal, lymphoma, leukemia, melanoma, etc.), neurodegenerative diseases (e.g. Alzheimer's disease, prion diseases), and other diseases.

References

1. Da Costa, D. J. *Microfluidic Technology for Screening and Selection of Monoclonal Antibodies from Single Cells*. 43 (University of British Columbia: 2011).
2. Murphy, K. M., Travers, P. & Walport, M. *Janeway's Immunobiology*. (Garland Science / Taylor & Francis LLC: 2011).
3. Kantor, A. & Herzenberg, L. Origin of Murine B-Cell Lineages. *Annu. Rev. Immunol.* **11**, 501–538 (1993).
4. Ackermann, B. L. & Berna, M. J. Coupling immunoaffinity techniques with MS for quantitative analysis of low-abundance protein biomarkers. *Expert Rev. Proteomics* **4**, 175–186 (2007).
5. Bradbury, A. *et al.* Antibodies in proteomics II: screening, high-throughput characterization and downstream applications. *Trends Biotechnol.* **21**, 312–317 (2003).
6. Foon, K. & Todd, R. Immunological Classification of Leukemia and Lymphoma. *Blood* **68**, 1–31 (1986).
7. Picker, L. J., Weiss, L. M., Medeiros, L. J., Wood, G. S. & Warnke, R. A. Immunophenotypic criteria for the diagnosis of non-Hodgkin's lymphoma. *Am J Pathol* **128**, 181–201 (1987).
8. Uhlen, M. Affinity as a tool in life science. *Biotechniques* **44**, 649–654 (2008).
9. Martin-Moe, S. *et al.* The Structure of Biological Therapeutics. *Formulation and Process Development Strategies for Manufacturing Biopharmaceuticals* 1–40 (2010).at <http://onlinelibrary.wiley.com/doi/10.1002/9780470595886.ch1/summary>
10. Zider, A. & Drakeman, D. L. The future of monoclonal antibody technology. *MAbs* **2**, 361–364 (2010).
11. Reichert, J. M. Monoclonal antibodies in the clinic. *Nat Biotech* **19**, 819–822 (2001).
12. Carter, P. J. Potent antibody therapeutics by design. *Nat Rev Immunol* **6**, 343–357 (2006).
13. Little, M. Antibody Libraries: How to Overcome the Discovery Log-Jam. *2006* **21**, 54–58
14. Love, J. C., Ronan, J. L., Grotenbreg, G. M., van der Veen, A. G. & Ploegh, H. L. A microengraving method for rapid selection of single cells producing antigen-specific antibodies. *Nat Biotech* **24**, 703–707 (2006).
15. Love, J. C. Making antibodies from scratch. *Nature Biotechnology* **28**, 1176–1178 (2010).
16. Braden, B. C. & Poljak, R. J. Structural features of the reactions between antibodies and protein antigens. *FASEB J.* **9**, 9–16 (1995).
17. Ganusov, V. V. & Boer, R. J. D. Do most lymphocytes in humans really reside in the gut? *Trends in Immunology* **28**, 514–518 (2007).
18. Arnaout, R. *et al.* High-Resolution Description of Antibody Heavy-Chain Repertoires in Humans. *PLoS ONE* **6**, e22365 (2011).
19. Tiller, T. *et al.* Efficient generation of monoclonal antibodies from single human B cells by single cell RT-PCR and expression vector cloning. *J. Immunol. Methods* **329**, 112–124 (2008).

20. Foote, J. & Milstein, C. Kinetic maturation of an immune response. , *Published online: 08 August 1991; | doi:10.1038/352530a0* **352**, 530–532 (1991).
21. Niels Jerne The Generative Grammar of the Immune System. at <http://nobelprize.org/nobel_prizes/medicine/laureates/1984/jerne-lecture.pdf>
22. Fooksman, D. R. *et al.* Development and Migration of Plasma Cells in the Mouse Lymph Node. *Immunity* **33**, 118–127 (2010).
23. Wrammert, J. *et al.* Rapid cloning of high-affinity human monoclonal antibodies against influenza virus. *Nature* **453**, 667–671 (2008).
24. McHeyzer-Williams, L. J. & McHeyzer-Williams, M. G. Antigen-Specific Memory B Cell Development. *Annual Review of Immunology* **23**, 487–513 (2005).
25. von Behring, E. & Kitasato, S. [The mechanism of diphtheria immunity and tetanus immunity in animals. 1890]. *Mol. Immunol.* **28**, 1317, 1319–1320 (1991).
26. Ehrlich, P. Partial Cell Functions. *Scandinavian Journal of Immunology* **31**, 4–13 (1990).
27. Pier, G. B. & Lyczak, J. B. *Immunology, Infection, and Immunity*. (ASM Press: 2004).
28. KOHLER, G. & MILSTEIN, C. Continuous cultures of fused cells secreting antibody of predefined specificity. *Nature* **256**, 495–497 (1975).
29. Davis, J. M., Pennington, J. E., Kubler, A.-M. & Conscience, J.-F. A simple, single-step technique for selecting and cloning hybridomas for the production of monoclonal antibodies. *Journal of Immunological Methods* **50**, 161–171 (1982).
30. Joyce, J. G. & Meulen, J. ter Pushing the envelope on HIV-1 neutralization. *Nature Biotechnology* **28**, 929–931 (2010).
31. Spieker-Polet, H., Sethupathi, P., Yam, P. C. & Knight, K. L. Rabbit monoclonal antibodies: generating a fusion partner to produce rabbit-rabbit hybridomas. *Proceedings of the National Academy of Sciences of the United States of America* **92**, 9348–9352 (1995).
32. Jones, P. T., Dear, P. H., Foote, J., Neuberger, M. S. & Winter, G. Replacing the complementarity-determining regions in a human antibody with those from a mouse. **321**, 522–525 (1986).
33. Riechmann, L., Clark, M., Waldmann, H. & Winter, G. Reshaping human antibodies for therapy. **332**, 323–327 (1988).
34. Winter, G. & Milstein, C. Man-made antibodies. *Nature* **349**, 293–299 (1991).
35. Beck, A., Wurch, T., Bailly, C. & Corvaia, N. Strategies and challenges for the next generation of therapeutic antibodies. *Nature Reviews Immunology* **10**, 345–352 (2010).
36. Karpas, A., Dremucheva, A. & Czepulkowski, B. H. A human myeloma cell line suitable for the generation of human monoclonal antibodies. *Proceedings of the National Academy of Sciences of the United States of America* **98**, 1799–1804 (2001).
37. Green, L. L. *et al.* Antigen–specific human monoclonal antibodies from mice engineered with human Ig heavy and light chain YACs. *Nature Genetics* **7**, 13–21 (1994).
38. Lonberg, N. *et al.* Antigen-specific human antibodies from mice comprising four distinct genetic modifications. **368**, 856–859 (1994).

39. Kellermann, S.-A. & Green, L. L. Antibody discovery: the use of transgenic mice to generate human monoclonal antibodies for therapeutics. *Current Opinion in Biotechnology* **13**, 593–597 (2002).
40. Lonberg, N. Fully human antibodies from transgenic mouse and phage display platforms. *Current Opinion in Immunology* **20**, 450–459 (2008).
41. Nelson, A. L., Dhimolea, E. & Reichert, J. M. Development trends for human monoclonal antibody therapeutics. *Nat Rev Drug Discov* **9**, 767–774 (2010).
42. L'Haridon, R. M., Bourget, P., Lefevre, F. & La Bonnardiere, C. Production of an Hybridoma Library to Recombinant Porcine Alpha I Interferon: A Very Sensitive Assay (ISBBA) Allows the Detection of a Large Number of Clones. *Hybridoma* **10**, 35–47 (1991).
43. Sogut, I., Hatipoglu, I., Kanbak, G. & Basalp, A. Monoclonal Antibodies Specific for Hepatitis B e Antigen and Hepatitis B Core Antigen. *Hybridoma* **30**, 475–479 (2011).
44. Pasqualini, R. & Arap, W. Hybridoma-free generation of monoclonal antibodies. *Proceedings of the National Academy of Sciences of the United States of America* **101**, 257–259 (2004).
45. Lanzavecchia, A., Corti, D. & Sallusto, F. Human monoclonal antibodies by immortalization of memory B cells. *Current Opinion in Biotechnology* **18**, 523–528 (2007).
46. Hoogenboom, H. R. Selecting and screening recombinant antibody libraries. *Nat Biotech* **23**, 1105–1116 (2005).
47. Harding, F. A., Stickler, M. M., Razo, J. & DuBridge, R. B. The immunogenicity of humanized and fully human antibodies. *MAbs* **2**, 256–265 (2010).
48. Bartelds, G. M. *et al.* Development of Antidrug Antibodies Against Adalimumab and Association With Disease Activity and Treatment Failure During Long-term Follow-up. *JAMA: The Journal of the American Medical Association* **305**, 1460–1468 (2011).
49. Corti, D. *et al.* A Neutralizing Antibody Selected from Plasma Cells That Binds to Group 1 and Group 2 Influenza A Hemagglutinins. *Science* **333**, 850–856 (2011).
50. Babcook, J. S., Leslie, K. B., Olsen, O. A., Salmon, R. A. & Schrader, J. W. A novel strategy for generating monoclonal antibodies from single, isolated lymphocytes producing antibodies of defined specificities. *Proceedings of the National Academy of Sciences of the United States of America* **93**, 7843–7848 (1996).
51. Jin, A. *et al.* A rapid and efficient single-cell manipulation method for screening antigen-specific antibody-secreting cells from human peripheral blood. *Nat Med* **15**, 1088–1092 (2009).
52. Owens, G. P. *et al.* Single-cell repertoire analysis demonstrates that clonal expansion is a prominent feature of the B cell response in multiple sclerosis cerebrospinal fluid. *J. Immunol* **171**, 2725–2733 (2003).
53. Wang, X. & Stollar, B. D. Human immunoglobulin variable region gene analysis by single cell RT-PCR. *J. Immunol. Methods* **244**, 217–225 (2000).
54. Sehgal, D., Schiaffella, E., Anderson, A. O. & Mage, R. G. Analyses of single B cells by polymerase chain reaction reveal rearranged VH with germline sequences in spleens of immunized adult rabbits: implications for B cell repertoire maintenance and renewal. *J. Immunol.* **161**, 5347–5356 (1998).

55. Ali, M., Hitomi, K. & Nakano, H. Generation of monoclonal antibodies using simplified single-cell reverse transcription-polymerase chain reaction and cell-free protein synthesis. *J. Biosci. Bioeng.* **101**, 284–286 (2006).
56. Küppers, R., Zhao, M., Hansmann, M. L. & Rajewsky, K. Tracing B cell development in human germinal centres by molecular analysis of single cells picked from histological sections. *EMBO J* **12**, 4955–4967 (1993).
57. Poulsen, T. R., Jensen, A., Haurum, J. S. & Andersen, P. S. Limits for Antibody Affinity Maturation and Repertoire Diversification in Hypervaccinated Humans. *J Immunol* **187**, 4229–4235 (2011).
58. Tiller, T., Busse, C. E. & Wardemann, H. Cloning and expression of murine Ig genes from single B cells. *Journal of Immunological Methods* **350**, 183–193 (2009).
59. Poulsen, T. R., Meijer, P.-J., Jensen, A., Nielsen, L. S. & Andersen, P. S. Kinetic, Affinity, and Diversity Limits of Human Polyclonal Antibody Responses against Tetanus Toxoid. *J Immunol* **179**, 3841–3850 (2007).
60. Smith, K. *et al.* Human monoclonal antibodies generated following vaccination with AVA provide neutralization by blocking furin cleavage but not by preventing oligomerization. *Vaccine* **30**, 4276–4283 (2012).
61. Wrammert, J. *et al.* Rapid and Massive Virus-Specific Plasmablast Responses during Acute Dengue Virus Infection in Humans. *J. Virol.* **86**, 2911–2918 (2012).
62. Niro, R. D. *et al.* Rapid Generation of Rotavirus-Specific Human Monoclonal Antibodies from Small-Intestinal Mucosa. *J Immunol* **185**, 5377–5383 (2010).
63. Whitesides, G. M. The origins and the future of microfluidics. *Nature* **442**, 368–373 (2006).
64. Manz, A. *et al.* Planar chips technology for miniaturization and integration of separation techniques into monitoring systems: Capillary electrophoresis on a chip. *Journal of Chromatography A* **593**, 253–258 (1992).
65. Agilent | Agilent Technologies' Microfluidics System Used in Breakthrough Breast Milk Study. (2010).at <http://www.agilent.ca/about/newsroom/presrel/2010/17aug-ca10051.html>
66. Jason-Moller, L., Murphy, M. & Bruno, J. Overview of Biacore Systems and Their Applications. *Current Protocols in Protein Science* (2001).at <http://onlinelibrary.wiley.com/doi/10.1002/0471140864.ps1913s45/abstract>
67. Metzker, M. L. Sequencing technologies - the next generation. *Nat. Rev. Genet.* **11**, 31–46 (2010).
68. Maerkl, S. J. & Quake, S. R. A Systems Approach to Measuring the Binding Energy Landscapes of Transcription Factors. *Science* **315**, 233–237 (2007).
69. Maerkl, S. J. Next generation microfluidic platforms for high-throughput protein biochemistry. *Current Opinion in Biotechnology* **22**, 59–65 (2011).
70. Einav, S. *et al.* Discovery of a hepatitis C target and its pharmacological inhibitors by microfluidic affinity analysis. *Nat Biotech* **26**, 1019–1027 (2008).
71. Lee, C.-C. *et al.* Multistep Synthesis of a Radiolabeled Imaging Probe Using Integrated Microfluidics. *Science* **310**, 1793–1796 (2005).
72. Anderson, M. J., Hansen, C. L. & Quake, S. R. Phase knowledge enables rational screens for protein crystallization. *Proceedings of the National Academy of Sciences* **103**, 16746–16751 (2006).

73. Hansen, C. L., Skordalakes, E., Berger, J. M. & Quake, S. R. A robust and scalable microfluidic metering method that allows protein crystal growth by free interface diffusion. *Proceedings of the National Academy of Sciences of the United States of America* **99**, 16531–16536 (2002).
74. Hansen, C. L., Sommer, M. O. A. & Quake, S. R. Systematic investigation of protein phase behavior with a microfluidic formulator. *Proceedings of the National Academy of Sciences of the United States of America* **101**, 14431–14436 (2004).
75. Heyries, K. A. *et al.* Megapixel digital PCR. *Nature Methods* **8**, 649–651 (2011).
76. Kartalov, E. P. *et al.* High-throughput multi-antigen microfluidic fluorescence immunoassays. *BioTechniques* **40**, 85–90 (2006).
77. Diercks, A. H. *et al.* A microfluidic device for multiplexed protein detection in nano-liter volumes. *Anal. Biochem* **386**, 30–35 (2009).
78. Falconnet, D. *et al.* High-throughput tracking of single yeast cells in a microfluidic imaging matrix. *Lab Chip* **11**, 466–473 (2011).
79. Leung, K. *et al.* A programmable droplet-based microfluidic device applied to multiparameter analysis of single microbes and microbial communities. *PNAS* (2012).doi:10.1073/pnas.1106752109
80. Lecault, V. *et al.* High-throughput analysis of single hematopoietic stem cell proliferation in microfluidic cell culture arrays. *Nat Meth* **8**, 581–586 (2011).
81. White, A. K. *et al.* High-throughput microfluidic single-cell RT-qPCR. *PNAS* (2011).doi:10.1073/pnas.1019446108
82. Lecault, V., White, A. K., Singhal, A. & Hansen, C. L. Microfluidic single cell analysis: from promise to practice. *Current Opinion in Chemical Biology* doi:10.1016/j.cbpa.2012.03.022
83. Marcus, J. S., Anderson, W. F. & Quake, S. R. Microfluidic Single-Cell mRNA Isolation and Analysis. *Analytical Chemistry* **78**, 3084–3089 (2006).
84. Duffy, D. C., McDonald, J. C., Schueller, O. J. & Whitesides, G. M. Rapid Prototyping of Microfluidic Systems in Poly(dimethylsiloxane). *Anal. Chem.* **70**, 4974–4984 (1998).
85. McDonald, J. C. *et al.* Fabrication of microfluidic systems in poly(dimethylsiloxane). *Electrophoresis* **21**, 27–40 (2000).
86. Unger, M. A., Chou, H.-P., Thorsen, T., Scherer, A. & Quake, S. R. Monolithic Microfabricated Valves and Pumps by Multilayer Soft Lithography. *Science* **288**, 113–116 (2000).
87. Thorsen, T., Maerkl, S. J. & Quake, S. R. Microfluidic Large-Scale Integration. *Science* **298**, 580–584 (2002).
88. NOSSAL, G. J. & LEDERBERG, J. Antibody production by single cells. *Nature* **181**, 1419–1420 (1958).
89. Viret, C. & Gurr, W. The Origin of the 'One Cell-One Antibody' Rule. *J Immunol* **182**, 1229–1230 (2009).
90. Story, C. M. *et al.* Profiling antibody responses by multiparametric analysis of primary B cells. *Proceedings of the National Academy of Sciences* **105**, 17902–17907 (2008).
91. Köster, S. *et al.* Drop-based microfluidic devices for encapsulation of single cells. *Lab on a Chip* **8**, 1110 (2008).

92. Debs, B. E., Utharala, R., Balyasnikova, I. V., Griffiths, A. D. & Merten, C. A. Functional single-cell hybridoma screening using droplet-based microfluidics. *PNAS* (2012).doi:10.1073/pnas.1204514109
93. Foote, J. & Eisen, H. N. Kinetic and affinity limits on antibodies produced during immune responses. *Proceedings of the National Academy of Sciences of the United States of America* **92**, 1254–1256 (1995).
94. Trisler, K. *et al.* A metalloantibody that irreversibly binds a protein antigen. *J. Biol. Chem.* **282**, 26344–26353 (2007).
95. Lauffenburger, D. A. & Linderman, J. *Receptors: Models for Binding, Trafficking, and Signaling*. (Oxford University Press, USA: 1996).
96. Northrup, S. H. & Erickson, H. P. Kinetics of protein-protein association explained by Brownian dynamics computer simulation. *Proceedings of the National Academy of Sciences of the United States of America* **89**, 3338–3342 (1992).
97. Shick, K. A., Xavier, K. A., Rajpal, A., Smith-Gill, S. J. & Willson, R. C. Association of the anti-hen egg lysozyme antibody HyHEL-5 with avian species variant and mutant lysozymes. *Biochimica et Biophysica Acta (BBA) - Protein Structure and Molecular Enzymology* **1340**, 205–214 (1997).
98. Edwards, B. M. *et al.* The Remarkable Flexibility of the Human Antibody Repertoire; Isolation of Over One Thousand Different Antibodies to a Single Protein, BLyS. *Journal of Molecular Biology* **334**, 103–118 (2003).
99. Sampson, J. H. *et al.* Unarmed, Tumor-Specific Monoclonal Antibody Effectively Treats Brain Tumors. *PNAS* **97**, 7503–7508 (2000).
100. Roost, H. P. *et al.* Early high-affinity neutralizing anti-viral IgG responses without further overall improvements of affinity. *Proc Natl Acad Sci U S A* **92**, 1257–1261 (1995).
101. Klasse, P. J. & Sattentau, Q. J. Occupancy and Mechanism in Antibody-Mediated Neutralization of Animal Viruses. *J Gen Virol* **83**, 2091–2108 (2002).
102. Boder, E. T., Midelfort, K. S. & Wittrup, K. D. Directed evolution of antibody fragments with monovalent femtomolar antigen-binding affinity. *Proceedings of the National Academy of Sciences of the United States of America* **97**, 10701–10705 (2000).
103. Rich, R. L. & Myszka, D. G. Higher-throughput, label-free, real-time molecular interaction analysis. *Analytical Biochemistry* **361**, 1–6 (2007).
104. Xavier, K. A., McDonald, S. M., McCammon, J. A. & Willson, R. C. Association and dissociation kinetics of bobwhite quail lysozyme with monoclonal antibody HyHEL-5. *Protein Eng.* **12**, 79–83 (1999).
105. Xavier, K. A. & Willson, R. C. Association and dissociation kinetics of anti-hen egg lysozyme monoclonal antibodies HyHEL-5 and HyHEL-10. *Biophys J* **74**, 2036–2045 (1998).
106. Bornhop, D. J. *et al.* Free-Solution, Label-Free Molecular Interactions Studied by Back-Scattering Interferometry. *Science* **317**, 1732–1736 (2007).
107. Homola, J., Yee, S. S. & Gauglitz, G. Surface plasmon resonance sensors: review. *Sensors and Actuators B: Chemical* **54**, 3–15 (1999).
108. D'Ulivo, L., Saint-Guirons, J., Ingemarsson, B. & Riekkola, M.-L. Quartz crystal microbalance, a valuable tool for elucidation of interactions between apoB-100

peptides and extracellular matrix components. *Analytical and Bioanalytical Chemistry* **396**, 1373–1380 (2010).
109. Pope, M. E., Soste, M. V., Eyford, B. A., Anderson, N. L. & Pearson, T. W. Anti-peptide antibody screening: Selection of high affinity monoclonal reagents by a refined surface plasmon resonance technique. *Journal of Immunological Methods* **341**, 86–96 (2009).
110. Leonard, P. *et al.* High throughput ranking of recombinant avian scFv antibody fragments from crude lysates using the Biacore A100. *Journal of Immunological Methods* **323**, 172–179 (2007).
111. Biacore Life Sciences > Product Range > Systems Overview > Biacore 3000 > System Information. at <http://www.biacore.com/lifesciences/products/systems_overview/3000/system_information/index.html?section=lifesciences&realsection=lifesciences&counter=4>
112. Singhal, A., Haynes, C. A. & Hansen, C. L. Microfluidic measurement of antibody-antigen binding kinetics from low-abundance samples and single cells. *Anal. Chem* **82**, 8671–8679 (2010).
113. Phillips, D. C. Symposium on Three-Dimensional Structure of Macromolecules of Biological Origin. by Invitation of the Committee on Arrangements for the Autumn Meeting. Presented before the Academy on October 19, 1966. Chairman, Walter Kauzmann: THE HEN EGG-WHITE LYSOZYME MOLECULE. *Proceedings of the National Academy of Sciences of the United States of America* **57**, 483 (1967).
114. Goldbaum, F. A. *et al.* Lack of significant differences in association rates and affinities of antibodies from short-term and long-term responses to hen egg lysozyme. *J. Immunol* **162**, 6040–6045 (1999).
115. Batista, F. D. & Neuberger, M. S. Affinity Dependence of the B Cell Response to Antigen: A Threshold, a Ceiling, and the Importance of Off-Rate. *Immunity* **8**, 751–759 (1998).
116. Ito, W., Yasui, H. & Kurosawa, Y. Mutations in the Complementarity-determining Regions do not cause Differences in Free Energy during the Process of Formation of the Activated Complex between an Antibody and the Corresponding Protein Antigen. *Journal of Molecular Biology* **248**, 729–732 (1995).
117. England, P., Nageotte, R., Renard, M., Page, A. L. & Bedouelle, H. Functional characterization of the somatic hypermutation process leading to antibody D1.3, a high affinity antibody directed against lysozyme. *J. Immunol* **162**, 2129–2136 (1999).
118. Tyn, M. T. & Gusek, T. W. Prediction of diffusion coefficients of proteins. *Biotechnology and Bioengineering* **35**, 327–338 (1990).
119. He, L.-Z. & Niemeyer, B. A Novel Correlation for Protein Diffusion Coefficients Based on Molecular Weight and Radius of Gyration. *Biotechnol. Prog.* **19**, 544–548 (2003).
120. Dubin, S. B., Clark, N. A. & Benedek, G. B. Measurement of the Rotational Diffusion Coefficient of Lysozyme by Depolarized Light Scattering: Configuration of Lysozyme in Solution. *The Journal of Chemical Physics* **54**, 5158–5164 (1971).

121. Abdiche, Y., Malashock, D., Pinkerton, A. & Pons, J. Determining kinetics and affinities of protein interactions using a parallel real-time label-free biosensor, the Octet. *Analytical Biochemistry* **377**, 209–217 (2008).
122. Bates, S. R. & Quake, S. R. Highly parallel measurements of interaction kinetic constants with a microfabricated optomechanical device. *Appl. Phys. Lett.* **95**, 073705 (2009).
123. Biacore Life Sciences > Technology > Introduction > Data from an interaction > Single-Cycle Kinetics. at <http://www.biacore.com/lifesciences/technology/introduction/data_interaction/SCK/index.html?backurl=%2Flifesciences%2Ftechnology%2Fintroduction%2Fdata_interaction%2Findex.html>
124. McKinney, K. L., Dilwith, R. & Belfort, G. Optimizing antibody production in batch hybridoma cell culture. *Journal of Biotechnology* **40**, 31–48 (1995).
125. Tan, W.-H. & Takeuchi, S. A trap-and-release integrated microfluidic system for dynamic microarray applications. *Proc. Natl. Acad. Sci. U. S. A.* **104**, 1146–1151 (2007).
126. Stevens, R. H. Immunoglobulin heavy chain mRNA in mitogen-stimulate B cells. *European Journal of Immunology* **5**, 47–53
127. Arbabi-Ghahroudi, M., Tanha, J. & MacKenzie, R. Prokaryotic expression of antibodies. *Cancer and Metastasis Reviews* **24**, 501–519 (2005).
128. Chiba, Y. & Akeboshi, H. Glycan Engineering and Production of 'Humanized' Glycoprotein in Yeast Cells. *Biological and Pharmaceutical Bulletin* **32**, 786–795 (2009).
129. Verma, R., Boleti, E. & George, A. J. . Antibody engineering: Comparison of bacterial, yeast, insect and mammalian expression systems. *Journal of Immunological Methods* **216**, 165–181 (1998).
130. Ma, J. K.-C., Drake, P. M. W. & Christou, P. The production of recombinant pharmaceutical proteins in plants. *Nat Rev Genet* **4**, 794–805 (2003).
131. Lagerkvist, A. C., Furebring, C. & Borrebaeck, C. A. Single, antigen-specific B cells used to generate Fab fragments using CD40-mediated amplification or direct PCR cloning. *BioTechniques* **18**, 862–869 (1995).
132. de Wildt, R. M. *et al.* A new method for the analysis and production of monoclonal antibody fragments originating from single human B cells. *J. Immunol. Methods* **207**, 61–67 (1997).
133. Heilmann, C. & Barington, T. Distribution of kappa and lambda light chain isotypes among human blood immunoglobulin-secreting cells after vaccination with pneumococcal polysaccharides. *Scand. J. Immunol.* **29**, 159–164 (1989).
134. Wang, Z. *et al.* Universal PCR amplification of mouse immunoglobulin gene variable regions: the design of degenerate primers and an assessment of the effect of DNA polymerase 3' to 5' exonuclease activity. *Journal of Immunological Methods* **233**, 167–177 (2000).
135. Saiki, R. *et al.* Primer-Directed Enzymatic Amplification of Dna with a Thermostable Dna-Polymerase. *Science* **239**, 487–491 (1988).
136. Ririe, K. M., Rasmussen, R. P. & Wittwer, C. T. Product differentiation by analysis of DNA melting curves during the polymerase chain reaction. *Anal. Biochem.* **245**, 154–160 (1997).

137. Rychlik, W. & Rhoads, R. E. A computer program for choosing optimal oligonudeotides for filter hybridization, sequencing and in vitro amplification of DNA. *Nucl. Acids Res.* **17**, 8543–8551 (1989).
138. Owczarzy, R. Melting temperatures of nucleic acids: Discrepancies in analysis. *Biophysical Chemistry* **117**, 207–215 (2005).
139. Bustin, S. A. Absolute Quantification of mRNA Using Real-Time Reverse Transcription Polymerase Chain Reaction Assays. *J Mol Endocrinol* **25**, 169–193 (2000).
140. Don, R. H., Cox, P. T., Wainwright, B. J., Baker, K. & Mattick, J. S. 'Touchdown' PCR to Circumvent Spurious Priming During Gene Amplification. *Nucl. Acids Res.* **19**, 4008–4008 (1991).
141. Hecker, K. & Roux, K. High and low annealing temperatures increase both specificity and yield in touchdown and stepdown PCR. *Biotechniques* **20**, 478–& (1996).
142. Invitrogen Dynabeads Oligo(dT)25 datasheet. at <http://tools.invitrogen.com/content/sfs/manuals/610%2002_05_50%20Dynabeads%20Oligo%28dT%2925%28rev006%29.pdf>
143. Phillips, R., Kondev, J. & Theriot, J. *Physical Biology of the Cell*. (Garland Science: 2008).
144. Subkhankulova, T. & Livesey, F. J. Comparative evaluation of linear and exponential amplification techniques for expression profiling at the single-cell level. *Genome Biology* **7**, R18 (2006).
145. Linke, D. Detergents: An Overview. *Guide to Protein Purification, Second Edition* **463**, 603–617 (2009).
146. Newman, M. A., Mainhart, C. R., Mallett, C. P., Lavoie, T. B. & Smith-Gill, S. J. Patterns of antibody specificity during the BALB/c immune response to hen eggwhite lysozyme. *J. Immunol* **149**, 3260–3272 (1992).
147. Gammon, G. *et al.* The Choice of T-Cell Epitopes Utilized on a Protein Antigen Depends on Multiple Factors Distant from, as well as at the Determinant Site. *Immunological Reviews* **98**, 54–73 (1987).
148. Brink, R., Phan, T. G., Paus, D. & Chan, T. D. Visualizing the effects of antigen affinity on T-dependent B-cell differentiation. *Immunology and Cell Biology* **86**, 31–39 (2008).
149. Lecault, V. *et al.* High-throughput analysis of single hematopoietic stem cell proliferation in microfluidic cell culture arrays. *Nature Methods* **8**, 581–586 (2011).
150. Corti, D., Sallusto, F. & Lanzavecchia, A. High throughput cellular screens to interrogate the human T and B cell repertoires. *Current Opinion in Immunology* **23**, 430–435 (2011).
151. Chan, T. D. & Brink, R. Affinity-based selection and the germinal center response. *Immunological Reviews* **247**, 11–23 (2012).
152. Lavoie, T. B. *et al.* Structural differences among monoclonal antibodies with distinct fine specificities and kinetic properties. *Mol. Immunol* **36**, 1189–1205 (1999).

153. Schwesinger, F. *et al.* Unbinding forces of single antibody-antigen complexes correlate with their thermal dissociation rates. *Proc. Natl. Acad. Sci. U.S.A.* **97**, 9972–9977 (2000).
154. Eisen, H. N. & Siskind, G. W. Variations in Affinities of Antibodies during the Immune Response*. *Biochemistry* **3**, 996–1008 (1964).
155. Banks, D. S. & Fradin, C. Anomalous Diffusion of Proteins Due to Molecular Crowding. *Biophys J* **89**, 2960–2971 (2005).
156. Xavier, K. A. & Willson, R. C. Association and dissociation kinetics of anti-hen egg lysozyme monoclonal antibodies HyHEL-5 and HyHEL-10. *Biophys. J* **74**, 2036–2045 (1998).
157. Ofek, G. *et al.* Relationship between Antibody 2F5 Neutralization of HIV-1 and Hydrophobicity of Its Heavy Chain Third Complementarity-Determining Region. *J Virol* **84**, 2955–2962 (2010).
158. Lavoie, T. B., Drohan, W. N. & Smith-Gill, S. J. Experimental Analysis by Site-Directed Mutagenesis of Somatic Mutation Effects on Affinity and Fine Specificity in Antibodies Specific for Lysozyme. *J Immunol* **148**, 503–513 (1992).
159. Xu, J. L. & Davis, M. M. Diversity in the CDR3 Region of VH Is Sufficient for Most Antibody Specificities. *Immunity* **13**, 37–45 (2000).
160. Boder, E. T. & Wittrup, K. D. Optimal Screening of Surface-Displayed Polypeptide Libraries. *Biotechnology Progress* **14**, 55–62 (1998).
161. Yancopoulos, G. D., Malynn, B. A. & Alt, F. W. Developmentally Regulated and Strain-Specific Expression of Murine VH Gene Families. *J Exp Med* **168**, 417–435 (1988).
162. Jiang, N. *et al.* Determinism and Stochasticity During Maturation of the Zebrafish Antibody Repertoire. *PNAS* **108**, 5348–5353 (2011).
163. Braden, B. C., Goldman, E. R., Mariuzza, R. A. & Poljak, R. J. Anatomy of an antibody molecule: structure, kinetics, thermodynamics and mutational studies of the antilysozyme antibody D1.3. *Immunol. Rev* **163**, 45–57 (1998).
164. Lötscher, M., Amstutz, H., Heusser, C. H. & Blaser, K. Fine specificity and heavy chain V gene usage of antibodies to the phosphorylcholine hapten. *Mol. Immunol.* **27**, 369–378 (1990).
165. Lötscher, M., Blaser, K. & Heusser, C. H. Specific V gene usage in anti-phosphorylcholine IgE antibodies. *Mol. Immunol.* **30**, 1573–1582 (1993).
166. Robert, R. *et al.* Restricted V gene usage and VH/VL pairing of mouse humoral response against the N-terminal immunodominant epitope of the amyloid β peptide. *Mol. Immunol.* **48**, 59–72 (2010).
167. Fernandez-Sanchez, A., Garcia-Ocana, M. & de los Toyos, J. R. Mouse monoclonal antibodies to pneumococcal C-polysaccharide backbone show restricted usage of VH-DH-JH gene segments and share the same kappa chain. *Immunol. Lett.* **123**, 125–131 (2009).
168. Adderson, E. E., Shackelford, P. G., Quinn, A. & Carroll, W. L. Restricted Ig H chain V gene usage in the human antibody response to Haemophilus influenzae type b capsular polysaccharide. *J. Immunol.* **147**, 1667–1674 (1991).
169. Breden, F. *et al.* Comparison of antibody repertoires produced by HIV-1 infection, other chronic and acute infections, and systemic autoimmune disease. *PLoS ONE* **6**, e16857 (2011).

170. McLean, G. R. *et al.* Recognition of human cytomegalovirus by human primary immunoglobulins identifies an innate foundation to an adaptive immune response. *J. Immunol.* **174**, 4768–4778 (2005).
171. Li, G.-M. *et al.* Pandemic H1N1 Influenza Vaccine Induces a Recall Response in Humans That Favors Broadly Cross-Reactive Memory B Cells. *PNAS* (2012).doi:10.1073/pnas.1118979109
172. Thomson, C. A. *et al.* Pandemic H1N1 influenza infection and vaccination in humans induces cross-protective antibodies that target the hemagglutinin stem. *Front. Immun.* **3**, 87 (2012).
173. Hangartner, L., Zinkernagel, R. M. & Hengartner, H. Antiviral antibody responses: the two extremes of a wide spectrum. *Nature Reviews Immunology* **6**, 231–243 (2006).
174. Hudziak, R. M. *et al.* p185HER2 monoclonal antibody has antiproliferative effects in vitro and sensitizes human breast tumor cells to tumor necrosis factor. *Mol Cell Biol* **9**, 1165–1172 (1989).
175. Han, M. Y., Gao, X. H., Su, J. Z. & Nie, S. Quantum-dot-tagged microbeads for multiplexed optical coding of biomolecules. *Nat. Biotechnol.* **19**, 631–635 (2001).
176. Lelli, D. *et al.* West Nile virus: characterization and diagnostic applications of monoclonal antibodies. *Virol. J.* **9**, (2012).
177. Wrammert, J. *et al.* Broadly Cross-Reactive Antibodies Dominate the Human B Cell Response Against 2009 Pandemic H1N1 Influenza Virus Infection. *J Exp Med* (2011).doi:10.1084/jem.20101352
178. Heyndrickx, L. *et al.* International Network for Comparison of HIV Neutralization Assays: The NeutNet Report II. *PLoS ONE* **7**, e36438 (2012).
179. Rimmelzwaan, G. F. *et al.* Use of GFP-expressing influenza viruses for the detection of influenza virus A/H5N1 neutralizing antibodies. *Vaccine* **29**, 3424–3430 (2011).
180. Katz, J. M., Hancock, K. & Xu, X. Serologic assays for influenza surveillance, diagnosis and vaccine evaluation. *Expert Review of Anti-infective Therapy* **9**, 669–683 (2011).
181. Tay, S. *et al.* Single-cell NF-κB dynamics reveal digital activation and analogue information processing. *Nature* **466**, 267–271 (2010).
182. Rathanaswami, P. *et al.* Demonstration of an in vivo generated sub-picomolar affinity fully human monoclonal antibody to interleukin-8. *Biochemical and Biophysical Research Communications* **334**, 1004–1013 (2005).
183. Ozawa, T., Kishi, H. & Muraguchi, A. Amplification and analysis of cDNA generated from a single cell by 5'-RACE: application to isolation of antibody heavy and light chain variable gene sequences from single B cells. *BioTechniques* **40**, 469–470, 472, 474 passim (2006).
184. Lao, K. Q. *et al.* mRNA-Sequencing Whole Transcriptome Analysis of a Single Cell on the SOLiD™ System. *J Biomol Tech* **20**, 266–271 (2009).
185. Singhal, A., Hansen, C. L. G., Schrader, J. W., Haynes, C. A. & Costa, D. J. D. Methods for Assaying Cellular Binding Interactions. at <http://www.google.com/patents/US20120015347>
186. Birch, J. R. & Racher, A. J. Antibody production. *Adv. Drug Deliv. Rev.* **58**, 671–685 (2006).

187. Holliger, P. & Hudson, P. J. Engineered antibody fragments and the rise of single domains. *Nat. Biotechnol.* **23**, 1126–1136 (2005).

Appendices

Appendix A - Primer Designs for Amplifying Mouse Antibody Genes

A.1 Highly Degenerate Primer Set for Amplifying Mouse Heavy and Light Chain Antibody Genes.

Primers sequences taken from Wang et al.[134]

Primer Name	Sequence
C_H Region (3')	
IgA	gga aga tct GAT GGT GGG ATT TCT CGC AGA CTC
IgE	gga aga tct TAA GGG GTA GAG CTG AGG GTT CCT G
IgM	gga aga tct GAC ATT TGG GAA GGA CTG ACT CTC
IgG1	gga aga tct ATA GAC AGA TGG GGG TGT CGT TTT GGC
IgG2A	gga aga tct CTT GAC CAG GCA TCC TAG AGT CA
IgG2B	gga aga tct AGG GGC CAG TGG ATA GAC TGA TGG
IgG3	gga aga tct AGG GAC CAA GGG ATA GAC AGA TGG
V_H Region (5')	
5' MH1	ctt ccg gaa ttc SAR GTN MAG CTG SAG SAG TC
5' MH2	ctt ccg gaa ttc SAR GTN MAG CTG SAG SAG TCW GG
5' MH3	ctt ccg gaa ttc CAG GTT ACT CTG AAA GWG TST G
5' MH4	ctt ccg gaa ttc GAG GTC CAR CTG CAA CAR TC
5' MH5	ctt ccg gaa ttc CAG GTC CAA CTV CAG CAR CC
5' MH6	ctt ccg gaa ttc GAG GTG AAS STG GTG GAA TC
5' MH7	ctt ccg gaa ttc GAT GTG AAC TTG GAA GTG TC
C_K Region (3')	
3' Kc	ggt gca tgc GGA TAC AGT TGG TGC AGC ATC
V_K Region (5')	
5' Mk	gg gag ctc GAY ATT GTG MTS ACM CAR WCT MCA

A.2 Low Degeneracy Nested PCR Primer Set for Amplifying Mouse Heavy and Light Chain Antibody Genes. (continued on next page)

Primer sequences taken from Tiller et al.[134]

Primer Name	Sequence
	IgH 1st round PCR
5′ MsVHE	GGGAATTCGAGGTGCAGCTGCAGGAGTCTGG
3′ Cμ outer	AGGGGGCTCTCGCAGGAGACGAGG
3′ Cγ1 outer	GGAAGGTGTGCACACCGCTGGAC
3′ Cγ2c outer	GGAAGGTGTGCACACCACTGGAC
3′ Cγ2b outer	GGAAGGTGTGCACACTGCTGGAC
3′ Cγ3 outer	AGACTGTGCGCACACCGCTGGAC
3′ Cα outer	GAAAGTTCACGGTGGTTATATCC
	IgH 2nd round PCR
5′ MsVHE	GGGAATTCGAGGTGCAGCTGCAGGAGTCTGG
3′ Cμ inner	AGGGGGAAGACATTTGGGAAGGAC
3′ Cγ1 inner	GCTCAGGGAAATAGCCCTTGAC
3′ Cγ2c inner	GCTCAGGGAAATAACCCTTGAC
3′ Cγ2b inner	ACTCAGGGAAGTAGCCCTTGAC
3′ Cγ3 inner	GCTCAGGGAAGTAGCCTTTGAC
3′ Cα inner	TGCCGAAAGGGAAGTAATCGTGAAT

A.3 (continued from previous page) Low Degeneracy Nested PCR Primer Set for Amplifying Mouse Heavy and Light Chain Antibody Genes.

Primer sequences taken from Tiller et al.[134]

Primer Name	Sequence
	Igκ 1st round PCR
5′ L-Vκ_3	TGCTGCTGCTCTGGGTTCCAG
5′ L-Vκ_4	ATTWTCAGCTTCCTGCTAATC
5′ L-Vκ_5	TTTTGCTTTTCTGGATTYCAG
5′ L-Vκ_6	TCGTGTTKCTSTGGTTGTCTG
5′ L-Vκ_6,8,9	ATGGAATCACAGRCYCWGGT
5′ L-Vκ_14	TCTTGTTGCTCTGGTTYCCAG
5′ L-Vκ_19	CAGTTCCTGGGGCTCTTGTTGTTC
5′ L-Vκ_20	CTCACTAGCTCTTCTCCTC
3′ mCκ	GATGGTGGGAAGATGGATACAGTT
	Igκ 2nd round PCR
5′ mVkappa	GAYATTGTGMTSACMCARWCTMCA
3′ BsiWI P-mJK01	GCCACCGTACGTTTGATTTCCAGCTTGGTG
3′ BsiWI P-mJK02	GCCACCGTACGTTTTATTTCCAGCTTGGTC
3′ BsiWI P-mJK03	GCCACCGTACGTTTTATTTCCAACTTTGTC
3′ BsiWI P-mJK04	GCCACCGTACGTTTCAGCTCCAGCTTGGTC

Appendix B - Labview Software for Hardware Automation and Image Analysis

B.1 Custom LabView Software to Automate CCD Camera, Brightfield Illumination, Microscope Stage Control, and Microfluidic Valve Operation.

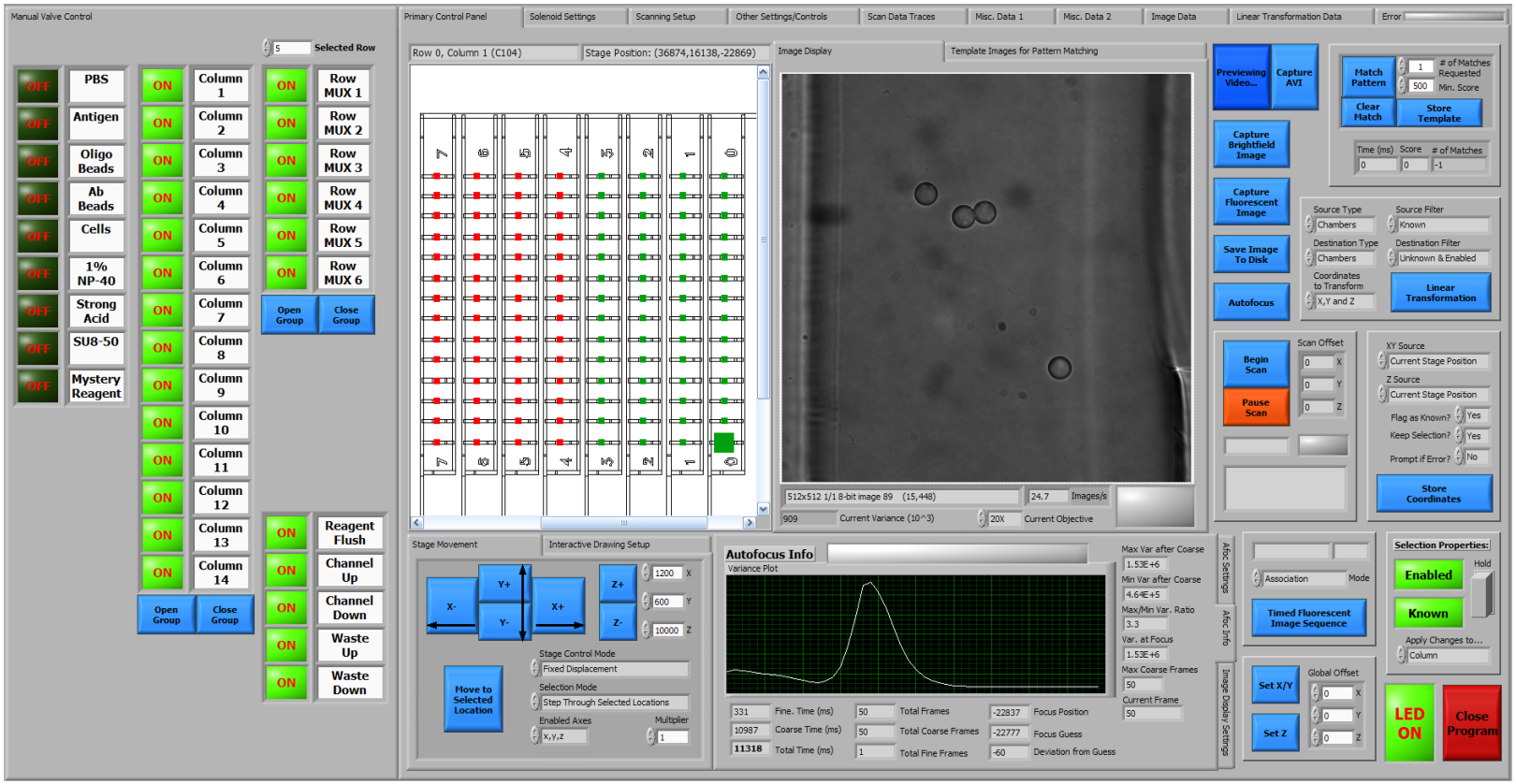

Image prepared by Daniel Da Costa.

B.2 Custom LabView Software for Automated Analysis of Images.

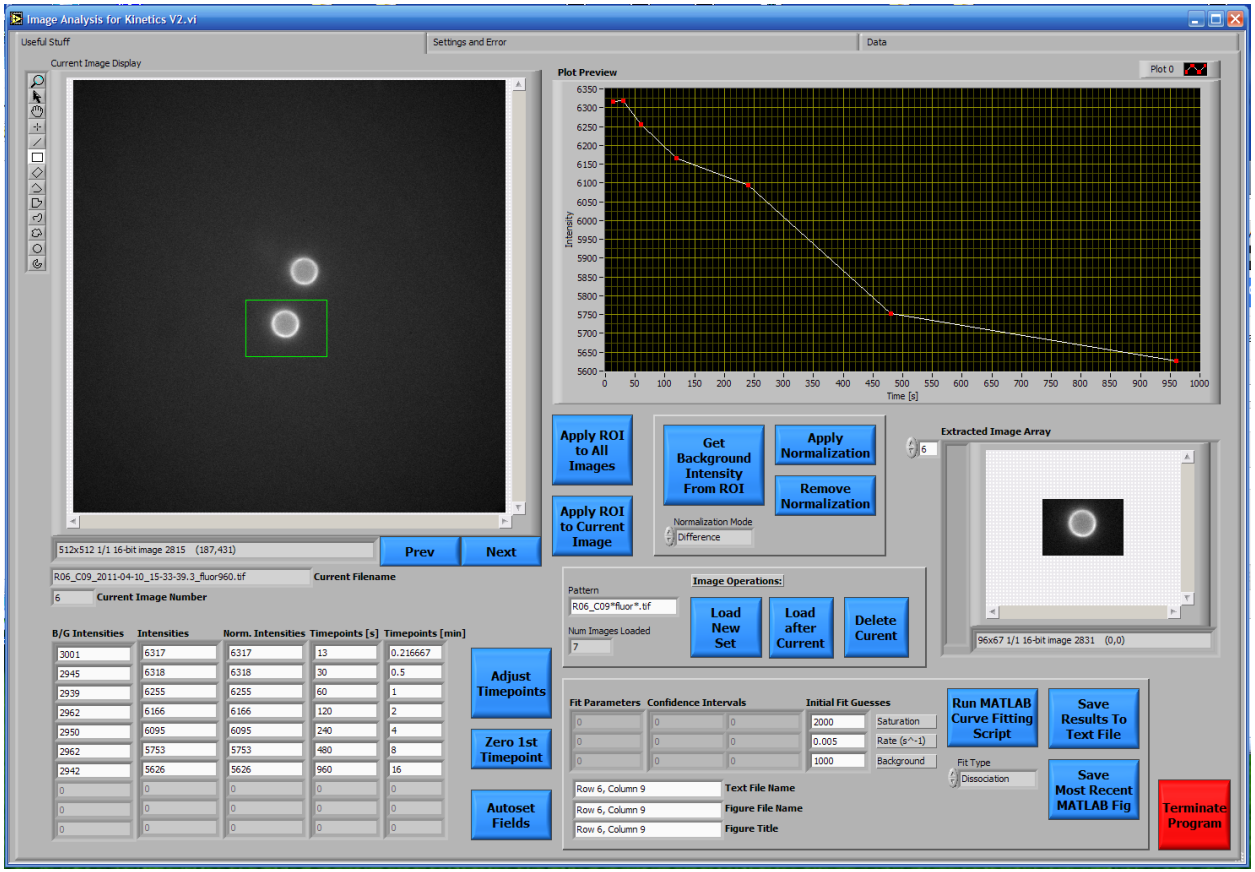

The user selects a region-of-interest and the program calculates the maximum fluorescence intensity within this region in all images. This program was used to measure fluorescence of all chambers as well as binding kinetics of individual chambers. Binding rate constants were determined by fitting the data to first-order mass-action equations (Chapter 2, Section 2.1.1) using nonlinear least squares minimization. Image prepared by Daniel Da Costa.